The effects of growth factors and mechanical tension on ocular fibroblasts in wound healing and scarring

Annegret Hella Dahlmann

Dr. med. FRCOphth FRCS(Ed) DipMedEd

This thesis is submitted to
University College London
for the degree of
Doctor of Philosophy

Institute of Ophthalmology
University College London
September 2006

ProQuest LLC
789 East Eisenhower Parkway
P.O. Box 1346
Ann Arbor, MI 48106-1346

To Erika and Herbert,

for love and education.

To Moni and Karl-Hermann,

who taught me observation.

To Alfred and to Nadim,

the most supportive boys,

and to young gorgeous Hamza,

who is my life and joy.

Acknowledgements

I would like to thank my supervisors, Peng Khaw and Maryse Bailly, for the continuous encouragement, inspiration, and fruitful discussions that have shaped this work. Senior colleagues in the laboratory, in particular Mark Eastwood, Claire Futter, Astrid Limb, Julie Daniels, Maria Balda, Karl Matter, Tim Levine, and Steve Moss, were always helpful by giving critical feedback on the work I presented at lab meetings. I learned all practical skills from postdocs, and am particularly grateful to Alison Cambrey, Alpa Ahir, Anna Tsapara and Minoo Agakhani for teaching me. Others contributed by discussing techniques and topics with me, and by enlarging my horizon in cell biology: Matt Hayes, Dongmin Shao, Catriona Brunton, Jean Lawrence, Tony Sourisseau, Saima Aijaz, Quian Garrett and Belen Martin Martin. Multiphoton imaging was only possible thanks to the expertise of Andrew Vaughan. Assistance with all administrative problems was expertly and liberately given by Stephen Griffiths, who also resolved many of my difficulties with operating lab equipment. Finally, this thesis, which was largely written in the hours around midnight, would not have seen the light of day without constant supplies of PGTips and Lindt chocolate.

Abstract

Processes of wound healing or scarring cause many blinding eye conditions and can limit the success of surgical eye treatments. The mechanisms underlying matrix remodelling and contraction by connective tissue cells (fibroblasts) are not fully understood. Two main theories dominate the field: firstly, that fibroblasts in a wound begin to express alpha smooth muscle actin and transdifferentiate into myofibroblasts with enhanced contractile properties, and secondly that fibroblast migration might underly matrix condensation. The purpose of this work was to develop novel imaging techniques to investigate the mechanisms of tissue contraction and force generation using live cell and matrix imaging during fibroblast-mediated collagen gel contraction, and to determine the role played by growth factors and mechanical tension in that process. We have shown that fibroblasts from different parts of the eye display marked differences in macroscopic matrix contraction profiles, and that four factors determine the early matrix contraction profile: 1) cell size, 2) intrinsic cellular force, 3) growth factor-mediated actomyosin-based dynamic cell protrusive activity and 4) net pericellular matrix displacement. Intrinsic cellular force and dynamic activity appear to be independent unique characteristics of each cell type and might serve as predictors of matrix contraction. In addition, in corneal fibroblasts, we have shown that the recently identified PDGF/rab5/RNTre-pathway mediates a specific type of cell protrusive activity leading to matrix contraction. Specific inhibitors of actomyosin- and rab5/RNTre-pathways are likely candidates to prevent corneal haze formation after surgery, trauma or inflammation. Finally, we explored novel models of contraction involving real tissue by developping techniques to maintain and microscopically study ocular surface tissue *ex vivo*. We achieved successful concomitant live imaging of

resident cells and extra-cellular matrix behaviour at high resolution in both conjunctival and corneal stroma by combining optimized strategies for tissue maintenance, fluorescent cell labeling, and confocal laser and/or two-photon microscopy.

In summary, this thesis presents novel pathways of matrix contraction and imaging techniques to study these events *in vitro* and *ex vivo*.

Declaration

I, Annegret Hella Dahlmann, confirm that the work presented in this thesis is my own. Where information has been derived from other sources, I confirm that this has been indicated in the thesis.

Cambridge, September 12, 2006

Table of contents

ACKNOWLEDGEMENTS 3

ABSTRACT 4

DECLARATION 6

TABLE OF CONTENTS 7

FIGURES AND TABLES 12

ABBREVIATIONS 18

CHAPTER 1: INTRODUCTION, REVIEW OF THE LITERATURE, AIMS 19

1.1. Cellular mechanisms of connective tissue contraction: actin dynamics versus the "contractile" phenotype 21

1.1.1. Actin cytoskeleton organisation and functions 21

1.1.2. Actin-based force generation: actin filament elongation versus actin-myosin interaction 36

1.1.3. Actin dynamics in matrix contraction 38

a) Pulling whilst moving: the locomotion concept of tractional structuring 39

b) Traction without migration: using the locomotion machinery for contraction 40

c) Tissue contraction by a contractile fibroblast phenotype: the myofibroblast 42

1.1.4. Measurements of traction and contraction forces 44

1.2. Growth factor signalling pathways in contraction 47

1.3. Matrix and Tension **52**

1.3.1. Connection between the cytoskeleton and matrix: transmembrane protein complexes transmit force 52

1.3.2. How cells sense matrix tension and react to changes 53

a) immediate responses 54

b) long-term responses 54

1.4. Relevance to the eye **56**

1.4.1. Corneal fibroblasts 56

1.4.2. Tenon's fibroblasts 57

1.4.3. Scleral fibroblasts 58

1.5 Hypotheses and Aims **59**

CHAPTER 2: MATERIALS AND METHODS **60**

2.1. Reagents **61**

2.1.1. Cell Culture 61

2.1.2. Collagen contraction assay 61

2.1.3. Organ Culture 62

2.1.4. Force measurement and application of external tension 62

2.1.5. Transfection reagents 63

2.1.6. Antibodies 64

2.1.7. Vital dyes 65

2.1.8. Plasmids 65

2.1.9. GFP adenovirus and plasmids 66

2.1.10.Inhibitory drugs 67

2.2. Cell and organ culture **68**

2.2.1. Human primary cell lines 68

2.2.2. Collagen matrices 68

2.2.3. Pig eyes 70

2.3. Macroscopic collagen contraction assay **70**

2.4. Circular ruffling assay **71**

2.5. Transfection of human corneal fibroblasts **73**

2.5.1. Lipofectamine™ transfection 73

2.5.2. Fugene™ transfection 73

2.5.3. Amaxa™ transfection 73

2.6. siRNA **74**

2.7. Western blotting **75**

2.7.1. Preparation of samples 75

2.7.2. SDS polyacrylamide gel electrophoresis (PAGE) 75

2.7.3. Western blotting 75

2.8. Viral transduction of cells **76**

2.9. Cell staining by vital dyes **76**

2.10. Microscopy **77**

2.10.1. Phase and fluorescence imaging 77

2.10.2. Confocal reflection microscopy 77

2.10.3. Quantitation of circular ruffling 78

2.10.4. Quantitation of three-dimensional protrusive activity 78

2.10.5. Quantitation of matrix displacement 80

2.11. Immunofluorescence **80**

2.12. Two photon excitation microscopy **81**

2.13. Force measurement and application of external tension **82**

2.14. Calculation of cell volume **82**

CHAPTER 3: RESULTS 83

3.1. Mechanics and dynamics of force generation and matrix contraction 84

3.1.1. Ocular fibroblasts differ in matrix contraction efficiency 85

3.1.2. Cell protrusive activity drives early matrix contraction and force generation 87

a) Protrusive activity is the main cellular behaviour in early matrix contraction and leads to matrix displacement 87

b) Development of the SIM-CFM: matrix displacement corresponds to force generation 94

3.2. The pathway from PDGF receptor to matrix contraction 103

3.2.1. PDGF is an important stimulator of matrix contraction in corneal fibroblasts 103

a) PDGF induces nearly as much matrix contraction as serum 104

b) PDGF inhibitors greatly reduce serum-induced matrix contraction by corneal fibroblasts 105

1. Identification of inhibitors of PDGF-mediated matrix contraction 106

2. Importance of PDGF-mediated matrix contraction by corneal fibroblasts in the presence of multiple growth factors 109

3. Assessment of toxic effects of AG1295 and Trapidil on corneal fibroblasts 113

3.2.2. PDGF stimulates a major protrusive activity in corneal fibroblasts: circular ruffling 115

a) Circular ruffling morphology and kinetics in corneal fibroblasts 115

b) Dose-response kinetics of circular ruffling 120

c) PDGF pathway blockers reduce the incidence of circular ruffling 122

d) Molecular pathways resulting in circular ruffling in corneal fibroblasts 125

3.2.3. The PDGF mediated circular ruffling pathway is involved in matrix contraction by corneal fibroblasts 134

a) PDGF inhibition reduces dynamic cellular activity 134

b) The circular ruffling pathway is involved in PDGF-mediated matrix contraction 140

1. Inhibition using actin assembly and myosin activation as a target 140

2. Inhibition using molecules specific to the circular ruffling pathway 150

3.3. Imaging tissue: confocal and two-photon microscopy combined with fluorescent probes visualise cells and matrix in conjunctiva and cornea 156

CHAPTER 4: DISCUSSION 162

4.1. Ocular fibroblasts differ in matrix contraction efficiency 163

4.2. The SIM-CFM 166

4.3. Protrusive activity drives early contraction and force generation 169

4.4. Two types of protrusive activity, spreading and steady-state, define two phases of early matrix contraction 173

4.5. PDGF is a major growth factor inducing matrix contraction by corneal fibroblasts 175

4.6. The signalling pathway downstream of the PDGF receptor induces circular ruffling in corneal fibroblasts 176

4.7. The circular ruffling pathway is a major pathway in early matrix contraction following PDGF stimulation 180

4.8. The role of the rab5/circular ruffling pathway in matrix contraction 188

4.9. Relevance to wound healing modulation and the eye 191

CONCLUSIONS 200

REFERENCES 201

Figures and tables

Figures

Fig. 1.1. Distribution of actin isoforms in a model cell

Fig. 1.2. Filament assembly and disassembly in response to extracellular signals

Fig. 1.3. Actin filament elongation and turnover

Fig. 1.4. Nucleation and actin filament network formation by the arp 2/3 complex

Fig. 1.5. Actin-based cellular structures

Fig. 1.6. Regulation of actin nucleation and protrusion formation

Fig. 1.7. Domain structure of WASP and WAVE/Scar proteins

Fig. 1.8. Auto- and trans-inhibitory conformation and activation of WASP and WAVE/Scar proteins

Fig. 1.9. The PDGF-receptor

Fig. 1.10. Molecules critically required for circular ruffling.

Fig. 1.11. Schematic illustration of the actin cytoskeleton in a migrating B16 melanoma cell

Fig. 1.12. Effects downstream from rac and cdc42 result in lamellipodia, ruffle, and filopodia formation, and in decreased actomyosin contractility

Fig. 1.13. Effects downstream from rho result in stress fibre formation and increased contractility

Fig. 1.14. Myosin-driven contractility is mediated through different pathways in cell centre and periphery

Fig. 2.1. Dynamic index calculation

Fig. 3.1.1. Ocular fibroblasts have different degrees of matrix contraction efficiency

Fig. 3.1.2. Contraction is linked to the presence of growth factors in the medium

Fig. 3.1.3. Establishment of cells in the matrix: in the first hours after matrix preparation, HCF and HTF form progressively longer protrusions, whilst HSF remain mostly spherical

Fig. 3.1.4. Cell length reaches a plateau 6 hours after matrix preparation

Fig. 3.1.5. Different types of ocular fibroblasts have different protrusive activity levels, reflected in their dynamic index at plateau value

Fig. 3.1.6. Protrusive activity is associated with traction on collagen fibres and net matrix displacement

Fig. 3.1.7 All types of fibroblasts induce net matrix displacement in the first hours after matrix preparation; only Tenon's fibroblasts sustain it

Fig. 3.1.8. The SIM-CFM allows simultaneous imaging of cells and matrix and measurement of force generation

Fig. 3.1.9. Whilst recording live cell behaviour, the SIM-CFM measures matrix contraction force

Fig. 3.1.10. Alteration of matrix strain

Fig. 3.1.11. Corneal fibroblasts generate more force than Tenon's fibroblasts, whilst scleral fibroblasts hardly generate any

Fig. 3.1.12. Ocular fibroblasts differ greatly in force generation

Fig. 3.1.13. Ocular fibroblasts differ greatly in size

Fig. 3.1.14. The intrinsic cellular force is in the same range for all three cell types, indicating the presence of a common mechanism of force generation

Fig. 3.1.15. Force generation, protrusive activity and matrix displacement increase initially, and after 6 hours reach a plateau

Fig. 3.2.1. In corneal fibroblasts, PDGF induces 70% of the matrix contraction observed after serum stimulation

Fig. 3.2.2. Anti-PDGF-BB-antibody efficiently reduces PDGF-induced matrix contraction

Fig. 3.2.3. The tyrphostin, AG1295, efficiently reduces PDGF-induced matrix contraction

Fig. 3.2.4. The PDGF-pathway inhibitor, Trapidil, efficiently reduces PDGF-induced matrix contraction

Fig. 3.2.5. AG1295 reduces serum-induced matrix contraction

Fig. 3.2.6. Trapidil reduces serum-induced matrix contraction to a similar degree as PDGF-induced contraction

Fig. 3.2.7. The effect of AG1295 on matrix contraction is not due to cellular toxicity

Fig. 3.2.8. Trapidil is toxic to corneal fibroblasts in collagen matrix

Fig. 3.2.9. In corneal fibroblasts, PDGF-BB induces a dramatic actin phenotype: circular ruffles

Fig. 3.2.10. Circular ruffles in corneal fibroblasts contain f-actin and components of the arp2/3 complex

Fig. 3.2.11. PDGF receptors are distributed over the cell surface, and are not arranged in circular structures

Fig. 3.2.12. Circular ruffling is associated with simultaneous retraction and protrusion of cellular processes

Fig. 3.2.13. The incidence of circular ruffles is dose-dependent and plateaus at stimulation with 50ng/ml PDGF

Fig. 3.2.14. Increasing concentrations of PDGF accelerate the appearance of CR

Fig. 3.2.15. Anti-PDGF-BB antibody reduces circular ruffling incidence in corneal fibroblasts after PDGF-BB stimulation

Fig. 3.2.16. The tyrphostin, AG1295, reduces circular ruffling incidence in corneal fibroblasts after PDGF-BB stimulation

Fig. 3.2.17. Trapidil reduces circular ruffling incidence in corneal fibroblasts after PDGF-BB stimulation

Fig. 3.2.18. Microinjection of the WA-domain of Scar or Wasp reduces the incidence of CR

Fig. 3.2.19. Microinjection of WA domain of Scar or Wasp alters CR morphology

Fig. 3.2.20. Myosin light chain kinase inhibition, but not rho kinase inhibition or application of blebbistatin, alters CR morphology

Fig. 3.2.21. Myosin light chain kinase inhibition, but not blebbistatin, reduces CR incidence

Fig. 3.2.22. Myosin light chain kinase inhibition specifically affects CR

Fig. 3.2.23. Combined inhibition of actin polymerization in ruffles and myosin light chain kinase has an additive inhibitory effect on CR incidence

Fig. 3.2.24. Following an initial period of growth factor starvation, PDGF enhances the rate of matrix contraction

Fig. 3.2.25. When stimulated with PDGF, corneal fibroblasts in three-dimensional matrix develop surface protrusions

Fig. 3.2.26. PDGF triggers protrusive and retractile activity in corneal fibroblasts in three-dimensional matrix

Fig. 3.2.27. After PDGF stimulation, cells remodel around 70% of their area every 10 minutes. The dynamic index largely remains stable during the first four hours after stimulation

Fig. 3.2.28. Pre-treatment with Trapidil or AG1295 reduces dynamic activity

Fig. 3.2.29. PDGF-induced matrix contraction is reduced when HCF express Scar-WA

Fig. 3.2.30. MLCK inhibition reduces PDGF-induced matrix contraction

Fig. 3.2.31. Rho-kinase inhibitor and blebbistatin reduce PDGF-induced matrix contraction

Fig. 3.2.32. Myosin inhibition strongly reduces PDGF-BB induced contraction after completion of the initial phase of cell spreading

Fig. 3.2.33. Overexpression of Scar combined with MLCK inhibition results in an additive inhibitory effect on matrix contraction

Fig. 3.2.34. Effect of myosin pathway inhibitors on protrusive activity after PDGF stimulation

Fig. 3.2.35. Rho-kinase inhibitor Y27632 and myosin inhibitor blebbistatin dramatically change protrusion morphology

Fig. 3.2.36. Specific inhibition of the rab5 circular ruffling signalling pathway through transfection with dominant negative plasmids reduces PDGF-induced matrix contraction

Fig. 3.2.37. Specific inhibition of the rab5 circular ruffling signalling pathway through siRNA reduces PDGF-induced matrix contraction

Fig. 3.2.38. Transfection with the RNTre plasmid and RNTre-siRNA transfection do not decrease protrusive activity

Fig. 3.2.39. Transfection with the RNTre plasmid and RNTre-siRNA transfection result in increased number of protrusions per cell

Fig. 3.3.1. Cornea in anterior segment perfusion chamber, which can be mounted onto an upright or an inverted microscope

Fig. 3.3.2. Keratocyte network in corneal stroma

Fig. 3.3.3. GFP-transduced keratocytes and corneal stroma visualised by two-photon excitation microscopy and second harmonic generation

Fig. 3.3.4. Cells and matrix in the conjunctival stroma (two-photon microscopy)

Fig. 3.3.5. Cells and matrix in the conjunctival stroma (confocal laser microscopy)

Fig. 4.1. Elements of the circular ruffling pathway

Fig. 4.2. Effect of all tested inhibitors on protrusive and retractile dynamic activity of corneal fibroblasts after PDGF stimulation

Fig. 4.3. Alternating cycles of protrusion formation, matrix binding, and protrusion retraction with matrix displacement are mediated by actomyosin dynamics

Fig. 4.4. Successful imaging strategies for imaging cells and stroma in whole conjunctiva and cornea

Tables

Table 1.1. Actin isoforms

Table 1.2. Magnitude of measured traction and contraction forces.

Table 2.1. Antibodies used

Table 2.2. Chemical modulators used

Abbreviations

ASMA	Alpha smooth muscle actin
CFM	Culture force monitor
CR	Circular ruffling, circular ruffles
EGF	Epidermal growth factor
GAP	GTPase-activating protein
GEF	GDP-GTP exchange factor
HCF	Human corneal fibroblast(s)
HSF	Human scleral fibroblast(s)
HTF	Human Tenon's fibroblast(s)
MLCK	Myosin light chain kinase
PAK	P21-activated kinase
PDGF	Platelet derived growth factor
ROCK	Rho-associated kinase
SEM	Standard error of the mean
SIM-CFM	Simultaneous imaging and culture force monitoring device
t-CFM	Tensioning culture force monitor
TGF-β	Transforming growth factor β

Chapter 1:

Introduction,

Review of the literature,

Aims

The processes of wound healing and scarring are involved in all severe and blinding eye conditions and can affect any part of the eye: from the surface (corneal and conjunctival scarring after injury, operations or inflammation) to the lens capsule (opacification and contraction after cataract surgery), to deeper structures such as vitreous and retina (proliferative vitreoretinopathy), the orbital fat tissue surrounding the eyeball (thyroid eye disease, socket contraction after removal of the eyeball) and the muscles moving the eye (in inflammatory muscle conditions, or after squint surgery) [Hales et al. 1994; Koumas et al. 2003; Zhao et al. 2004; Fuchshofer et al. 2005; Kirwan et al. 2005]. Currently used interventions to inhibit scarring, such as β-irradiation and cytotoxic agents, can in themselves cause severe complications and blindness [Khaw et al. 1991; Khaw et al. 1992]. Antibodies to growth factors involved in the scarring response have shown promise, but have so far not been more effective than standard treatments [Siriwardena et al. 2002]. Whilst more specific to the treatment of wound healing than cytotoxic drugs, these antibodies still treat a target at the beginning of the cascade of wound healing events. Better understanding of the players downstream of growth factor receptors might facilitate the development of more specific scarring modulators [Dahlmann et al. 2005].

Tissue or matrix contraction is an important component of scarring, and the players involved in contraction might be suitable and specific targets for intervention. However, the cellular mechanisms underlying matrix contraction are not fully understood, and there is a need for investigations into cell behaviour and cell-matrix interaction during contraction. The backbone of dynamic cell activity is the cytoskeleton, and the following section reviews its most active component: actin.

1.1. Cellular mechanisms of connective tissue contraction: actin dynamics versus the "contractile" phenotype

1.1.1. Actin cytoskeleton organisation and functions

Cells need an internal structure to form and maintain their shape and to mechanically interact with their surroundings. The cytoskeleton provides cells with this internal support. There are three main types of cytoskeletal filaments: microtubules, intermediate filaments, and the actin network. Microtubules direct the traffic and positioning of intracellular organelles, and intermediate filaments provide mechanical strength and resistance to shear stress. All dynamic processes related to cell movement, however, require the actin cytoskeleton. In addition, actin filaments determine the shape of the cell's surface, play a role in cell division and endocytosis, and can generate sufficient force to move small beads and bacteria [Cameron et al. 1999; Alberts et al.; Marcy et al. 2004; Paavilainen et al. 2004].

Actin is a 43 KD globular protein which polymerises into helical filaments. Based on slight differences in structure, three main isoforms are distinguished: α, β, and γ. Whilst α-actins are found in muscle cells, β- and γ-actins are cytosolic proteins in non-muscle cells (Table 1).

Class I: non-muscle actins	Class II: muscle actins	Class III: actin-related
Non-muscle (β)	Cardiac (α)	Actin-related proteins
Non-muscle (γ)	Skeletal (α)	
	Smooth muscle (α)	

Table 1.1. Actin isoforms. Modified from [Herman 1993].

The three actin isoforms show >90% amino acid homology. The majority of the heterogeneity is located in the aminoterminal end of the molecule, which is the region interacting with myosin. These slight structural differences translate into different functional roles and subcellular localisation (Fig. 1.1).

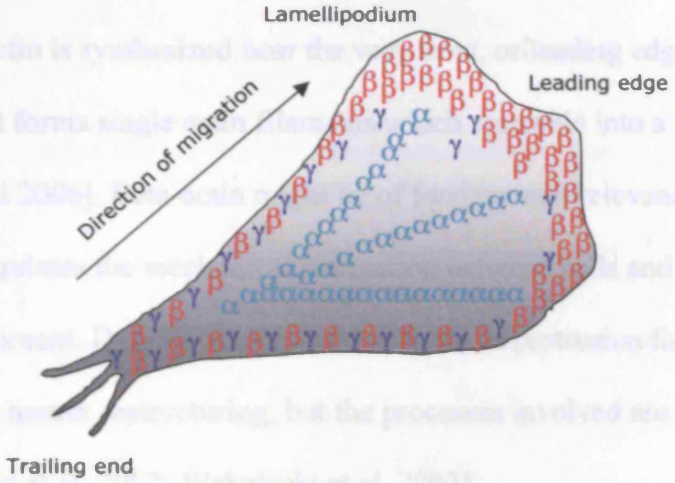

Fig. 2.1. Distribution of actin isoforms in a model cell, after [Herman 1993]. The cell cortex and regions of moving cytoplasm such as lamellipodia contain class I actins (β and γ), whereas contractile bundles such as stress fibres or myofibrils are predominantly composed of class II actins.

The muscle or α-actins are found in skeletal and cardiac myocytes and in vascular smooth muscle cells and pericytes. They are mainly located in stress fibres, contractile intracellular actin bundles. Alpha-actins more easily incorporate into myofibrils than the other actin isoforms, which might explain their affinity for contractile cellular elements [Herman 1993]. In the context of wound healing, scarring and tissue contraction in general, much focus has been placed on the de-novo expression of **alpha smooth muscle actin (ASMA)** by fibroblasts, resulting in a phenotype with enhanced contractile properties, the myofibroblast [Gabbiani et al. 1971]. However, although

myofibroblasts are present in healing and fibrosing tissues, there is no conclusive evidence that these cells are at the origin of tissue contraction, and do not occur as a result of increasing tissue tension.

Beta-actin, on the other hand, is ubiquitously expressed in the cortical cytoplasm of mammalian cells, where it underlies the formation and retraction of all cellular protrusions. Beta-actin is synthesized near the very front, or leading edge, of moving fibroblasts, where it forms single actin filaments which assemble into a fibrous meshwork [Bulinski 2006]. Beta-actin might be of fundamental relevance to contraction, as it regulates the mechanical interaction between cells and their surrounding environment. Dynamic cell behaviour such as protrusion formation is intimately linked to matrix restructuring, but the processes involved are not fully understood [Tamariz et al. 2002; Wakatsuki et al. 2003].

The actin cytoskeleton is a highly dynamic structure which undergoes continuous turnover. The following sections review the basic principles of actin assembly into organised structures, and molecules which regulate actin dynamics.

Actin polymerisation

About half of cellular actin in eukaryotic cells is in momomeric form, called globular or G-actin, whilst the other half is polymerised in filaments. Actin filaments are highly dynamic structures which are continuously broken down into monomers and re-assembled again, allowing cells to rapidly change their shape and orientation in response to external signals (Fig. 1.2).

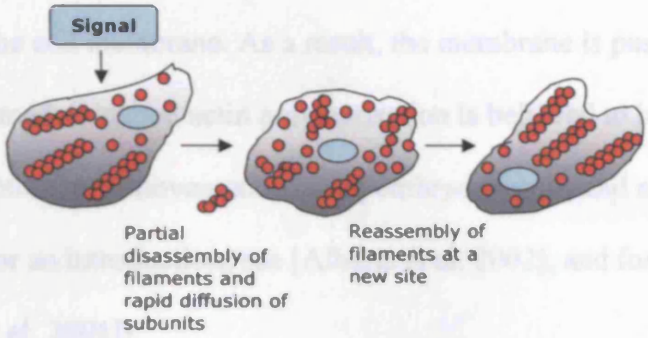

Fig. 1.2. Filament assembly and disassembly in response to extracellular signals. After [Alberts et al. 2002].

Actin filaments are composed of a helix of actin monomers. Monomers are continuously added to one end of the actin filament, called the "plus side" or "barbed end", and other monomers simultaneously disassemble from the other end, called the "minus side" or "pointed end". At steady state, this process is known as "treadmilling" (Fig. 1.3).

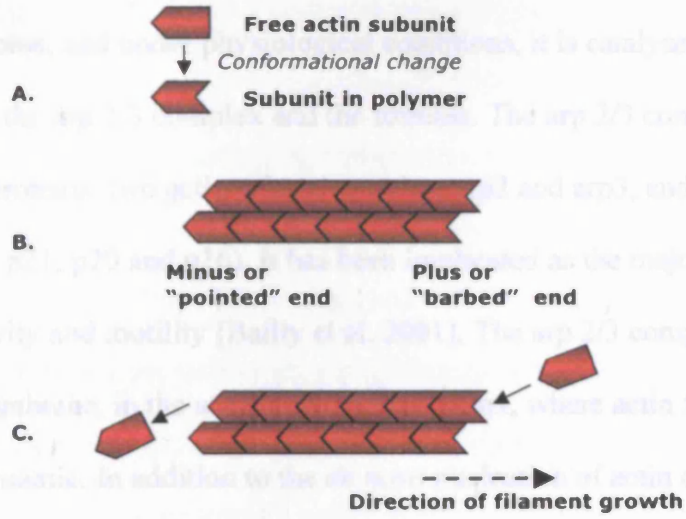

Fig. 1.3. Actin filament elongation and turnover. After [Alberts et al. 2002].

In most physiological situations, actin filaments extend at the barbed end, which is pointing towards the cell membrane. As a result, the membrane is pushed outwards, and protrusions are formed. Directed actin polymerisation is believed to be the driving force behind cell locomotion, cell movements during embryogenesis, and many intracellular transport events (for an introduction, see [Alberts et al. 2002], and for a recent review, see [Paavilainen et al. 2004]).

Actin assembly and disassembly are tightly regulated events, and recent years have seen the characterisation of several initiators and regulators of actin polymerisation, such as the arp2/3 complex and the WASP family of proteins.

The arp2/3 complex mediates actin nucleation

The initial step of actin assembly is the formation of a nucleus or core from three actin monomers. Two actin molecules bind to each other relatively weakly, but addition of a third actin monomer makes the group more stable. Further monomers can be added on, making the initial trimer a nucleus for polymerisation. The assembly of a nucleus is a relatively slow process, and under physiological conditions, it is catalysed by **nucleators** such as the arp 2/3 complex and the formins. The arp 2/3 complex is a complex of seven proteins: two actin-related proteins, arp2 and arp3, and five additional subunits (p41, p34, p21, p20 and p16). It has been implicated as the major catalyst of cell protrusive activity and motility [Bailly et al. 2001]. The arp 2/3 complex is enriched close to the cell membrane, in the actin-rich cellular cortex, where actin filament turnover is most dynamic. In addition to the *de novo* nucleation of actin cores from monomers, the arp 2/3 complex mediates filament growth at the end of existing

filaments and, as it can also attach to the side of existing filaments, creates a branching actin network (Fig. 1.4).

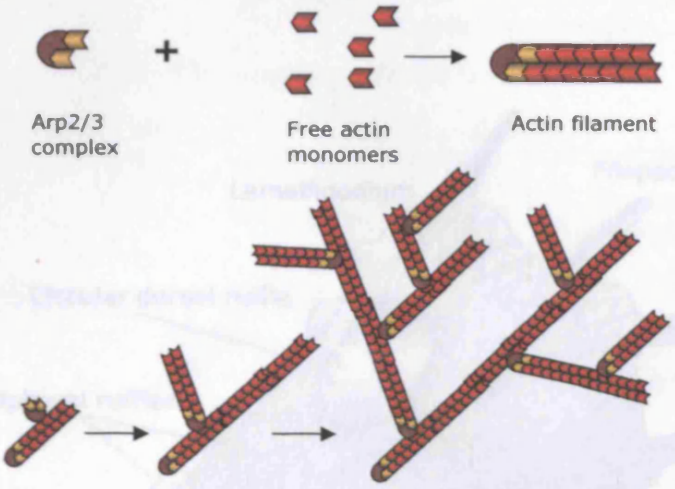

Fig. 1.4. Nucleation and actin filament network formation by the arp 2/3 complex. After [Alberts et al. 2002].

Actin-based cellular structures

Depending on the signalling pathway which activates the polymerisation of actin molecules into filaments and organised structures, distinct surface structures or protrusions are formed. In cells growing on a planar surface, three main types of actin-based protrusions can be distinguished: lamellipodia, filopodia, and ruffles. Lamellipodia are flat, protrusive veils composed of a network of branched actin filaments, which extend parallel to the substratum and are involved in cell motility. Filopodia are thin, finger-like protrusions which contain spiky actin bundles. Ruffles are thin protrusions which contain networked actin filaments and which form elevations perpendicular to the substratum [Small et al. 2002]. There are two types of ruffles: peripheral ruffles, located at the cell edge, and circular ruffles, located on the dorsal cell

surface (Fig. 1.5). When cells are cultured in three-dimensional environments, the distinction between lamellipodia, filopodia, and ruffles is much less clear. In these assays, all cell projections are called "pseudopodia" [Friedl et al. 2000].

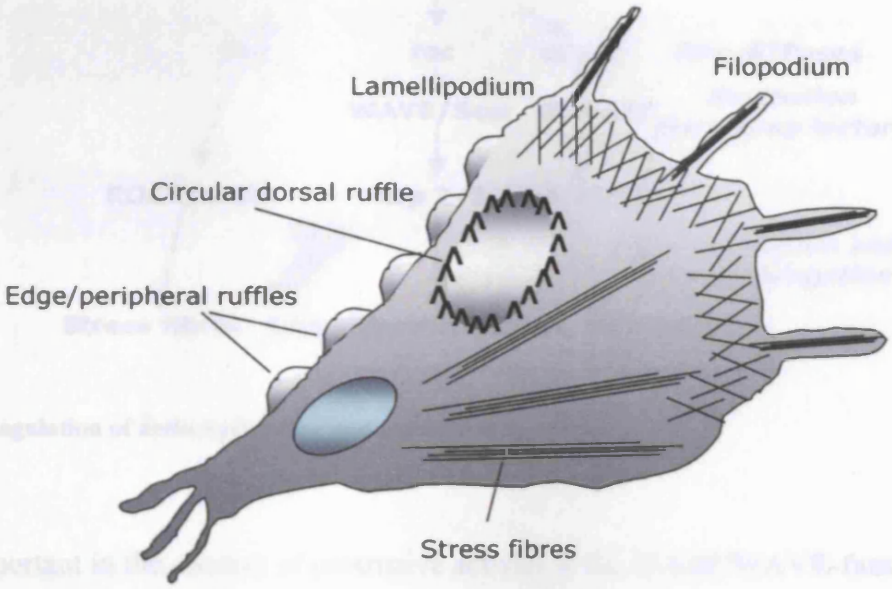

Fig. 1.5. Actin-based cellular structures.

Regulation of protrusion formation

The previous sections have described how, under the control of **nucleators** such as the arp2/3 complex, actin monomers are assembled into filaments, and how filaments are organized into different protrusions. The polymerisation of actin into surface protrusions is under the control of **nucleation promoting factors,** which are required to activate the constitutively inactive arp2/3 complex (Fig. 1.6).

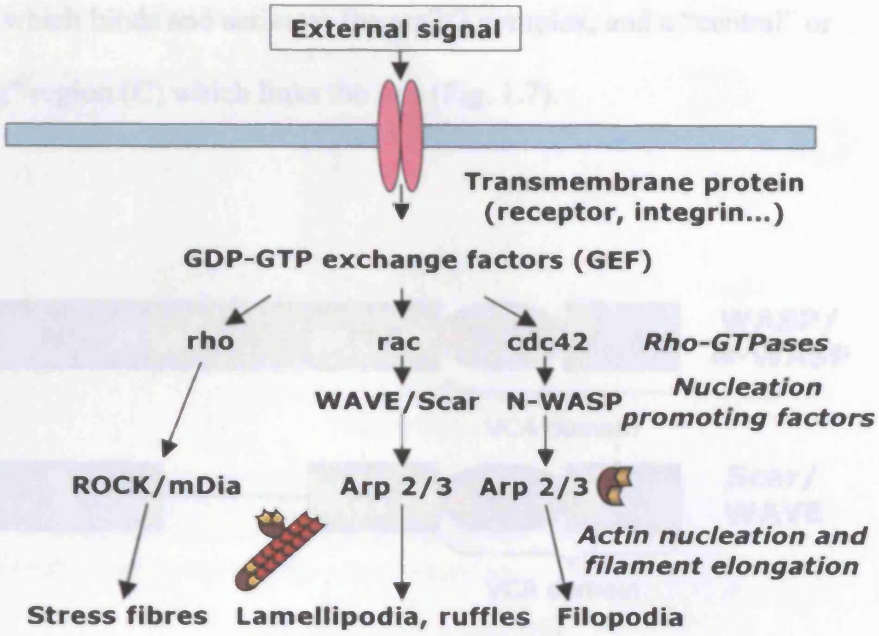

Fig. 1.6. Regulation of actin nucleation and protrusion formation.

Most important in the context of protrusive activity is the **WASP/WAVE-family** of proteins, which comprises 5 members: WASP, N-WASP, and WAVE 1-3, also known as Scar 1-3. Lamellipodia formation is the result of signalling through WAVE/Scar, whilst filopodia result from signalling through N-WASP. In turn, the WASP/WAVE proteins are regulated by a group of enzymes known as the small rho GTPases, whose most prominent members are rac, cdc42, and rho. Rac activates WAVE/Scar, leading to lamellipodia formation, and cdc 42 activates N-WASP, resulting in filopodia formation. However, there is increasing recognition of cross-talk between these signalling pathways [Burridge et al. 2004].

From an investigative point of view, the inhibition of the different players in these signalling cascades allows detailed studies of pathways from external signals to actin polymerisation. An *in vivo* inhibitor of WASP makes use of the binding characteristics of its C-terminal VCA or WA domain, which is composed of a domain homologue to the yeast verprolin protein (V motif or WH2 domain) which binds G actin, an acidic

region (A), which binds and activates the arp2/3 complex, and a "central" or "connecting" region (C) which links the two (Fig. 1.7).

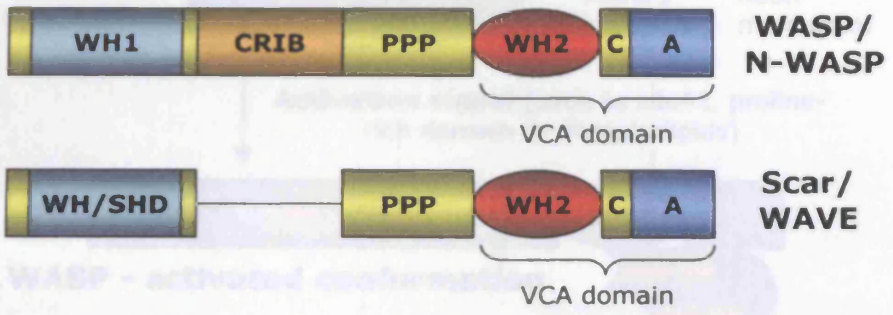

Fig. 1.7. Domain structure of WASP and WAVE/Scar proteins. The N-terminal region of WASP contains a WASP homology (WH)1 domain and a Cdc42- and Rac1-interactive binding (CRIB) region that are important for the regulation of WASP. The C-terminal actin-binding WH2 domain and acidic region (A) promote the interaction of WASP with actin monomers and the arp2/3 complex. PPP: proline-rich domain including SH3 domain binding sites; linking site for a wide range of signaling proteins. VCA or WA domain: WH2 or V motif = homolog to the yeast verprolin protein, followed by a "connecting" or "central" region, and a highly negatively charged, mostly acidic (A) region. The V/WH2 region interacts with actin monomers, while the A motif interacts directly with the arp2/3 complex. The WAVE/Scar proteins lack a GTPase binding site, but can bind to rac indirectly. From [Paavilainen et al. 2004].

In the resting state, the activity of the actin- and arp2/3-binding WA domain is masked by interaction with other domains, resulting in autoinhibition (WASP) or transinhibition (WAVE/Scar). Binding of activated small GTPases (Cdc 42 for WASP or Rac for Scar) or phospholipids releases this inhibition (Fig. 1.8).

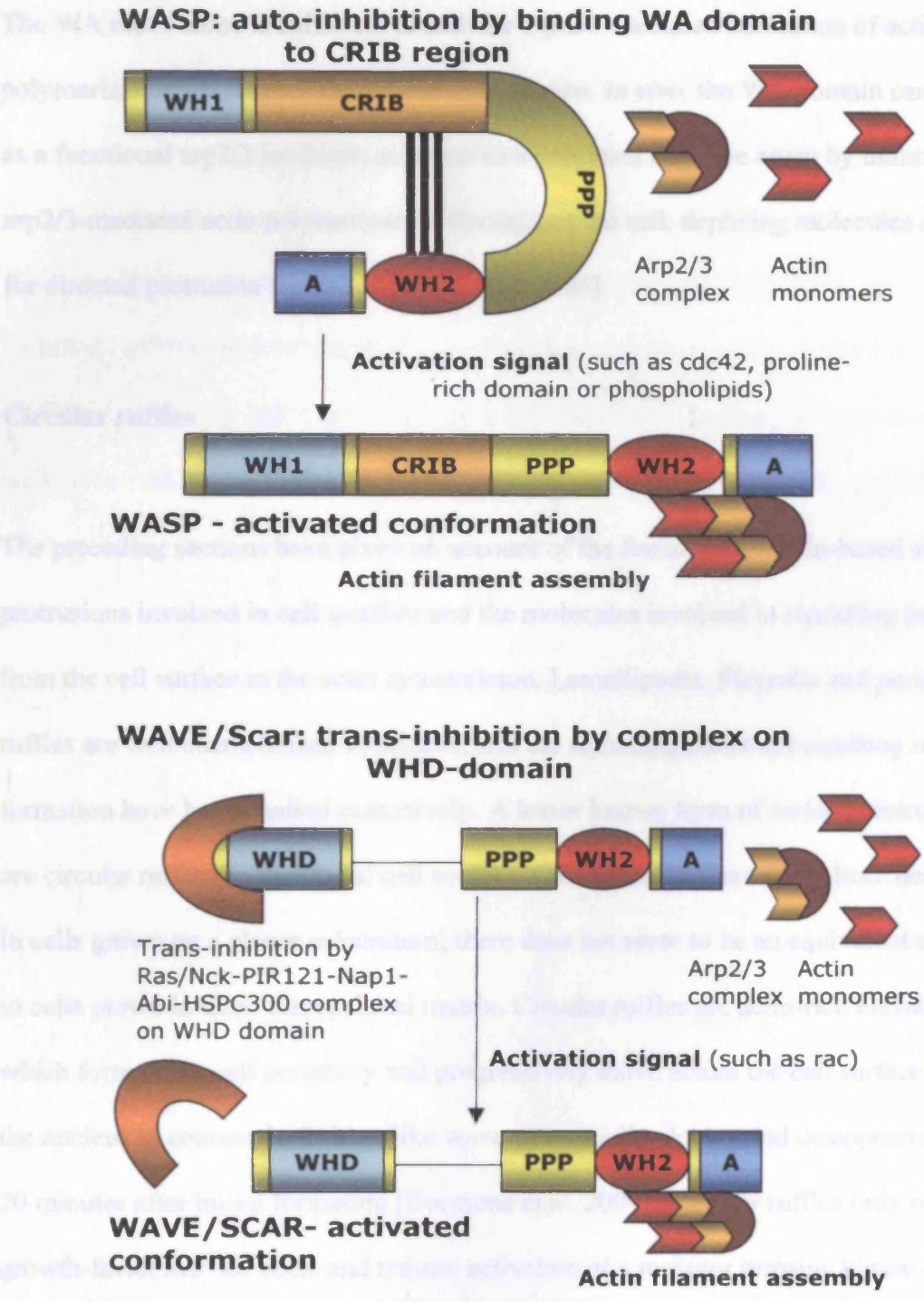

Fig. 1.8. Auto- and trans-inhibitory conformation and activation of WASP (top) and WAVE/Scar (bottom) proteins. Modified from [Paavilainen et al. 2004].

The WA motif alone is sufficient to activate arp 2/3-mediated nucleation of actin polymerization and branching of filaments *in vitro*. *In vivo*, the WA domain can be used as a functional arp2/3 inhibitor, as it acts as a dominant negative agent by inducing arp2/3-mediated actin polymerization throughout the cell, depleting molecules available for directed protrusion formation [Shao et al. 2006].

Circular ruffles

The preceding sections have given an account of the formation of actin-based surface protrusions involved in cell motility and the molecules involved in signalling pathways from the cell surface to the actin cytoskeleton. Lamellipodia, filopodia and peripheral ruffles are well characterised structures, and the signalling pathways resulting in their formation have been studied extensively. A lesser known form of surface protrusions are circular ruffles on the dorsal cell surface. Circular ruffles have only been described in cells grown on a planar substratum; there does not seem to be an equivalent structure in cells grown in three-dimensional matrix. Circular ruffles are actin-rich elevations which form in the cell periphery and progressively move across the cell surface towards the nucleus in concentric fashion like waves, eventually closing and disappearing about 20 minutes after initial formation [Buccione et al. 2004]. Circular ruffles only occur in growth-factor starved cells, and require activation of a receptor tyrosine kinase (RTK) [Lanzetti et al. 2004]. Members of the tyrosine kinase receptor family include the epidermal growth factor (EGF) receptor, the insulin and insulin-like-growth factor (IGF) receptors, the macrophage-colony-stimulating factor (M-CSF) receptor, fibroblast growth factor (FGF) receptors, the hepatocyte growth factor (HGF) receptor, the vascular endothelial growth factor (VEGF) receptor, and the β-isoform of the platelet

derived growth factor (PDGF) receptors. Circular ruffling has been described after stimulation of any of these receptors, albeit in different cell types.

Most recent investigations have studied this phenomenon in mouse embryonic and human fibroblasts stimulated by PDGF-BB [Lanzetti et al. 2004; Su et al. 2005]. PDGF is a potent mitogen and chemoattractant. PDGF receptors are a family of dimers of two identical or different subunits (Fig. 1.9). The best studied members of this family are the PDGF-αα, -αβ, and -ββ type receptors. Whilst all of these induce cell migration and peripheral ruffling, only the ββ-receptor stimulates the formation of circular ruffles. During wound healing and inflammation, the PDGF-β receptor is upregulated in fibroblasts and blood vessels. In tumour cells, PDGF-β receptor-mediated signalling acts in a paracrine fashion, regulating cell growth and proliferation [Mellstrom et al. 1988; Arvidsson et al. 1992; Wennstrom et al. 1992; Heldin 1997; Heldin et al. 1999; Hooshmand-Rad et al. 2000; Anton et al. 2003; Funa et al. 2003].

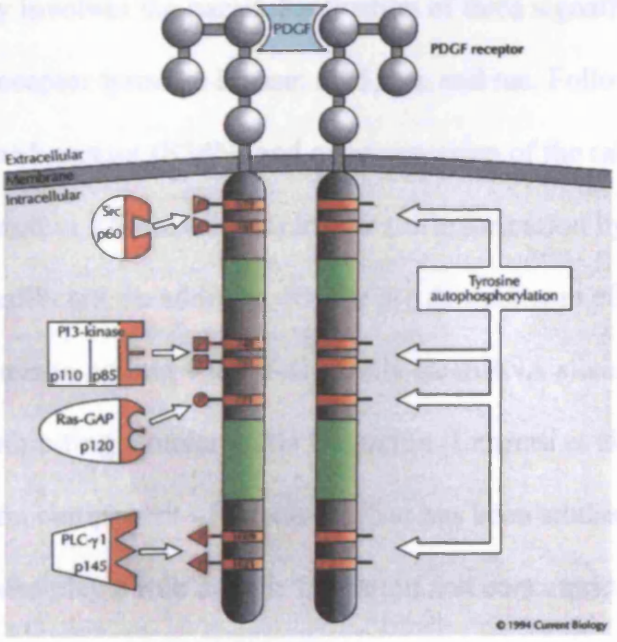

Fig. 1.9. The PDGF-receptor. From [Wennstrom et al. 1994].

An intriguing feature of circular ruffles is that they only occur once after growth factor stimulation, whereas peripheral ruffling continues. The switch which prevents further circular ruffling is not known, although several autoregulatory negative feedback mechanisms which effectively downregulate PDGF receptor activity after growth factor binding have been described [Funa et al. 2003].

The presence of several distinct proteins has been demonstrated in circular ruffles: rac, WAVE1, p21-activated kinase 1 (PAK1), arp2/3, dynamin and cortactin [Dharmawardhane et al. 1997; Heldin 1997; Hooshmand-Rad et al. 2000; McNiven et al. 2000; Anton et al. 2003; Krueger et al. 2003; Suetsugu et al. 2003].

Recently, a specific signalling pathway has been uncovered, which critically involves the activation of a small GTPase initially described in the context of endocytosis, but later found to have a direct effect on actin remodelling in lamellipodia formation and migration in NIH3T3 fibroblasts: **rab5** (Fig. 1.11) [Lanzetti et al. 2001; Lanzetti et al. 2004]. This pathway involves the parallel activation of three signalling cascades downstream of the receptor tyrosine kinase: rab5, ras, and rac. Following this model, a dominant negative rab5 mutant (S34N) and overexpression of the rab5-specific GTPase-activating protein RN-tre inhibit circular ruffle formation by PDGF, but leave peripheral ruffles unaffected. In addition, RN-tre is a downstream effector of rab5 in this pathway, and binds to actinin 4 and f-actin. RN-tre mRNA silencing is another specific method of inhibiting circular ruffle formation [Lanzetti et al. 2004].

To date, only the actin component of circular ruffles has been studied in depth. However, myosins also play a role in their formation and concentric closure, as the use of a myosin II inhibitor impairs circular ruffle co-ordination [Araki et al. 2003].

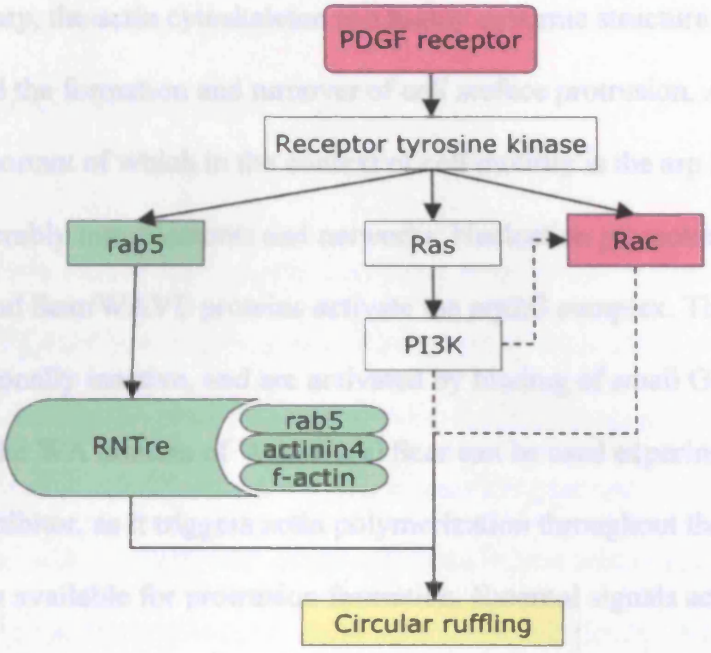

Fig. 1.10. Molecules critically required for circular ruffling.

The physiological significance of circular ruffling is unknown. A functional role in endocytosis, and more specifically macropinocytosis, has been suggested [Dowrick et al. 1993; Swanson et al. 1995; Araki et al. 2000]. Macropinocytosis is a route for uptake of solute macromolecules, but might also be involved in directed cell movement. It allows cells to rapidly internalise large areas of plasma membrane and to re-direct them to the leading edge of the cell, thereby contributing to the membrane flow required for cell movement [Bretscher 1996; Bretscher et al. 1998]. The matrix-degrading enzyme MMP-2 co-localises with WAVE1 in circular ruffles, which might be another indicator for a possible role of the circular ruffling pathway in cell migration. However, whilst MMP-inhibition reduces WAVE1-dependent cell migration through matrix by 70%, it does not inhibit ruffle formation [Suetsugu et al. 2003]. Apart from macropinocytosis and cell migration, another possible functional context of circular ruffling might be receptor internalisation after ligand binding [Dowrick et al. 1993; Suetsugu et al. 2003; Buccione et al. 2004].

In summary, the actin cytoskeleton is a highly dynamic structure which mediates cell shape and the formation and turnover of cell surface protrusion. Actin nucleators, the most important of which in the context of cell motility is the arp 2/3 complex, regulate actin assembly into filaments and networks. Nucleation promoting factors such as WASP and Scar/WAVE proteins activate the arp2/3 complex. These proteins are constitutionally inactive, and are activated by binding of small GTPases such as rac and cdc 42. The WA domain of WASP and Scar can be used experimentally as a functional arp2/3 inhibitor, as it triggers actin polymerization throughout the cell and depletes molecules available for protrusion formation. External signals activate rac, cdc 42 and rho, and induce the formation of actin-based surface protrusions via the above pathways.

In some cells, activation of a tyrosine kinase receptor through binding of specific growth factors such as PDGF triggers the formation of a special type of surface protrusion, circular ruffles. In addition to the signalling molecules involved in other ruffling activities, the circular ruffling pathway critically involves activation of the small GTPase, rab5. The functional role of this pathway is not known; macropinocytosis, cell migration and receptor internalization and recycling have been suggested.

Both actin-based cell surface protrusions and actin-based structures in the centre of the cell such as stress fibres are involved in cell-matrix interaction and in particular in the creation of a mechanical continuum between cells and their environment. In the context of wound healing and scarring, the generation of contractile force by cells is of particular interest and is discussed in the following sections.

1.1.2. Actin-based force generation: actin filament elongation versus actin-myosin interaction

Cells use two mechanisms to generate force, both of which require actin [Fehrenbacher et al. 2003]. Firstly, elongating filaments generate force which pushes the cell membrane outwards, resulting in protrusion formation required for cell movement [Condeelis et al. 1984]. This actin polymerisation generates sufficient force to move micrometer-sized polystyrene beads and intracellular bacteria [Cameron et al. 1999]. The second mechanism is based on actin-myosin interaction. Bipolar myosin II filaments associate with actin filaments to form contractile bundles at different locations throughout the cell (Fig. 1.11) [Small et al. 2005]. Myosin activation results in traction on actin filaments and generation of force.

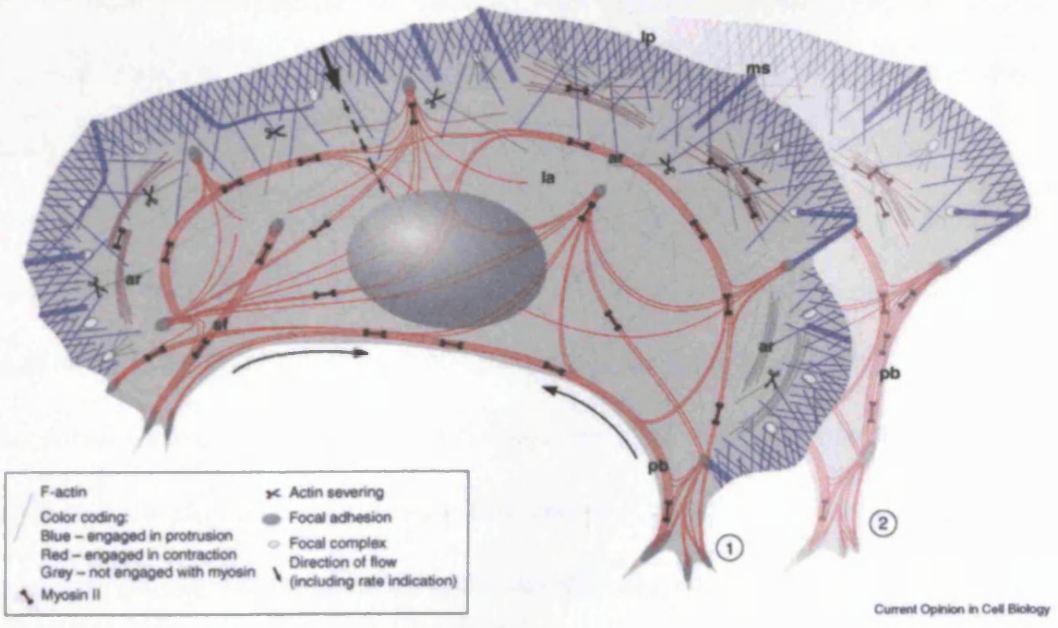

Fig. 1.11. Schematic illustration of the actin cytoskeleton in a migrating B16 melanoma cell.

Contractile assemblies with myosin: arcs (ar), stress fibers (sf) and peripheral bundles (pb). From [Small et al. 2005].

Amongst the different types of contractile actomyosin bundles, stress fibres are particularly relevant to matrix contraction activities. Stress fibres allow cells to generate tension internally in response to extracellular signals, and also to transmit cell tension onto their environment. At the base of lamellipodia in cells in planar culture, and within cellular protrusions in three-dimensional matrix, myosin II is also involved in cellular „probing" of the mechanical conditions of the environment: minute rearward actomyosin-based contractions inform the cell about substrate rigidity and are essential for dynamic protrusion behaviour [Giannone et al. 2004]. Lastly, in migrating cells, myosin located at the rear of the cell pulls the trailing end in, pushing the cell forward [Alberts et al. 2002].

1.1.3. Actin dynamics in matrix contraction

As described in the preceding sections, cells use the actin machinery to form protrusions to interact with their environment. Protrusion dynamics are commonly studied in the context of cell migration or "locomotion". Actin polymerisation in protrusive activity generates sufficient force to drive cell motility [Condeelis et al. 1984]. Cells exert force onto their environment, and when they are grown on or in deformable substrates, such as sheets of soft silicone or collagen, the force deforms the matrix, resulting in wrinkling of silicone and alignment of collagen fibres in tight bundles or straps [Harris et al. 1980; Harris et al. 1981]. When associated with cell migration, the matrix deflections are transient. However, when the tractional force is sustained, it results in progressive pulling of the matrix towards the cell and permanent **matrix contraction.** Whilst actin polymerisation has been shown to generate sufficient force to drive cell protrusive activity, there is debate whether it is sufficient to induce matrix contraction. Early histological work on healing wounds indicated the presence of a special, contractile fibroblast phenotype, the myofibroblast, whose main characteristic is the *de novo* expression of α-smooth muscle actin [Gabbiani et al. 1971; Majno et al. 1971]. To date, most studies on matrix contraction have concentrated on the myofibroblast, whilst tractional matrix structuring associated with protrusive activity, which is driven mainly by β-actin dynamics, has received less attention. The following section describes the evidence for matrix restructuring involving the „protrusion" or „locomotion" machinery.

a) Pulling whilst moving: the locomotion concept of tractional structuring

The paradigm of wound healing is the closure of a skin wound, which involves the migration of fibroblasts from adjacent, intact tissue into the wound bed. In 1979, Bell et al. introduced a three-dimensional *in vitro* model of wound healing: the fibroblast-populated collagen lattice, which allows the study of contraction and fibroblast behaviour in a pseudo-physiological environment [Bell et al. 1979]. In brief, liquid collagen is added to a suspension of trypsinised fibroblasts; when the pH of the solution is neutralised, the collagen polymerises, with the fibroblasts dispersed throughout the resulting gel-like matrix. Initially rounded up, the embedded fibroblasts spread out extensions and establish themselves in the matrix. During this process, they pull on the surrounding matrix, generating sufficient force to bend individual collagen fibres bound to their surface [Lee et al. 1999]. Initially only collagen fibres in the immediate vicinity of cells are moved, but as fibres are linked, the tractional forces are subsequently propagated throughout the matrix, resulting in global remodelling [Grinnell et al. 1984; Guidry et al. 1987]. However, it is unclear whether these tractional forces might be sufficient to induce *in vivo* wound closure as well as *in vitro* matrix contraction [Ehrlich et al. 1990].

The pathways involved in protrusion formation are the same in two- and three-dimensional culture conditions, but the resulting cellular phenotypes differ. In three-dimensional matrix, all cell protrusions are called „pseudopodia" [Friedl et al. 2000]. Fibroblasts migrating through a three-dimensional collagen matrix form new pseudopodia at the front of the cell, which become anchored to matrix fibres at focal adhesions sites. When protrusions are retracted, fibres are pulled towards the cell. The retraction of protrusions with fibre displacement requires both cortical β-actin and

myosin II. In a simplified two-dimensional assay of lamellipodia binding to loose, individual matrix fibres, the process of lamellipodium retraction with fibre displacement involves cell-matrix attachment via $\alpha_2\beta_1$ integrin and cyclic myosin II-B assembly and contraction within the lamellipodium. In the more complex three-dimensional collagen matrix assay, myosin IIB is localised in the cell periphery, particularly along collagen fibre contacts of the cell protrusions, suggesting a similar mechanism of protrusion-mediated matrix remodeling [Meshel et al. 2005].

b) Traction without migration: using the locomotion machinery for contraction

The classic locomotion theory of matrix contraction states that protrusion formation serves cell migration and induces matrix contraction as a side-effect. However, there is some evidence that matrix contraction can occur without cell migration, and that the same mechanisms are involved. When cell protrusions which are symetrically anchored to matrix contract, matrix fibres are drawn towards the cell whilst the cell itself remains stationary [Sawhney et al. 2004]. In a different assay with clusters of fibroblasts planted on top of a collagen layer, the matrix fibres become aligned along the axis between the cell clusters, resulting in the formation of a dense collagen „strap". The movement of individual fibres on the axis between the cell clusters is small, but the collagen fibres on both sides of this axis are pulled towards the strap over large distances and at considerable speed, as traction forces are transmitted across the collagen network and amplified in the direction orthogonal to the strap axis. The cell behaviour generating force and inducing its „orthogonal amplification" is not migration, but the extension and spreading of protrusions [Sawhney et al. 2002]. Chemical agents that lead to actin filament disassembly or block myosin activity inhibit strap formation, indicating that

the players involved in migration are also at the basis of traction without migration [Sawhney et al. 2004].

The same link between force development and spreading morphology has been observed in fibroblasts contracting a collagen-glycosaminoglycan matrix, where matrix deformation and force development are associated with cell elongation after trypsinisation, but not migration [Freyman et al. 2001].

The binding of cell protrusions to matrix fibres depends on the presence of growth factors. In the absence of these, fibroblasts in collagen matrix still display continuous protrusion and retraction of cell processes, but fibre binding and dislocation only occur when growth factors such as PDGF or lysophosphatidic acid (LPA) are present in the medium [Tamariz et al. 2002; Wozniak et al. 2004].

The preceding paragraphs summarise available evidence that protrusion dynamics involving cortical β-actin and myosin II in conjunction with cell-matrix binding can generate sufficient force to displace matrix fibres. However, the field of matrix contraction studies is dominated by investigations into α-smooth muscle actin expressing myofibroblasts. The following section reviews the evidence in favour of an essential role of myofibroblast transformation in the generation of matrix contraction forces.

c) Tissue contraction by a contractile fibroblast phenotype: the myofibroblast

Work on matrix contraction by myofibroblasts began with Gabbiani's description, in 1971, of modified fibroblasts with smooth-muscle like features in an experimental animal model of wound healing. He suggested that these cells, characterised by an irregular nucleus, densely packed cytoplasmic fibrils, and numerous sites of attachment with the extracellular matrix (fibronexus), are responsible for the contraction of granulation tissue during skin healing [Gabbiani et al. 1971; Majno et al. 1971]. Subsequently, these modified fibroblasts were also found in pathological connective tissue conditions, such as fibrosis of parenchymal organs, fibromatosis, and stromal reaction to tumours [Gabbiani 1992]. Today, the presence of α-smooth muscle actin (ASMA) in stress fibres is considered to be the main defining characteristic of this cell, named „myofibroblast" by Gabbiani's group [Gabbiani et al. 1971; Skalli et al. 1986; Benzonana et al. 1988; Darby et al. 1990].

For long, the *in vitro* induction of the myofibroblast phenotype was difficult to achieve, as it requires special culture conditions. A subpopulation of fibroblasts cultured in medium with serum expresses ASMA, but reproducible enhancement of ASMA expression *in vitro* was first achieved 22 years after Gabbiani's original paper [Desmouliere et al. 1992]. The first identified substance to enhance ASMA expression was heparin, but the effect was only observed in dividing fibroblasts [Desmouliere et al. 1992]. Later, transforming growth factor β (TGF-β) was found to reproducibly induce myofibroblast transformation even of quiescent fibroblasts *in vitro* [Desmouliere et al. 1993]. Further work demonstrated that in addition to TGF-β, two other factors are required: tension and time. The usual timespan from TGF-β stimulation to demonstration of ASMA incorporation into stress fibres is 72 hours, although mRNA

expression presumably occurs much earlier [Desmouliere et al. 1993; Serini et al. 1998]. To induce ASMA expression, cells also need to be exposed to mechanical tension by growing either on rigid substrata or in restrained or non-compliant collagen matrices [Mochitate et al. 1991; Tomasek et al. 1992; Arora et al. 1994; Grinnell et al. 1999]. Both ordinary fibroblasts and myofibroblasts exert tractional forces onto the surrounding matrix [Majno et al. 1971; Harris et al. 1980; Harris et al. 1981; Arora et al. 1994]. However, some authors consider contraction proper to start only when increasing stiffness and tension in the matrix have induced myofibroblast transformation [Hinz et al. 2001; Tomasek et al. 2002]. On the other side, both *in vitro* collagen matrix contraction and early *in vivo* wound closure proceed in the absence of tissue rigidity and myofibroblasts, casting doubt on their indispensability [Ehrlich et al. 1990; Grinnell 1994].

One aspect of cell-matrix interaction and contraction important for this debate is the magnitude of the generated force. The measurement of the minute forces produced by individual cells or populations of cells poses great technical challenges. The following section gives a summary of traction force measurements obtained by different techniques.

1.1.4. Measurements of traction and contraction forces

Different methods have been used to quantify the force cells generate and transmit onto their surrounding matrix. Most experimental devices measure the deformation of matrix, which reflects the **strain** cells exert onto a substratum or matrix *in vitro*.
The net tractional forces measured are minute, and differ greatly depending on the setup used for measurements. Two units are commonly used to describe cell-generated forces, newton and dyne, with 1 dyne = 10^{-5}N (Table 1.2). A single-cell assay studying keratocytes migrating on top of a collagen layer reported that the highest traction force was generated in the equatorial region of cells, and amounted to $2x10^{-8}$N or 20 nanonewton (nN) [Lee et al. 1994]. Similarly, actively invading cancer cells generate approximately 2nN per cell, with a peak of 10-20nN for short periods in the most actively invading cells [Wyckoff et al. 2006]. The force generated purely at the leading edge and used to propel fibroblasts forward during migration on a collagen layer is much greater, in the order of 0.2 dyne or 2 micronewton [Dembo et al. 1999].
Measurement of forces in three-dimensional matrix is more complex, as individual cells are difficult to probe. One approach is to measure the overall strain exerted by a population of cells embedded in matrix. Culture force monitors detect the deflection of a force transducer probe when matrix is contracted, and measure the strain along one axis of matrix contraction. Strain measurements obtained by culture force monitors are orders of magnitude smaller than forces measured in individual cell assays. There are two main reasons for this. Firstly, only uniaxial strain is measured, along the axis perpendicular to the deflection of the force transducer probe, whilst strain in other axes is ignored. Secondly, forces of opposite direction along the measurement axis, such as during traction on fibres on one side of a cell with simultaneous relaxation on the other

side, can cancel each other out, as only the overall sum of strain is measured. Values of 30-60 dyne per million cells (0.3 to 0.6 nN per cell) have been reported for skin fibroblasts [Eastwood et al. 1994; Zhang et al. 2006].

Assay	Newton	Dyne
Single-cell assay, keratocytes migrating on top of a collagen layer [Lee et al. 1994]	$2x10^{-8}$N (20 nN) per cell	20 dyne per cell
Fibroblasts migrating on a collagen layer [Dembo et al. 1999]	$2x10^{-6}$N (2000 nN) per cell	0.2 dyne in equatorial region of cell
Uniaxial strain exerted on 3D collagen matrix by skin fibroblasts [Eastwood et al. 1994]	$4\text{-}6x10^{-10}$N (0.4-0.6 nN) per cell	40-60 dyne per million cells
Uniaxial strain exerted on 3D collagen matrix by skin fibroblasts [Zhang et al. 2006]	$3x10^{-10}$N (0.3 nN) per cell	30 dyne per million cells

Table 1.2. Magnitude of measured traction and contraction forces.

Culture force monitors have been used to measure the strain exerted by fibroblasts in response to external stimuli such as growth factors, and to test the influence of other factors such as matrix adhesion formation and matrix rigidity.

Different growth factors induce characteristic profiles of force generation: following growth factor starvation, the addition of serum or LPA to the medium induces an immediate, intense increase in force by around 80 to 90 dyne/million cells (0.8 to 0.9

nN per cell). PDGF induces a slower and less intense increase of 30 dyne/million cells (0.3 nM per cell). The molecular mechanisms underlying these differences are not clear [Kolodney et al. 1993].

Previous sections have described the association between force generation and the extension and spreading of cells after trypsinisation. The matrix-deflecting force generated by spread cells flattened against a planar surface is in the range of 20-40 nN per cell, depending on cell surface area [Tan et al. 2003]. In a three-dimensional collagen matrix, culture force monitors demonstrate that spreading activity is associated with force development, but the dynamic link between cell morphology and force generation has not been established [Eastwood et al. 1996].

In summary, actin-based protrusive cellular activity has been shown to generate force that can be transmitted to surrounding matrix. Protrusion formation is based on β-actin dynamics in the cell periphery, but the expression of α-smooth muscle actin in the cell centre of myofibroblasts might enhance contractility. Actomyosin interaction in cell protrusions has been connected to matrix fibre displacement. Force generation is increased in the presence of growth factors, and is likely to involve signalling pathways from growth factor receptors to the actin cytoskeleton. The following section reviews our knowledge about the growth factor signalling pathways involved in matrix contraction.

1.2. Growth factor signalling pathways in contraction

Growth factors are critical modulators of the wound healing response. Following injury, growth factors such as TGF-β, PDGF and LPA are released into the wound by injured cells, from storage places in the matrix, and by chemotactically attracted cells [Clark et al. 1989; Gullberg et al. 1990; Tingstrom et al. 1992]. Amongst these numerous growth factors, most attention has focussed on TGF-β, as it plays a key role in myofibroblast transformation with subsequent tissue contraction and new matrix deposition. Part of the signalling pathway from TGF-β receptor to ASMA expression has been identified [Lee et al. 2000].

However, much less is known about the role of the other growth factors such as PDGF or LPA in wound healing and tissue contraction. In particular, the role of LPA in wound healing *in vivo* is unclear. The following review focuses on PDGF pathways, which are known to be of considerable importance *in vivo*.

PDGF is well known to be involved in the immediate response to injury. Its best known contribution follows its release from storage in circulating platelets in the cascade leading to effective haemostasis after vascular injuries. Extracellular locations such as the corneal epithelial basement membrane also store PDGF. Injuries to the basement membrane release PDGF, activating local wound healing response cascades.
In vitro, PDGF induces the contraction of collagen matrices by fibroblasts. Dermal fibroblasts grown in collagen matrix and stimulated by PDGF form cell protrusions and establish a network of dendritic cells, but the mechanism by which this cellular network effects tissue contraction is not known [Tamariz et al. 2002; Grinnell et al. 2003]. PDGF

does not induce ASMA expression nor myofibroblast transformation [Rubbia-Brandt et al. 1991; Desmouliere et al. 1992]. However, it has an immediate effect on actin cytoskeleton re-arrangement and induces the formation of lamellipodia, filopodia and ruffles. The signalling pathways begin with activation of the rho GTPases, rac and cdc 42, which have traditionally been associated with a decrease in cell contractility in favour of protrusive activity and cell migration (Fig. 1.12). P21-activated kinase 1 (PAK) and ruffling activity are essential for matrix contraction, but the pathway leading to cell contractility is unknown [Rhee et al. 2006].

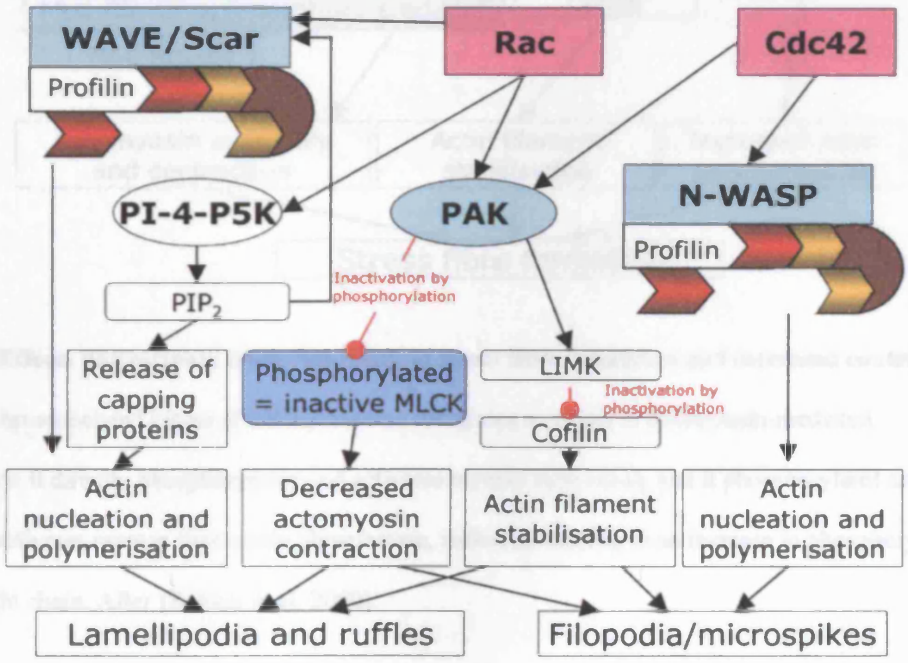

Fig. 1.12. Effects downstream from rac and cdc42 result in lamellipodia, ruffle, and filopodia formation, and in decreased actomyosin contractility. Note that through p21-activated kinase 1 (PAK), both rac and cdc42 activation result in phosphorylation and inactivation of myosin light chain kinase (MLCK), leading to a reduction in active, phosphorylated myosin light chain and cell contractility. After [Bishop et al. 2000].

PDGF-induced matrix contraction is difficult to explain, as contractile actomyosin assembly is mediated through the third classic rho GTPase, rho (Fig. 1.13). Although PDGF activates rac and cdc 42, but not rho, PDGF-induced matrix contraction is rho, ROCK and myosin II dependent [Abe et al. 2003; Lee et al. 2003].

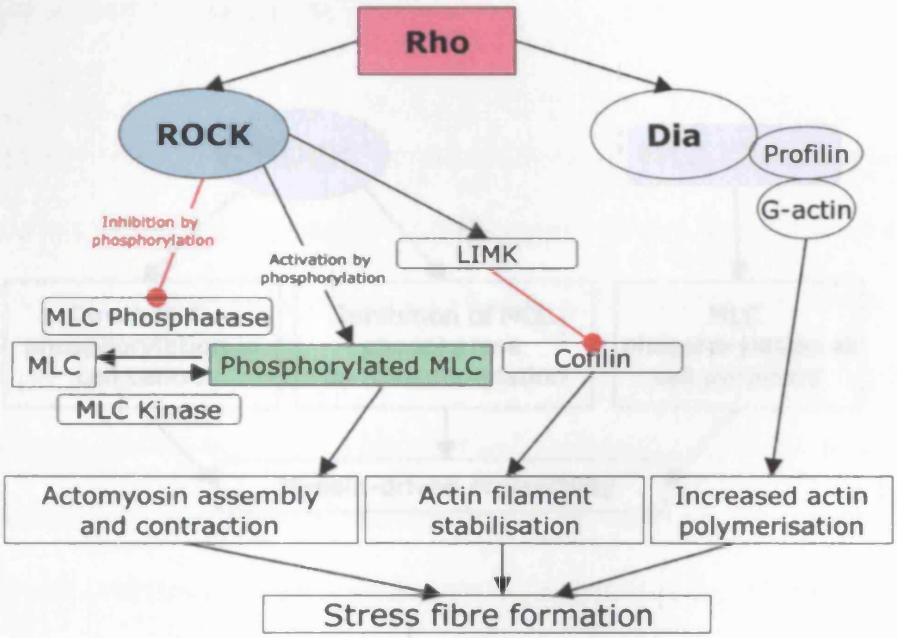

Fig. 1.13. Effects downstream from rho result in stress fibre formation and increased contractility. Note that rho-associated kinase (ROCK) has two substrates involved in actomyosin-mediated contractility: it directly phosphorylates and activates myosin light chain, and it phosphorylates and thereby inactivates myosin light chain phosphatase, indirectly leading to an increase in phosphorylated myosin light chain. After [Bishop et al. 2000].

There is some crosstalk between the signalling pathways, and rac can activate rho in growth-factor starved cells. In this situation, PDGF activates rac, inducing rapid formation of membrane ruffles, followed by weak rho-mediated stress fibre formation [Ridley et al. 1992; Ridley et al. 1992]. Another potential path to PDGF-induced rho activation might be the co-operation between PDGF receptor and integrin signalling: PDGF stimulation induces $\alpha_2\beta_1$ integrin expression on protrusions, and integrins can

activate rho signalling [Barry et al. 1997; Ahlen et al. 2004; Huang et al. 2005]. A third possible explanation is the localised activation of rho-dependent contraction events in cell protrusions. Myosin light chain phosphorylation in the cell periphery and in protrusions depends on myosin light chain kinase activity (Fig. 1.14).

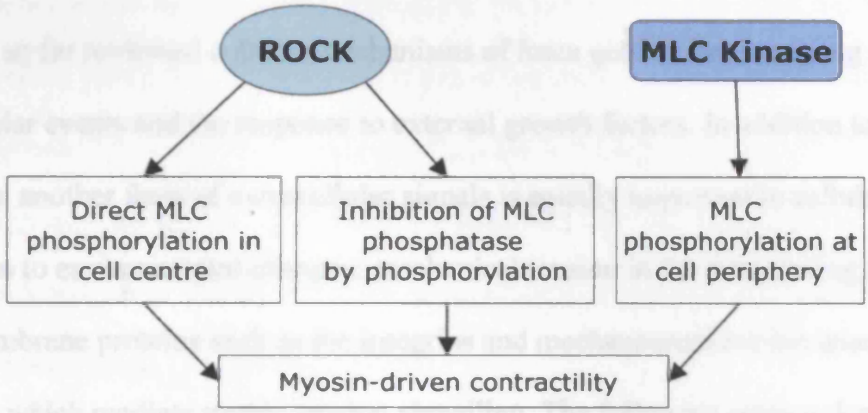

Fig. 1.14. Myosin-driven contractility is mediated through different pathways in cell centre and periphery.

Recently, actomyosin co-operation has been reported to occur in lamellipodia in migrating cells, in the form of periodic contractions during lamellipodia extension. These contractions generate waves of actin-bound α-actinin and MLCK, which activate myosin II at the base of the lamellipodium, causing contraction. Wave formation depends on MLCK, but not ROCK, which is consistent with previous findings about MLCK phosphorylating myosin light chain in the cell periphery [Giannone et al. 2004].

In summary, the PDGF signalling pathway involved in matrix contraction is only partially known. P21-activated kinase 1 (PAK) is essential for ruffling activities and matrix contraction. However, PDGF-mediated matrix contraction is rho, ROCK and myosin II dependent, and the link between PDGF receptor or PAK and these contractility mediators is unknown.

We have so far reviewed cellular mechanisms of force generation, focussing on intracellular events and the response to external growth factors. In addition to soluble cytokines, another form of extracellular signals is equally important in cellular adaptation to environmental changes: mechanical tension in the surrounding matrix. Transmembrane proteins such as the integrins and mechanosensitive ion channels act as receptors which mediate matrix tension signalling. The following section describes these important interfaces between cell and matrix and how their activation can affect the state of the cell.

1.3. Matrix and Tension

The transmission of tension from the cell onto the matrix is a prerequisite for matrix remodelling. Cell-matrix interaction occurs at specialised points of contact between cell protrusions and matrix. These contact points are dynamic structures which depend on tension in the matrix as well as the presence of growth factors and other molecules. Cells use these points of adhesion both to sense the tension in their environment and to transmit intracellular tension onto the matrix. Matrix rigidity influences cell morphology and growth, and cells bring the tension within their surrounding environment to a level characteristic for each cell type, a phenomenon known as tensional homeostasis [Brown et al. 1998].

1.3.1. Connection between the cytoskeleton and matrix: transmembrane protein complexes transmit force

Transmembrane proteins such as mechanosensitive ion channels, integrins and focal adhesions transmit forces in both directions between extracellular matrix and intracellular cytoskeleton and other proteins.

Integrins are a direct link between extracellular matrix fibrils and the cytoskeleton (for a review see [Hynes 1992]). Integrin activation initiates both immediate and long-term cellular responses, such as actin remodeling and alteration of gene expression [Lygoe et al. 2004]. Integrin engagement is involved in focal adhesion and stress fibre formation, myofibroblast transformation, downregulation of collagen expression during contraction, and induction of matrix-degrading enzymes [Chrzanowska-Wodnicka et al. 1996; Amano et al. 1997; Ren et al. 1999; Arthur et al. 2000; Lygoe et al. 2004].

In planar cell cultures, the presence of mechanical tension and other factors induces the formation of adhesion sites of different size and molecular composition: focal complexes, focal adhesions, and fibrillar adhesions. Focal adhesions typically contain $\alpha_v\beta_3$ integrin, paxillin, vinculin, and focal adhesion kinase, whilst fibrillar adhesions are predominantly composed of $\alpha_5\beta_1$ integrin and tensin [Cukierman et al. 2001]. As a general rule, larger adhesions are observed at longer-term points of anchorage to the matrix and transmit more force [Galbraith et al. 2002]. Cells grown in three-dimensional matrices form a different type of contact point: the three-dimensional matrix adhesion, which contains components of both focal and fibrillar adhesions: $\alpha_5\beta_1$ integrin, paxillin, vinculin, focal adhesion kinase, tensin, and other cytoskeletal components [Cukierman et al. 2001].

1.3.2. How cells sense matrix tension and react to changes

Matrix composition and stiffness influence cell morphology and motility, both in two-dimensional and three-dimensional models [Pelham et al. 1997; Cukierman et al. 2001; Pizzo et al. 2005].

Cells actively probe the mechanical compliance of the extracellular matrix, in part by locally deforming it with nanonewton-scale traction forces [Choquet et al. 1997]. The actin cytoskeleton plays a vital part in mechanotransduction by maintaining a certain amount of intracellular tension or prestress [Ingber 1997; Geiger et al. 2001; Grinnell et al. 2002]. Matrix tension influences the response to growth factor stimulation: in tension-free matrices, TGF-β stimulates contraction directly via actin and rho, and indirectly by pre-activating cells to become myofibroblasts. In restrained matrices, on the other hand, TGF-β only activates fibroblasts to become myofibroblasts, and does

not have any direct effect [Grinnell et al. 2002]. External forces induce both immediate and long-term cellular responses, such as gene expression, proliferation, differentiation and apoptosis [Ingber 2003].

a) immediate responses

In a three-dimensional matrix, an increase in external tension leads to immediate reduction of overall cell-mediated contraction. However, force quickly recovers to its original level ("tensional homeostasis") [Brown et al. 1998; Mizutani et al. 2004]. Tensional homeostasis has important implications: cells exert the same level of force, regardless of matrix rigidity. As a result, overall contraction of a pliable matrix is higher than that of a rigid matrix [Freyman et al. 2002].

On a cellular level, stretch induces initial cell elongation, quickly followed by disengagement and retraction of protrusions. Relaxation of tension induces rapid cell shortening, followed by protrusion formation. Both contraction and protrusion formation are blocked by ROCK and actin inhibitors [Petroll et al. 2004]. From these findings it becomes obvious that the common downstream mediator of external signals such as growth factors and mechanical tension is the actin cytoskeleton.

b) long-term responses

Changes in tension also induce changes in gene expression, both by activating intracellular signalling cascades and by directly activating stress-responsive elements in gene promoters [Huang et al. 2004]. An increase in tension induces cells to produce new extracellular matrix proteins, reduces the expression of matrix-degrading proteases,

and increases gene expression for components of focal adhesions and the cytoskeleton. The term "synthetic phenotype" has been coined for this cellular state [Kessler et al. 2001]. Conversely, a reduction in tension increases the secretion of matrix-degrading enzymes [Langholz et al. 1995; Riikonen et al. 1995; Martin 1997].

This brief review of the points of contact between cells and their surrounding matrix highlights the fact that mechanically, cells and their environment form a continuum. Integrins link the intracellular actin cytoskeleton to extracellular matrix fibres. Changes in external tension result in actin remodelling similar to that seen after growth factor stimulation; the actin cytoskeleton mediates responses to both types of extracellular signals: cytokines and matrix changes.

The following last part of this introduction reviews current knowledge about growth factor signalling and force generation in matrix remodelling by the three types of ocular cells which are the focus of this work: corneal, Tenon's and scleral fibroblasts.

1.4. Relevance to the eye

The health of the outer layers of the eye is vital for vision. Scarring processes of the cornea cause haziness and at worst blindness. Obstruction of glaucoma surgery sites by Tenon's fibroblasts causes treatment failure. Scleral remodelling is involved in a form of short-sightedness, axial myopia, and in childhood glaucoma. Better understanding of matrix remodelling by these cells is critical for the development of new treatment strategies.

1.4.1. Corneal fibroblasts

The corneal response to injury is complex. The corneal stroma, which constitutes 90% of corneal thickness, consists of highly arranged extracellular matrix proteins with interspersed resident cells, the keratocytes. After corneal injury, injured epithelial basement membrane and keratocytes release cytokines, as does the lacrimal gland, which secretes cytokines into the tear film. These cytokines activate quiescent keratocytes to become fibroblasts, which proliferate and migrate towards the site of injury. Several cytokines are involved, including PDGF, interleukin 1α, bone morphogenic proteins 2 and 4, and tumour necrosis factor α [Kim et al. 1999]. Some characteristics of the corneal wound healing response are unusual and differ from skin healing, such as the importance of PDGF in this system. High levels of PDGF, isoforms A and B, are stored in the epithelial basement membrane and are released upon injury, inducing keratocyte proliferation and migration. Of these isoforms, PDGF-BB exerts the strongest chemoattractant effect [Wilson et al. 2001]. PDGF-BB and EGF

(epidermal growth factor) are more effective in promoting matrix contraction by corneal fibroblasts than other cytokines [Assouline et al. 1992]. Endothelial cells, quiescent stromal keratocytes and activated fibroblasts strongly express the PDGF-β receptor, which might explain their particularly strong response to PDGF-BB [Hoppenreijs et al. 1993]. PDGF is also the only growth factor which is absent from the tear fluid of most healthy eyes, but strongly expressed after corneal surgery [Vesaluoma et al. 1998]. In the cornea, myofibroblast transformation involves PDGF as well as TGF-β signalling [Jester et al. 2002]. Lastly, corneal fibroblasts have been reported to contract matrix without undergoing myofibroblast transformation. This is associated with growth-factor dependent formation of protrusions, stress fibres and matrix adhesions [Roy et al. 1999].

1.4.2. Tenon's fibroblasts

Tenon's fibroblasts efficiently remodel matrix, and myofibroblast transformation has been demonstrated in this process [Cordeiro et al. 2000]. The appearance of optically empty spaces in the matrix next to the cells on electron microscopical samples led to speculation that cell migration might also occur during matrix remodelling [Porter et al. 1998].

Most studies on Tenon's fibroblasts have investigated the effect of TGF-β2, the predominant isoform found in the aqueous fluid of eyes that have undergone surgery and also in non-operated eyes with raised intraocular pressure [Connor et al. 1989; Jampel et al. 1990; Pasquale et al. 1993; Tripathi et al. 1994]. The force generation profile of Tenon's fibroblasts differs from that of skin fibroblasts. Tenon's cells show a slow and linear increase in force development over 24 hours after collagen matrix preparation, as opposed to the initial rapid increase followed by a plateau seen in dermal

fibroblasts. In addition, they produce less force, around 16 dyne/million cells, about a quarter of that produced by dermal fibroblasts [Porter et al. 1998]. Mechanisms of force development by Tenon's fibroblasts have not been studied in detail.

1.4.3. Scleral fibroblasts

Scleral remodelling has mostly been studied in response to mechanical stretching to model childhood glaucoma, or to blurring of vision to induce myopia by disrupting the optical feedback mechanisms important to normal eye growth [Phillips et al. 2004]. MMPs and their natural antagonists, the tissue-inhibitors of metalloproteinases (TIMPs), are players in scleral remodelling, but to date no study has investigated cellular mechanism of matrix contraction by scleral fibroblasts [Guggenheim et al. 1996; Rada et al. 1999; Yamaoka et al. 2001; Cui et al. 2004].

1.5 Hypotheses and aims

Both prevailing theories about the mechanism underlying matrix contraction (myofibroblast transdifferentiation versus fibroblast migration) revolve around remodelling of the actin cytoskeleton, but the dynamic cell behaviour underlying early matrix contraction is not known. The general hypothesis tested in this thesis is that actin remodelling and actin-mediated dynamic cell behaviour are involved in matrix contraction by ocular fibroblasts. To this extent, we have addressed 3 specific aims:

a) actin-mediated dynamic cell behaviour triggered by growth factors results in the generation of matrix tension and contraction *in vitro:* in order to test this hypothesis, we developed a novel set up allowing us to acquire live images of cells and collagen matrix in 3D whilst simultaneaously measuring the strain exerted by the cells on the matrix, and designed a novel parameter to quantitate cell dynamic activity in 3D

b) specific growth factor activation of cell dynamics and actin remodelling is involved in matrix contraction: to test this second hypothesis, we have studied the effect of PDGF on corneal fibroblasts dynamic activity in 2 and 3D, characterised the specific signalling pathway downstream of tyrosine kinase receptors leading to the cellular dynamic activity and actin remodelling observed, and tested the involvement of this pathway in the in vitro matrix contraction by these cells

c) actin remodelling and actin-mediated dynamic cell behaviour involved in matrix contraction can be tested on more physiological ex-vivo systems: to test this final hypothesis, we developed novel tissue culture and microscopy techniques, combining live cell and matrix imaging in intact ocular tissue.

Chapter 2:

Materials and Methods

2.1. Reagents

2.1.1. Cell Culture

All cell culture flasks were purchased from Nunc (nalgenunc, Rochester, USA), with the exception of 35mm glass-bottomed culture dishes (MatTek Corporation, Ashland, USA). For immunolabelling, cells were grown on glass coverslips (CoverGlass BDH 406 / 0187 / 35).

Cell culture media used were DMEM (Dulbecco's modified Eagle's medium, DMEM with 4500mg/ml glucose, L-glutamine and pyruvate, Invitrogen catalogue number 41966-029) with 10% FBS (Fetal Bovine Serum, Invitrogen 10108-165 or Sigma F9665) and 100U/ml penicillin, 100mg/ml streptomycin and 2mM L-glutamine (Life Technologies), serum-free DMEM with 0.7% BSA (Bovine serum albumin, Fisher Scientific, Pittsburgh, USA), and Leibovitz L-15 medium 1x with L-glutamine, without phenol-red (Invitrogen 21083-027).

2.1.2. Collagen contraction assay

Materials used for the preparation of cell-seeded collagen matrices were: Trypsin-EDTA 1x in HBSS without Ca and Mg with EDTA 4x (Invitrogen 25300-054), trypan blue (Invitrogen 15250-061), L-glutamine (Invitrogen/Life Technologies, Paisley, UK), sodium bicarbonate solution 7.5% (Sigma S8761), Dulbecco's modified Eagle's medium 10x (Sigma D2429), and liquid rat tail collagen type I in acetic acid (initially

Sigma C8897; later First Link 60-30-810, collagen 2.1mg/ml in 0.6% acetic acid). The final collagen concentration in the matrix was 1.5mg/ml.

2.1.3. Organ Culture

Pig eyes were obtained fresh from a local abattoir and prepared for use within 5 hours of the animals being killed. Serum-free DMEM with penicillin 100U/ml, streptomycin 100µg/ml, amphotericin B 0.25µg/ml and gentamycin 50µg/ml (Invitrogen) was used for tissue maintenance. Two ocular tissues were retrieved and maintained as whole tissue: conjunctiva and cornea. Pieces of conjunctiva of about 0.5 x 0.5 cm were maintained floating under a glass coverslip in medium. Whole corneas were maintained in a modified and custom-built anterior segment perfusion chamber [Thiel et al. 2001].

2.1.4. Force measurement and application of external tension

Based on the previously described tensioning culture force monitor (t-CFM) [Eastwood et al. 1994; Eastwood et al. 1998], a novel device allowing simultaneous microscopic imaging, measurement of force generation by cells in collagen matrix, and application of external tension was developed, the SIM-CFM. A force transducer was mounted onto a Zeiss Axiovert 100 microscope stage, and a microstepping motor (Micromech systems ltd, Braintree, Essex, UK) was used to apply tension onto specimens placed on the microscope stage. Both force transducer and motor were connected to a personal computer and operated via software control (PicoLog, pico technology ltd, and XWare 6.0.4, Parker). The system was complemented by a custom-built microscope incubation chamber and a humidifier (Zeiss).

2.1.5. Transfection reagents

Lipofectamine 2000™ (Invitrogen 11668-027), Oligofectamine™ (Invitrogen 12252-011) and Fugene 6™ (Roche 11 815 091 001), and Amaxa™ nucleofection (Amaxa Biosystems) were used to transfect cells.

2.1.6. Antibodies

The following antibodies were used:

Primary antibodies	*Supplier and catalogue number*	*Dilution used*
anti-c-myc: sc-40	Santa Cruz 9E10	1:100
anti-PDGFR-β: sc-339	Santa Cruz P-20	1:100
anti-PDGF-BB neutralizing antibody	R&D AF220NA	0.1, 0.5,1µg/ml
anti-cortactin (p80/85) clone 4F11	Upstate 05-180	1:50, 1:2000
anti-dynamin II	BD Biosciences 610263	1:25, 1:100
anti-cortactin	BD Biosciences, 610049	1:50, 1:200
anti-paxillin	Sigma, P 1093	1:50, 1:200
anti-human vinculin	Sigma V9131	1:50
anti-ASMA FITC conjugate	Sigma F3777	1:50
rabbit IgG Purified Immunoglobulin	Sigma I5006	
anti-p34-antibody	M. Bailly [Bailly et al. 2001]	1:40
polyclonal antibodies against components of the arp2/3 complex (AE 351, AE 360, AE 366)	M. Bailly [Bailly et al. 2001]	1:100, 1:50/ 1:50/ 1:50, 1:30
monoclonal antibodies against components of the arp2/3 complex (49B6, p16Arc)	gift from J. Wehland	Undiluted (hybridoma supernatant)
monoclonal antibody against RNTre	gift from L. Lanzetti	Undiluted (hybridoma supernatant)

Secondary antibodies	*Supplier and catalogue number*	*Dilution used*
rhodamine (TRITC)-conjugated affinipure donkey anti-mouse IgG	Jackson ImmunoResearch 715-025-150	1:50
rhodamine (TRITC)-conjugated affinipure donkey anti-rabbit IgG	Jackson ImmunoResearch 715-025-152	1:50
Cy2-conjugated donkey anti-rabbit IgG	Jackson 711-225-152	1:50
fluorescein (FITC)-conjugated affinipure donkey anti-mouse IgG	Jackson 715-095-150	1:50
fluorescein (FITC)-conjugated affinipure donkey anti-rabbit IgG	Jackson 715-095-152	1:50

Table 2.1. Antibodies used

2.1.7. Vital dyes

Fluorescent dyes which permeate into living cells were purchased from Molecular probes: the Vybrant CFDA-SE Cell Tracer Kit (V12883) and CellTracker Green CMFDA (5-chloromethylfluorescein diacetate, C7025).

2.1.8. Plasmids

Plasmids encoding proteins relevant for actin assembly (Scar) or GTPases involved in the circular ruffling pathway were transfected into corneal fibroblasts. Plasmids used

were pEGFP-C1 vector (Clontech 6084-1) (control), H-Scar-WA-myc [Machesky et al. 1998], pEGFP-4-Rab5a, pCDNA3-Rab5^{S34N}-myc and pEGFP-RN-tre (gifts from L. Lanzetti and P. Di Fiore [Lanzetti et al. 2004]).

2.1.9. GFP-adenovirus and plasmids

GFP transgene carrying adenovirus V209 with hCMV promoter was a gift from P. Turowski (Institute of Ophthalmology, London).

2.1.10. Inhibitory drugs

The following chemical modulators were used to inhibit collagen matrix contraction and cell protrusive activity:

Agent	*Manufacturer, Cat. No.*	*Concentrations used*
Myosin light chain kinase inhibitors, ML-7 and ML-9	Sigma I2764 and C-1172	10, 25, 50, 100μM
Blebbistatin, a small molecule inhibitor of muscle and non-muscle myosin	Calbiochem 203391	10, 25, 50,100μM
rho kinase and PRK2 inhibitor, Y27632	Calbiochem 688000	10, 25, 50, 100μM
broad-spectrum MMP inhibitor, GM6001	Chemicon CC1100	100μM
PDGF receptor tyrosine kinase inhibitor, AG1295	Calbiochem 658550	10, 25, 100μM
PDGF pathway blocker, Trapidil	gift from Rodleben Pharma GmbH, 06862 Rodleben, Germany	100, 200, 400μg/ml

Table 2.2. Chemical modulators used

Concentrations were chosen based on published studies using these inhibitors, and no cell toxic effects were observed.

2.2. Cell and organ culture

2.2.1. Human primary cell lines

Cells were obtained from P. T. Khaw's laboratory as cultured primary cell lines isolated from cornea, episclera (Tenon's layer) and sclera of human donor eyes by dispase digestion [Daniels et al. 2000]. Corneal and Tenon's fibroblasts from three different donors and scleral fibroblasts from one donor were used. Cells were maintained in complete medium in tissue culture incubators with 5% CO_2 and 95% humidity. Experiments used cells of passage 2 to 10. During these passages, we did not experience any problems with cell growth. Cells reached confluence and were split on average once or twice a week; we therefore did not perform formal cell growth analyses.

2.2.2. Collagen matrices

Collagen matrices were prepared as previously described [Garrett et al. 2004]. In brief, cells were trypsinised and counted using a hemocytometer. Where appropriate, cell viability counts were performed using trypan blue (Invitrogen 15250-061). Cell suspension containing the desired number of cells was diluted in PBS and centrifuged. The cell pellet was resuspended in pure fetal calf serum or serum-free medium with 0.7% BSA. Concentrated medium (350µl L-glutamine, 900µl sodium bicarbonate solution 7.5%, 3.5ml Dulbecco's modified Eagle's medium 10x), and liquid rat tail collagen type I in acetic acid were added. Adjustment of the pH to 7 by NaOH induces rapid collagen polymerisation. The final collagen concentration was 1.4mg/ml to 1.5mg/ml.

Two standard cell concentrations were used: a low cell density of 40 or 60,000 cells/ml matrix volume to study global matrix contraction and dynamic behaviour of individual cells, and a high cell density of 10^6 cells/ml matrix volume for force measurement experiments.

Matrices were either cast in the shape of 150µl buttons of 14mm diameter using the central well of 35mm MatTek tissue culture dishes, or in 14 x 22mm rectangular moulds. After 30 minutes of polymerisation at 37°C in a tissue culture incubator, the matrices were manually detached from the wells or moulds and floated in medium. The standard medium used was DMEM with either 10% FBS or 0.7% BSA (serum-free controls), with or without modulators such as PDGF. Medium was not changed after matrix preparation, with the exception of specimens used for live cell imaging, whose medium was switched to colourless L15. In experiments on PDGF-induced matrix contraction, three different concentrations of PDGF-BB were used: 20 ng/ml in assays determining global contraction over one week without acquisition of microscopical images (see 2.3.), and a higher concentration of 50ng/ml in assays involving cell microscopy immediately after addition of growth factor. A third concentration, 100ng/ml, was used in the first two exploratory experiments attempting to visualise the cellular response to PDGF in matrix. The higher concentrations was used to compensate for a possible delay and reduction in PDGF-triggered cellular activities if PDGF bound to collagen fibres whilst penetrating the matrix.

Every 24 hours digital photographs of the matrices were acquired. The surface area relative to the area at matrix preparation was measured with the software ImageJ.

2.2.3. Pig eyes

Pig eyes were immersed in 5% povidone iodine solution for 10 minutes within 5 hours after the animals had been killed. They were then rinsed in PBS with penicillin 1000U/ml, streptomycin 1000µg/ml, amphotericin B 2.5µg/ml and gentamycin 500µg/ml and dissected. Whole cornea with an 8mm scleral rim was mounted onto a perfusion chamber [Thiel et al. 2001]. Conjunctival specimens were placed in tissue culture dishes. Serum-free DMEM with penicillin 100U/ml, streptomycin 100µg/ml, amphotericin B 0.25µg/ml and gentamycin 50µg/ml was used for perfusion or tissue maintenance.

2.3. Macroscopic collagen contraction assay

Whole matrix contraction was monitored by digital photographs taken immediately following release of the polymerised matrices and then daily over 7 days. Images were imported into NIH image or Image J software. The gel/well diameter ratio R in pixels was entered into a Microsoft Excel spreadsheet. Gel surface area was normalised to the area calculated at T0 and expressed as percentage of the initial surface area, according to the following formula: $A(Tx)$ in % = $100-(100xR_{1x}^2/R_{10}^2)$ with A=area, Tx=Timepoint between 24 and 168 hours after matrix preparation. Statistical analysis (mean area, standard error) was performed on the values of triplicates of gels under different conditions, in Microsoft Excel.

Contraction was induced by floating the matrices in either DMEM with 10% FBS or 20ng/ml PDGF (R&D 220-BB) in serum-free medium with 0.7% BSA. Negative controls were floated in serum-free DMEM with 0.7% BSA. Contraction was

modulated by either transfecting cells with the plasmids or siRNA detailed in paragraph 2.5 and 2.6, or by adding chemical modulators listed in 2.10 to the culture medium the matrices were floated in.

2.4. Circular ruffling assay

Human corneal fibroblasts were plated at a cell density of 35,000 cells per 35mm MatTek dish. To enhance cell attachment to the central glass well, the dishes were pretreated by a wash with 1 M HCl for 3-5 min ("acid-wash"), two rinses with sterile PBS, followed by a rinse with 95% ethanol and a final wash with sterile PBS. Following serum starvation by incubation in DMEM with 0.7% BSA over night, cells were stimulated with PDGF-BB at a concentration of 20-100ng/ml to determine circular ruffling characteristics, and 50ng/ml thereafter. Circular ruffles were imaged either using timelapse phase or fluorescent microscopy. For f-actin staining and immunolabeling, cells were fixed with 3.7% formaldehyde in cytobuffer[1] after 7 minutes of PDGF stimulation and processed as described in section 2.11.

To modulate circular ruffling, the following agents were used:

a) anti-PDGF-BB neutralising antibody (R&D AF-220-NA)

b) human WASp-WA and Scar1-WA domains [Machesky et al. 1998] , which D. Shao had expressed in bacteria and purified as GST-fusion proteins. The GST tag was removed by thrombin (Sigma) digestion, and the WA domains were further purified by Mono-Q and Superdex-75 filtration (Amersham) [Shao et al. 2006].

[1] 2 x cytobuffer: 10mM Kcl, 274 mM NaCl, 8 mM $NaHCO_3$, 0.8mM KH_2PO_4, 4mM $MgCl_2$, 10mM PIPES, 4mM EGTA, 11mM Glucose, pH to 6.0 – 6.1

To evaluate the effect of anti-PDGF-BB-neutralising antibody on circular ruffling, cells were grown on MatTek dishes as previously described [Bailly et al. 2001], and serum-starved overnight. The next day, 0.1 to 1.0μg/ml of antibody and 20ng/ml PDGF-BB were simultaneously added to incubation medium.

For microinjection experiments, cells were grown on MatTek dishes and serum-starved overnight as above. Microinjection was conducted using an Eppendorf semi-automated microinjection system using needles pulled on a Sutter p87 micropipette puller. WA domains at a concentration of 136μM PBS (phosphate buffered saline) were mixed with FITC-labeled dextran (0.8mg/ml final concentration for identification of injected cells). Cells were allowed to recover for a minimum of 30 minutes, then stimulated with human recombinant PDGF-BB and imaged with timelapse phase microscopy, or fixed and stained with rhodamin-phalloidin. Control cells were injected with PBS mixed with FITC-labelled dextran.

The effect of chemical modulators (ML9, Y27632, AG1295, Trapidil) on circular ruffling was studied by pre-incubating cells in DMEM with 0.7% BSA and modulator in the same concentrations as detailed in section 2.3 for 30 to 60 minutes prior to PDGF stimulation.

2.5. Transfection of human corneal fibroblasts

2.5.1. Lipofectamine™ transfection

Cells were plated at a density of 35,000 per 35mm or 100,000 per 60mm culture dish. The following day, transfection of cells in 35mm dishes was performed using 4µl of Lipofectamine and 1.5µg plasmid DNA in 1ml serum-free medium without antibiotics. Volumes were trebled for 60mm diameter dishes. Transfected cells were allowed to recover in complete medium for one night before further processing.

2.5.2. Fugene™ transfection

Cells were plated at a density of 35,000 per 35mm or 100,000 per 60mm culture dish. The following day, transfection of cells in 35mm dishes was performed using 6µl Fugene™, 2µg DNA and in 1100µl serum-free medium without antibiotics. Volumes were trebled for 60mm diameter dishes. Transfected cells were allowed to recover in complete medium for one night before further processing.

2.5.3. Amaxa™ transfection

Cells were trypsinised and counted. For each plasmid assay, 5 x 10^5 cells were centrifuded for 7 minutes at 4°C at 1300 revolutions per minute. The supernatant was aspirated. Each pellet was resuspended in: 100µl Nucleofector solution for Normal Human Dermal Fibroblasts (NHDF solution) and 2µg DNA. Cells were nucleofected using the pre-set program U23. Five hundred microliter of DMEM with 10% fetal calf

serum were added , and the resulting suspension was divided between two culture flasks. Transfected cells were allowed to recover in complete medium for 24 to 48 hours before further processing.

2.6. siRNA

Fluorescently labelled silencing RNA against RN-tre was obtained custom-made from Qiagen: Target sequences for siRNA tagged with AlexaFluor 488 were: for RN-tre, 5`-AACAATCCTTATTCCATGTGC-3`; a control oligo was designed by introducing three mismatched nucleotides: 5`-AGCAGTCGTTATTCCATGTGC-3`.
Human corneal fibroblasts were plated at a cell density of 25,000 per 35mm or 60,000 per 60mm culture dish. The following day, they were transfected with 5µl siRNA, 8µl Oligofectamine in 1ml serum-free medium without antibiotics antibiotics (threefold these volumes for 60mm dishes). The final concentration of the small interfering RNA duplex in the culture medium was 100nM. Transfected cells were serum-starved overnight, then stimulated with 50ng/ml PDGF-BB and fixed and stained with rhodamine phalloidin to assess the effect on circular ruffling. Alternatively, transfected cells were cast into collagen matrices to assess the effect on matrix contraction. Downregulation of RNTre was evaluated by Western blotting.

2.7. Western blotting

2.7.1. Preparation of samples

To confirm the downregulation of RNTre after transfection with siRNA, cells were incubated in DMEM with 10% FBS for 20 hours after transfection. After washing cells with PBS, cells were lysed and scraped into 1x sample buffer. The samples were boiled at 95°C for 3 minutes and briefly centrifuged to remove debris.

2.7.2. SDS polyacrylamide gel electrophoresis (PAGE)

Typically, 10µl of cell lysate or 5µl of rainbow molecular weight markers (Amersham) were loaded into each well. Samples were resolved by SDS-PAGE using a 12% polyacrylamide gel run at 1Amp (per mini-gel) for 60 minutes.

2.7.3. Western blotting

After SDS-PAGE, proteins were transferred to Protran nitrocellulose transfer membrane (Schleicher and Schuell) using the BioRad Transfer unit at 100V for 60 minutes. Membranes were washed in PBS and then blocked in 5% (w/v) dried powdered skimmed milk for 30 minutes at room temperature. After blocking, membranes were incubated with primary antibody in PBS/milk for one hour at room temperature or overnight at 4°C. Membranes were washed in PBS/Tween before incubation with secondary antibody-HRP conjugate (1.5µl of goat anti-mouse antibody in 3ml milk) for

45 minutes at room temperature. Membranes were washed thoroughly in PBS/Tween before incubation with Supersignal West Pico Chemiluminescent substrate (Pierce). Antibody binding was visualised using Fujifilm intelligent dark box II and Las-1000 Pro software (version 2.3).

2.8. Viral transduction of cells

Human corneal fibroblasts grown on MatTek dishes were incubated with GFP-adenovirus at a titre of 400 and 1000pfU/ml complete medium per cell for 24 hours prior to further processing. Corneal tissue was injected with 50µl containing $2x10^{11}$ pfU/ml.

2.9. Cell staining by vital dyes

Vital dyes were used to highlight cells in conjunctival and corneal tissue. To assess cell penetration, corneal fibroblasts grown on MatTek dishes were exposed to a 10µM CFDA-SE or 25µM CMFDA dilution in prewarmed PBS for 20 minutes. Medium was then changed to DMEM with 10% FBS for 30 minutes prior to imaging. Tissue was stained following the same protocol.

2.10. Microscopy

2.10.1. Phase and fluorescence imaging

Phase and epifluorescence microscopy were performed on a Zeiss Axiovert 100M using standard x10, x20, x40 objectives and a x60 long working distance air objective (Olympus LCP Plan FI 60x, NA 0.70, infinity corrected, with correction collar, Olympus Optical, UK). Images were taken using a CCD camera coupled to an OpenLab-driven image acquisition system (Improvision). Confocal fluorescence microscopy was performed on a Zeiss Axiovert S100 TV coupled to a Biorad Radiance 2000 confocal microscope. During live timelapse microscopy, the medium in the culture dishes containing the specimens was covered with a layer of heavy mineral oil (Aldrich 33.076-0) to slow down evaporation.

2.10.2. Confocal reflection microscopy

Collagen matrix fibrils were imaged by reflection microscopy as previously described [Brightman et al. 2000]. Briefly, a long working distance x60 air objective (Olympus LCP Plan FI 60x, NA 0.70, infinity corrected, with correction collar, Olympus Optical, UK) was fitted to a Zeiss Axiovert S100 TV/Biorad Radiance 2000 confocal microscope. Specimens were illuminated with an argon laser emitting light at 488nm for excitation (Biorad). Only the 488nm reflected light was detected by a photomultiplier tube (PMT) through a polarisation filter to image matrix fibres. Simultaneous green fluorescence of transfected cells was imaged along the same optical pathway and

separated from back-scattered (reflected) light before reaching a longer band pass emission filter in front of a second PMT. Differential interference images of cells were acquired in a third channel. In this manner, both matrix fibrils and cellular activity could be imaged together. Images were taken in z-stacks with 3µm steps in a fixed x-y plane and used for quantitation of fiber movement and cell protrusive and retractile activity as detailed in section 2.10.3. Images were acquired every 10 or 15 minutes for 4-15 hours, using LaserSharp software (Biorad).

2.10.3. Quantitation of circular ruffling

The proportion of cells displaying circular ruffling was quantified manually on live imaging timelapse sequences consisting of phase images acquired every minute for 5 minutes prior and 30 minutes after PDGF stimulation, and on cells fixed with formaldehyde 7 minutes after PDGF stimulation and stained with fluorescent labelled phalloidin. Images were viewed in Openlab software (Improvision).

2.10.4. Quantitation of three-dimensional protrusive activity

Cells in collagen gels were imaged with z-stacks of 11 to 16 sections of 3µm each. For the investigation of cell spreading behaviour and protrusive activity during the first 15 hours after matrix preparation, z-stacks were acquired every 15 minutes. To study cellular responses to PDGF stimulation, matrices were floated in serum-free medium with 0.7% BSA for the initial 24 hours after preparation. After growth factor stimulation, cells were imaged every 10 minutes for 4 hours. The acquired z-stacks were exported into ImageJ software and compressed into single images using the maximum

intensity setting. The outline of individual cells was manually traced to allow accurate image thresholding. Cell area and changes in cell shape were quantified using a modification of the colocalisation module of Metamorph, and summarised as "dynamic index", defined as (areas of new protrusions + areas of retractions) / cell area (Fig. 2.1). The dynamic index represents the percentage of cell area that is redistributed between timepoints.

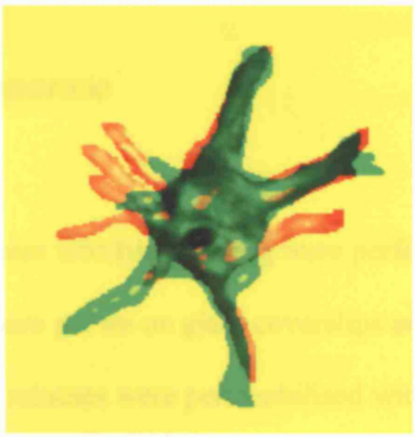

Fig. 2.1. Dynamic index calculation, based on change in cell shape from one timepoint to the next. Purely red areas represent newly formed protrusions, whilst purely green areas reflect processes that have been retracted between the first and the second timepoint. Using Metamorph, the areas of new protrusions and the areas of retractions were measured, and the dynamic index defined as (areas of new protrusions + areas of retractions) /cell area at first timepoint.

2.10.5. Quantitation of matrix displacement

Of each z-stack of matrix images one single corresponding layer was selected. Collagen fibre displacement was quantified by manually tracking individual fibres on subsequent timepoints using Openlab software. The first hour of imaging was excluded, as small vertical drifts of the specimen prevented accurate maintenance of the same focal plane.

2.11. Immunofluorescence

F-actin and immunofluorescent labelling staining were performed as described [Bailly et al. 2001]. In brief, cells were grown on glass coverslips and in collagen gels. Cells fixed in formaldehyde for 5 minutes were permeabilised with 0.5% Triton X100 (Sigma T9284) in cytobuffer for 20 minutes and incubated in 0.1M glycine in cytobuffer for 10min. Non-specific staining was blocked and filamentous actin labelled simultaneously by staining with 0.5μM fluorescent labelled phalloidin (AlexaFluor 488 phalloidin or rhodamine phalloidin, Molecular Probes, A-12379/R-415) in TBS[2]/1%BSA/1%FBS in a humidified chamber for 20 min. When additional labelling with antibodies was required, the phalloidin/TBS was aspirated and replaced by primary antibody diluted in TBS/1% BSA for an incubation of 1 hour at room temperature in a humidified chamber, followed by a rinse and incubation with a secondary antibody for 1 hour in TBS/1% BSA at room temperature.

Cells in collagen gel were fixed in 2% formaldehyde in cytobuffer for 30 minutes at room temperature, extracted with 1% triton X100 in cytobuffer for 15 minutes, then

[2] 2xTBS: 40mM Tris, 308mM NaCl, H_2O 500ml, pH to 8.0

washed twice for 10 minutes in glycine 0.1M in cytobuffer. Non-specific staining was blocked by incubation with TBS/10%FBS/1%BSA for one hour. Filamentous actin was labelled by incubation with 0.5μM fluorescent labelled phalloidin in TBS/1%BSA for 20 minutes at room temperature in a humidified chamber. When additional labelling with antibodies was required, the phalloidin/TBS was aspirated and replaced by primary antibody diluted in TBS/1% BSA for an incubation of 1 hour at room temperature in a humidified chamber, followed by incubation with a secondary antibody for 1 hour in TBS. Lastly, specimens were washed four times for 5 minutes in TBS/1%BSA and once for 5 minutes in TBS only, and mounted on glass slides using N-Propyl gallate/glycerol-based mounting medium.

2.12. Two photon excitation microscopy

Pig conjunctiva and cornea were examined using a Bio-Rad Radiance 2100 MP microscope mounted on a Nikon E1000 upright stand, with a two-photon pulsed laser (Coherent Mira 900). Two objectives were used: a x20 multi-immersion objective, NA 0.75, with the correction collar set to water-dipping, and a x60 water-dipping objective, NA 1.0.

Visualisation of conjunctival cells relied on cytosolic autofluorescence, and was performed using an excitation wavelength of 780nm. Conjunctival stroma was visualised by an excitation wavelength of 920nm, which uses the autofluorescent properties of collagen. Corneal cells were visualised after transduction with GFP-adenovirus, using an excitation wavelength of 880nm. Corneal stroma was visualised using an excitation wavelength of 780 to 800nm, using second harmonic generation.

2.13. Force measurement and application of external tension

Force measurements were obtained by placing the culture force monitor in a tissue culture incubator (37°C, 95% humidity, 5% CO_2) and recording force development over 24 hours after matrix preparation. For simultaneous imaging, the SIM-CFM (37°C, 70% humidity, no CO_2) was used. Image z-stacks were acquired every 15 minutes over the first 6 hours after matrix preparation using DIC and confocal reflection microscopy. External tension was applied in the form of a single stretch at 6 hours after matrix preparation. For 30 minutes prior to and 60 minutes after application of external tension via the microstepping motor, images of individual cells were acquired every 5 minutes. Further images were acquired every 15 minutes for 15 hours.

2.14. Calculation of cell volume

Corneal, Tenon's and scleral fibroblasts were trypsinised and fixed using 3.7% formaldehyde in cytobuffer. Using a confocal microscope, photos were taken of cells in suspension. The cell diameter of 20 to 40 cells of each type was measured on two axes on these digital photos using ImageJ, and the cell volume was calculated from the cell diameter, using the formula for the calculation of the volume of a sphere:

$V = 4/3\ \pi\ r^3$ (r = radius).

Chapter 3:

Results

3.1. Mechanics and dynamics of force generation and matrix contraction

Ocular fibroblasts are involved in numerous conditions which can affect vision, but details of how these cells mediate wound healing and scarring events are not known. In particular, potential differences between ocular fibroblasts from different parts of the eye have not been studied systematically. We therefore began our investigation by studying the remodelling and contraction of collagen matrix by three types of ocular fibroblasts, which is the standard *in vitro* assay to study matrix contraction. Cells were stimulated by a mix of growth factors by adding fetal calf serum to the incubation medium.

3.1.1. Ocular fibroblasts differ in matrix contraction efficiency

We measured the global contraction of collagen matrices by human corneal, Tenon's, and scleral fibroblasts (HCF, HTF, HSF) over 7 days (Fig. 3.1.1). HCF contract matrix by about 55% within the first 24 hours, and contraction reaches a plateau after 72 hours. HTF remodel matrix more slowly: matrix contraction reaches 10% after 24 hours, but steadily continues, until maximal contraction is reached after 6 days. The final degree of contraction is the same for HCF and HTF. Matrices seeded with the same number of HSF hardly contract at all, but a 75 fold increase in cell density results in a contraction profile similar to that of HTF.

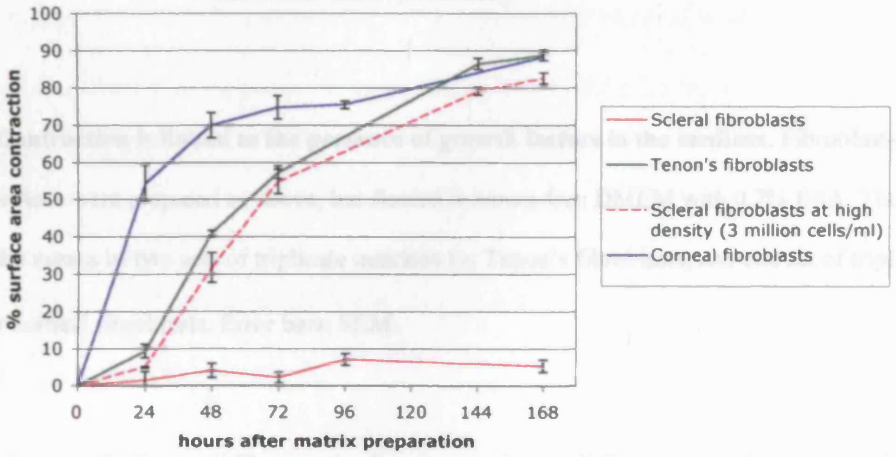

Fig. 3.1.1. Ocular fibroblasts have different degrees of matrix contraction efficiency. Collagen matrices were seeded with corneal or Tenon's fibroblasts at a density of 40,000 cells/ml, and with scleral fibroblasts at densities of 40,000 and 3 million cells/ml. The matrices were released from the casting well 30 minutes after preparation, and were freely floated in DMEM with 10% FBS. Surface area contraction was calculated from the matrix diameter measured on digital photographs obtained at daily intervals. The data shown are the means of two sets of triplicate matrices for corneal and Tenon's fibroblasts, and one set of triplicate matrices for scleral fibroblasts. Error bars: standard error of the mean (SEM).

To ensure that the observed matrix contraction was related to the presence of growth factors in the medium, we repeated the experiment in the absence of externally added growth factors. Under these conditions, matrix contraction is minimal (Fig. 3.1.2).

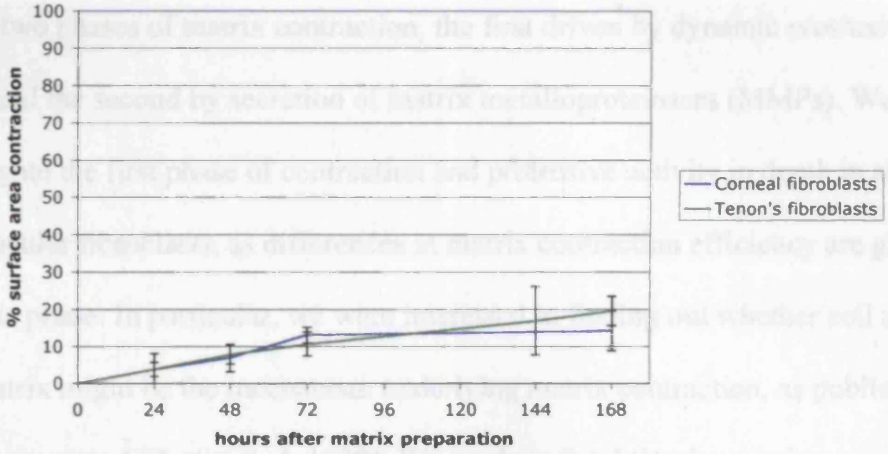

Fig. 3.1.2. Contraction is linked to the presence of growth factors in the medium. Fibroblast-seeded collagen matrices were prepared as above, but floated in serum-free DMEM with 0.7% BSA. The data shown are the means of two sets of triplicate matrices for Tenon's fibroblasts, and one set of triplicate matrices for corneal fibroblasts. Error bars: SEM.

In conclusion, cells from different ocular tissues have different matrix contraction profiles, and differences are most marked in the early phase of matrix contraction, i.e. in the first 24 to 48 hours after matrix preparation.

3.1.2. Cell protrusive activity drives early matrix contraction and force generation

The first 24 hours after matrix preparation see the greatest degree of matrix remodelling and contraction. Work on scleral fibroblasts in our laboratory had demonstrated that there are two phases of matrix contraction, the first driven by dynamic protrusive cell activity, and the second by secretion of matrix metalloproteinases (MMPs). We decided to investigate the first phase of contraction and protrusive activity in depth in all three types of ocular fibroblasts, as differences in matrix contraction efficiency are greatest during this phase. In particular, we were interested in finding out whether cell migration across matrix might be the mechanism underlying matrix contraction, as published literature suggested [Porter et al. 1998]. We used confocal timelapse microscopy with simultaneous acquisition of phase contrast images to visualise the cells and reflection microscopy to visualise the matrix.

a) Protrusive activity is the main cellular behaviour in early matrix contraction and leads to matrix displacement

Timelapse microscopy shows that immediately after matrix preparation, cells are rounded and devoid of protrusions. In the following hours, cells extend and retract protrusions of increasing length. In corneal and Tenon's fibroblasts, the overall cell shape changes from rounded to star- or spindle shape. The scleral fibroblasts used here only extend short processes, and their cell shape remains mostly spherical. Regardless of cell type, protrusion formation is a highly dynamic process. Existing protrusions are continuously retracted, whilst new processes form (Fig. 3.1.3). Cell migration, on the

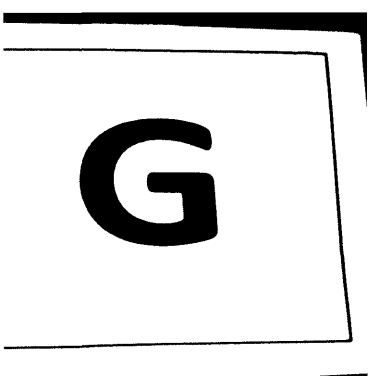
G

6other hand, is a rare event. Of 8 cells imaged for 16 hours after matrix preparation (3 corneal, 3 Tenon's, 2 scleral fibroblasts), no cell migrated across the matrix. An additional 32 corneal and Tenon's fibroblasts were observed for 4 hours each. Of these, only one cell showed directional movement.

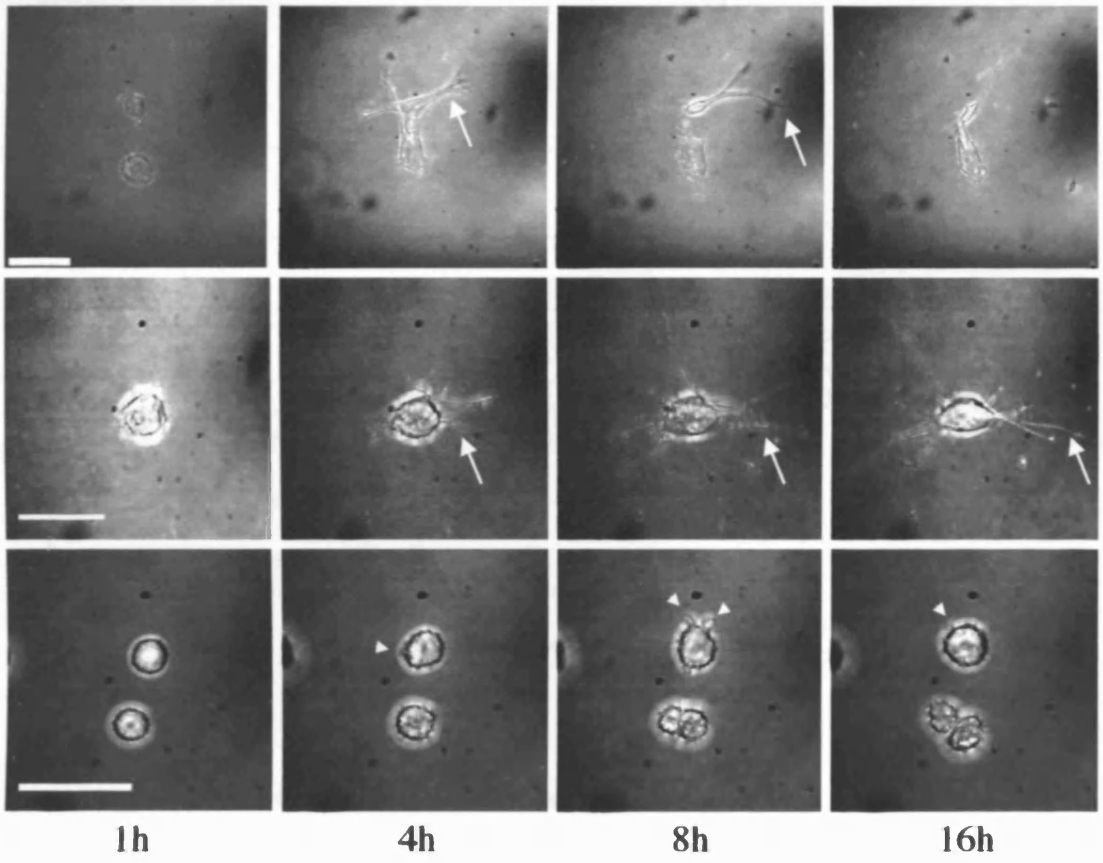

Fig. 3.1.3. Establishment of cells in the matrix: in the first hours after matrix preparation, HCF and HTF form progressively longer protrusions, whilst HSF remain mostly spherical. Collagen matrices were seeded with ocular fibroblasts at a reduced cell density of 20,000 cells/ml to facilitate single-cell imaging. The matrices were released from the casting well 30 minutes after preparation, and were freely floated in Leibowitz' L-15 medium with 10% FBS and transferred to a confocal microscope. Timelapse z-stack phase contrast images of individual cells were obtained every 15 or 20 minutes for 16 hours after matrix preparation. Z-stacks were compressed into single images for each timepoint. Montage shows projection images of corneal (top), Tenon's (middle) and scleral (bottom) fibroblasts at selected timepoints. Scalebars = 50μm.

During the first hours after matrix preparation, the length of protrusions of both corneal and Tenon's fibroblasts seems to increase rapidly and then reach a plateau. We quantified this impression by measuring maximal cell length between opposite extension tips, which confirms that a plateau value is reached about 6 hours after matrix preparation (Fig. 3.1.4).

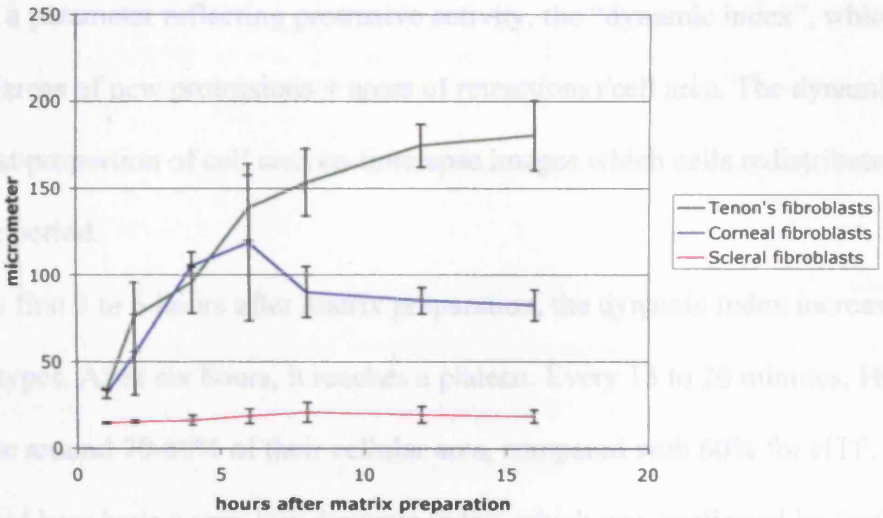

Fig. 3.1.4. Cell length reaches a plateau 6 hours after matrix preparation.

The maximum cell length (tip of one protrusion to tip of another protrusion) was measured in compressed z-stack images in ImageJ. The data shown are the means of three corneal, three Tenon's and two scleral fibroblasts. Error bars: SEM.

Measuring cell length at selected timepoints does not reflect the dynamic protrusive activity observed on timelapse movies, which consists of continuing retraction of existing and formation of new protrusions. We therefore developed a new method to quantify cell protrusive activity, by digitally subtracting the area of a cell on a selected timelapse image from the area on the previous timelapse image. This results in two numerical values, one for the area of retracted protrusions, and one for the area of newly formed protrusions. Based on these values and on total cell area on these images, we calculated a parameter reflecting protrusive activity, the "dynamic index", which we define as (areas of new protrusions + areas of retractions)/cell area. The dynamic index reflects that proportion of cell area on timelapse images which cells redistribute over a given time period.

During the first 3 to 6 hours after matrix preparation, the dynamic index increases in all three cell types. After six hours, it reaches a plateau. Every 15 to 20 minutes, HCF redistribute around 70-80% of their cellular area, compared with 60% for HTF. The HSF studied here have a very low dynamic index, which was confirmed by further work on these cells performed in our laboratory. The dynamic index is an intrinsic characteristic of each cell type (Fig. 3.1.5).

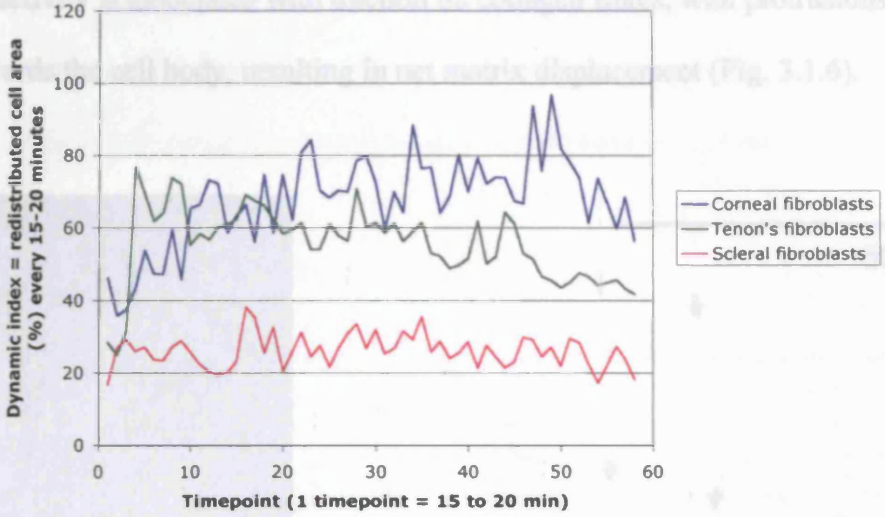

Fig. 3.1.5. Different types of ocular fibroblasts have different protrusive activity levels, reflected in their dynamic index at plateau value.

Collagen matrices were prepared with low cell density (25,000 cells/ml), and floated in L15/10%FBS medium. Cells and matrix were imaged on a confocal microscope using phase contrast and confocal reflection microscopy settings, acquiring a z-stack of images of individual cells at high magnification every 15 to 20 minutes for 15 hours. Image acquisition was started 1 hour after matrix preparation. The z-stack images were compressed into a single image. Cell outline was tracked in ImageJ and changes in cell area analysed using the colocalisation module of Metamorph. Changes in cell area reflect formation of new protrusions and retraction of existing processes. These areas were quantified and summarised as "dynamic index", defined as (areas of new protrusions + areas of retractions) / cell area per 15-20 minutes. The dynamic index represents the percentage of cell area that is redistributed between timepoints. The analysis is based on three cells of each type each. The SEM of three measurements at each timepoint lies between 0.03 and 31%, and is not shown on this graph for reasons of density of data points.

Whilst cell protrusive activity is the main cell behaviour observed during the first 24 hours after matrix preparation, it does not in itself explain matrix contraction. In order to investigate whether there is a link between formation and retraction of protrusions and matrix contraction, we measured the displacement of individual collagen fibres in

the immediate vicinity of cells at selected timepoints. We found that protrusive / retractile activity is associated with traction on collagen fibres, with protrusions pulling fibres towards the cell body, resulting in net matrix displacement (Fig. 3.1.6).

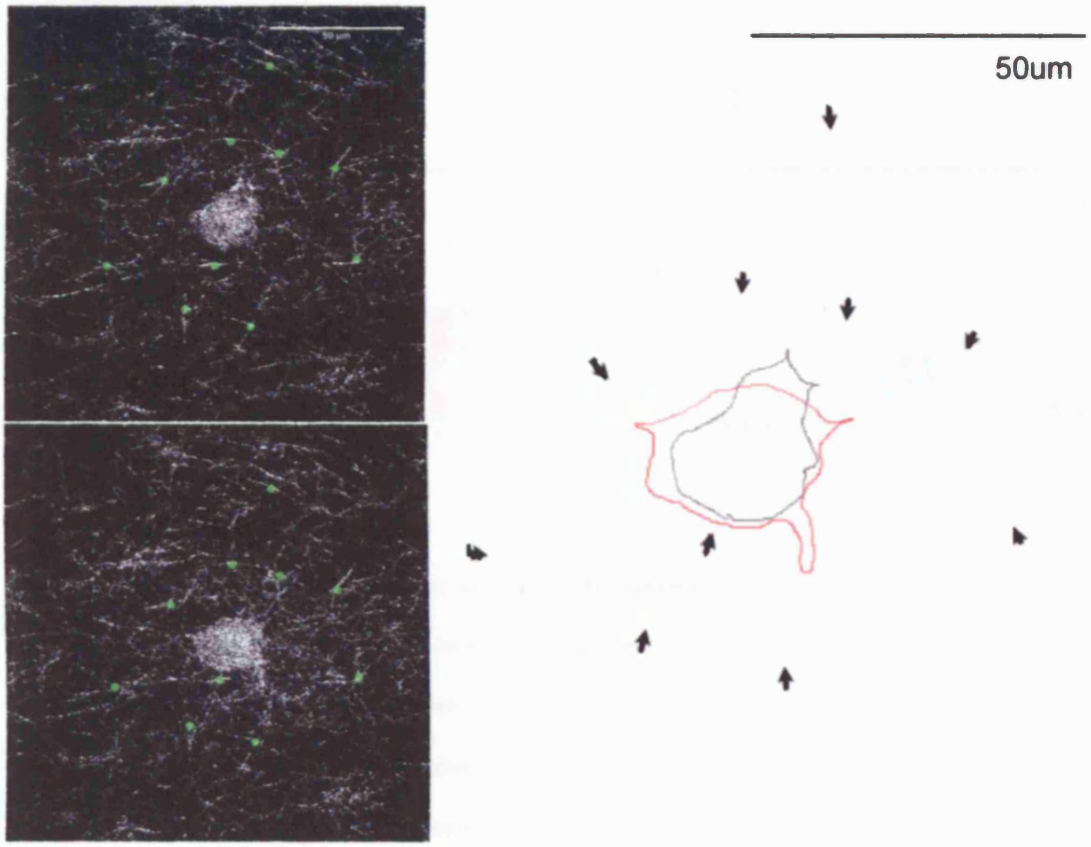

Fig. 3.1.6. Protrusive activity is associated with traction on collagen fibres and net matrix displacement.

Left: Confocal reflection images showing cell reflection and individual collagen fibrils acquired one (top) and two (bottom) hours after matrix preparation. The displacement of 10 individual fibres (green) was tracked. Right: the movement of the tracking points was measured in ImageJ. Arrows indicate the direction of fibre displacement, with arrow length corresponding to the net displacement, in this example an average of 1.27μm over one hour. Superimposed the change in cell shape over the same time period (grey outline: first timepoint, red outline: second timepoint). Note retraction of protrusion at the top and extension of new protrusion towards the bottom of the image. Scale bar: 50μm.

To assess potential changes in matrix contraction intensity over time, we measured the fibre displacement between the first and second, and between the 6th and 8th hour after matrix preparation. In all three cell types, net matrix displacement is greater in the first two hours after matrix preparation than in the plateau phase of protrusive activity (Fig. 3.1.7).

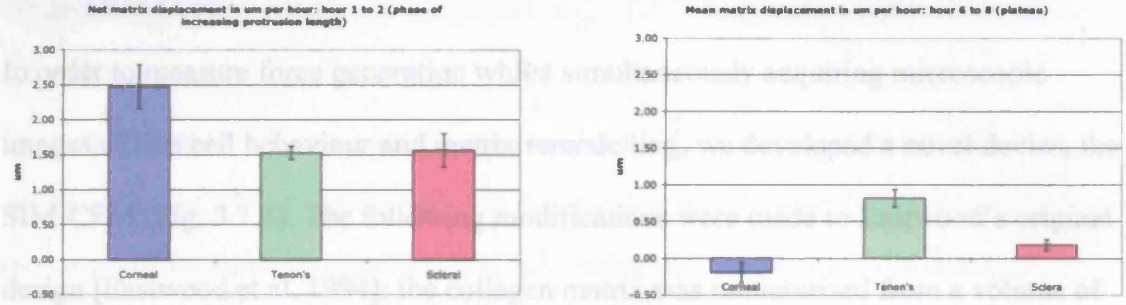

Fig. 3.1.7 All types of fibroblasts induce net matrix displacement in the first hours after matrix preparation; only Tenon's fibroblasts sustain it. Left: Net displacement of individual collagen fibres per hour in µm and standard error for three Tenon's, three corneal and two scleral fibroblasts, during the first hour of imaging (starting one hour after matrix preparation). Fibre displacement towards the cell body or towards cell extensions was allocated a positive value, displacement away from cell extensions and cell body a negative value. Net displacement was calculated by adding all measured values, and forming the average of three corneal, three Tenon's and two scleral fibroblasts. Right: Same for the period from 6 to 8 hours after matrix preparation.

In summary, we have demonstrated that in the early phase after matrix preparation, the main cell behaviour is protrusive and retractile activity, and that this is associated with net matrix displacement towards the cell. The three types of ocular fibroblasts have different matrix contraction efficiency, different dynamic indices and different matrix displacement characteristics.

In order to link protrusive activity and fibre displacement to global matrix contraction, we investigated the strain exerted by the cells onto their surrounding matrix by use of a modified culture force monitor.

b) Development of the SIM-CFM: matrix displacement corresponds to force generation

In order to measure force generation whilst simultaneously acquiring microscopic images of live cell behaviour and matrix remodelling, we developed a novel device, the SIM-CFM (Fig. 3.1.8). The following modifications were made to Eastwood's original design [Eastwood et al. 1994]: the collagen matrix was miniaturised from a volume of 5ml to 2ml, fitting into a rectangular mould in a 35mm diameter glass-bottom microscopy culture dish, and mounted onto an Zeiss Axiovert microscope stage; a microstepping motor was also mounted onto the microscope stage; the stage was surrounded by a custom-built incubator box which provided constant temperature of 37°C; the air in the chamber was humidified via a Zeiss humidifier; evaporation from the medium-air interface was further reduced by covering matrices and medium with heavy mineral oil.

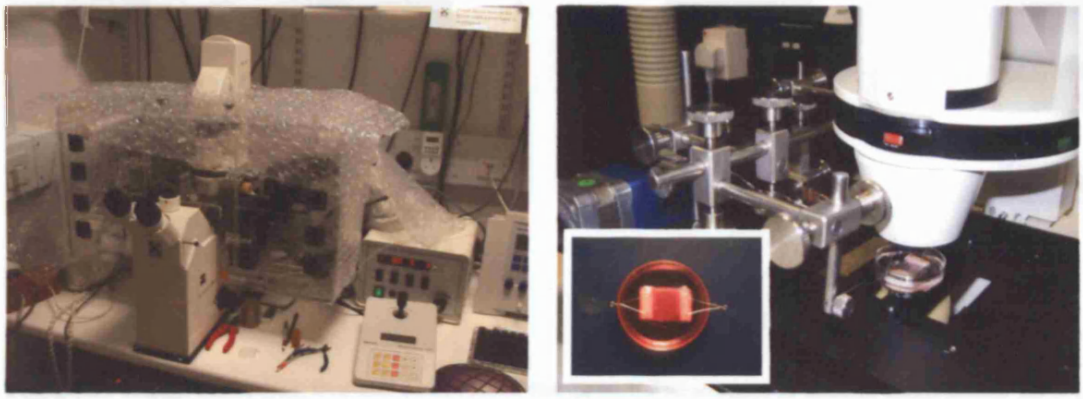

Fig. 3.1.8. The SIM-CFM allows simultaneous imaging of cells and matrix and measurement of force generation. Left: Incubator box and CFM stage set up on Zeiss Axiovert epifluorescence microscope. Right: Matrix set up on SIM-CFM. Inset: freshly cast collagen matrix with embedded floatation bars and hooks to connect it to CFM suspension wires.

For SIM-CFM-studies, fibroblasts are seeded into liquid collagen as usual. The matrix is cast into a rectangular shape, and Vyon™ floatation bars and metal hooks are embedded at the short sides of the matrix before the collagen polymerises. After thirty minutes of polymerisation, the mould is removed, the matrix is floated in medium, covered with heavy mineral oil, and connected to the metal suspension wires of the SIM-CFM. One wire is fixed, whilst the other one is attached to a flexible metal strip whose deflection is recorded by a force transducer (Fig. 3.1.9). As the fibroblasts contract the matrix, the transducer converts the mechanical deflection signal into an electrical one, which is recorded on a PC, using the software package picolog™. The glass-bottom culture dish with the matrix is mounted on the stage of an epifluorescence or confocal microscope, allowing the acquisition of timelapse and z-stack microscopical images.

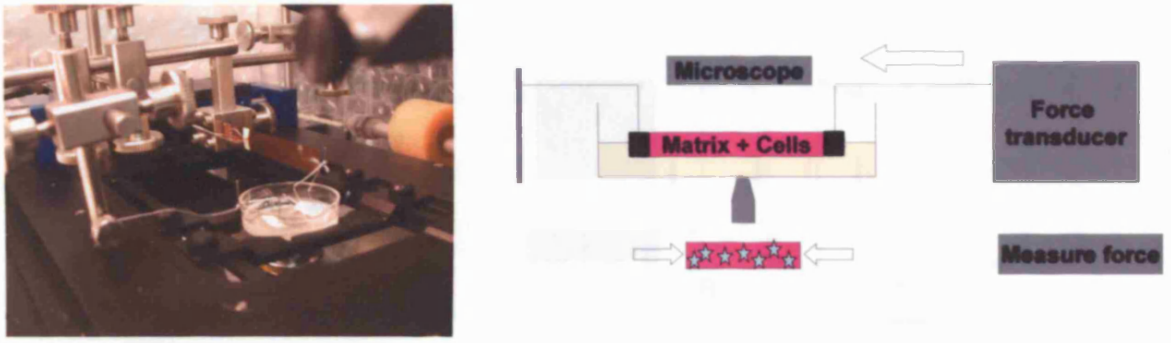

Fig. 3.1.9. Whilst recording live cell behaviour, the SIM-CFM measures matrix contraction force. Left: Setup without matrix, demonstrating fixed suspension wire (left) and flexible metal strip connected to force transducer (right). Right: Working principles of the SIM-CFM. As fibroblasts contract matrix, a flexible metal strip connected to one of the embedded floatation bars is deflected. A force transducer converts the mechanical into an electrical signal, which is recorded as force measurement on a PC. Cell behaviour and matrix interaction are visualised using epifluorescence or confocal microscopy.

The SIM-CFM can also be used to study the effect of changes in external tension on cellular behaviour in matrix. A micro-stepping motor can be programmed to apply external stretch to the matrix by pulling on the suspension wire that is connected to the transducer (Fig. 3.1.10. A) The force transducer measures the cellular adaptation to changes in the level of tension, and the microscope visualises changes in cell behaviour (Fig. 3.1.10. B, C). Stretching the matrix induces a shift in the image recorded by the microscope. We corrected this shift by superimposing consecutive timelapse images and correcting their position relative to each other, by using the "registration" module of the software package Openlab (Improvision).

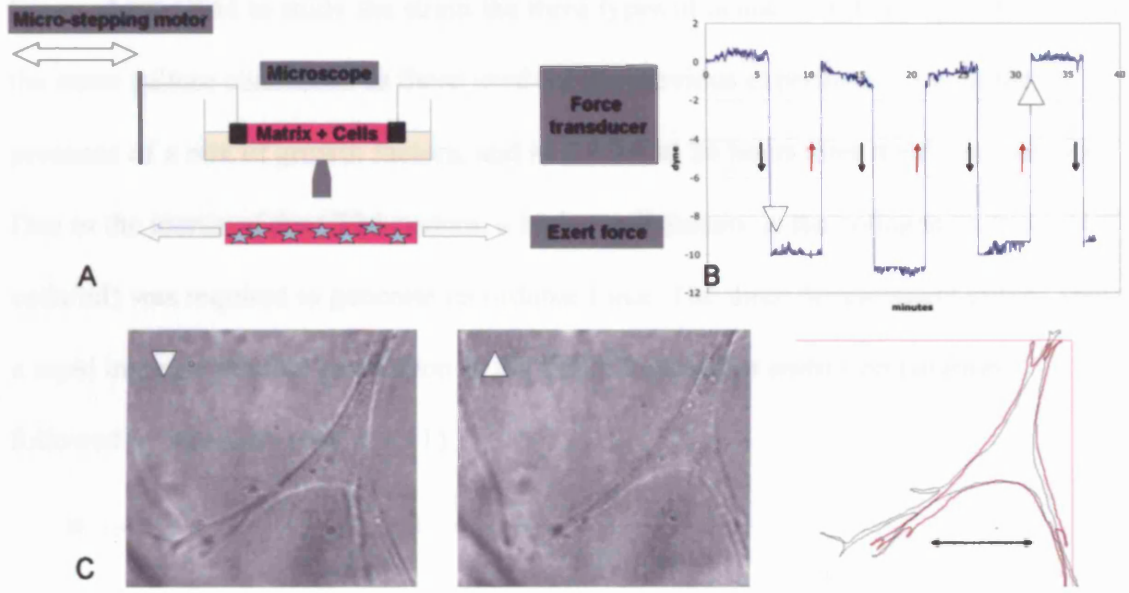

Fig. 3.1.10. Alteration of matrix strain. A: A microstepping motor applies external tension onto the fibroblast-populated collagen matrix, or relaxes cell-generated internal strain. The cellular response both in terms of dynamic behaviour and of force generation can be recorded as previously described. **B and C: Recording of cell behaviour following changes in external strain: force recording and cell shape reflect changes in matrix tension.** Human corneal fibroblasts were seeded into collagen matrix at a cell density of 0.25×10^6 cells/ml. **B:** The tension was manually set to zero, and then altered using a cycle of stretching and relaxation episodes of 10D each every 5 minutes, repeated 4 times, as reflected in the force recording curve (black arrows: tension reduced, red arrows: tension increased). **C:** Left: Cell imaged after first relaxation, at the timepoint indicated on the force recording. Centre: Same cell, imaged after external tension applied several times, as indicated on the force recording. Right: After adjustment for changes in cell position by using the Registration module in Openlab, the response of the cell to the stretching regime (red outline) is reflected in a decrease in the angle between the cell processes at the bottom (arrow), with elongation of the cell in the direction of the strain. The number of branching points in these protrusions has also decreased.

We used the CFM to study the strain the three types of ocular fibroblasts generate under the same culture conditions as those used for the previous experiments, i.e. in the presence of a mix of growth factors, and in the initial 24 hours after matrix preparation. Due to the inertia of the CFM system, a higher cell density in the collagen matrices (10^6 cells/ml) was required to generate recordable force. The force development curves show a rapid increase in force generation in the first 6 hours after matrix preparation, followed by a plateau (Fig. 3.1.11).

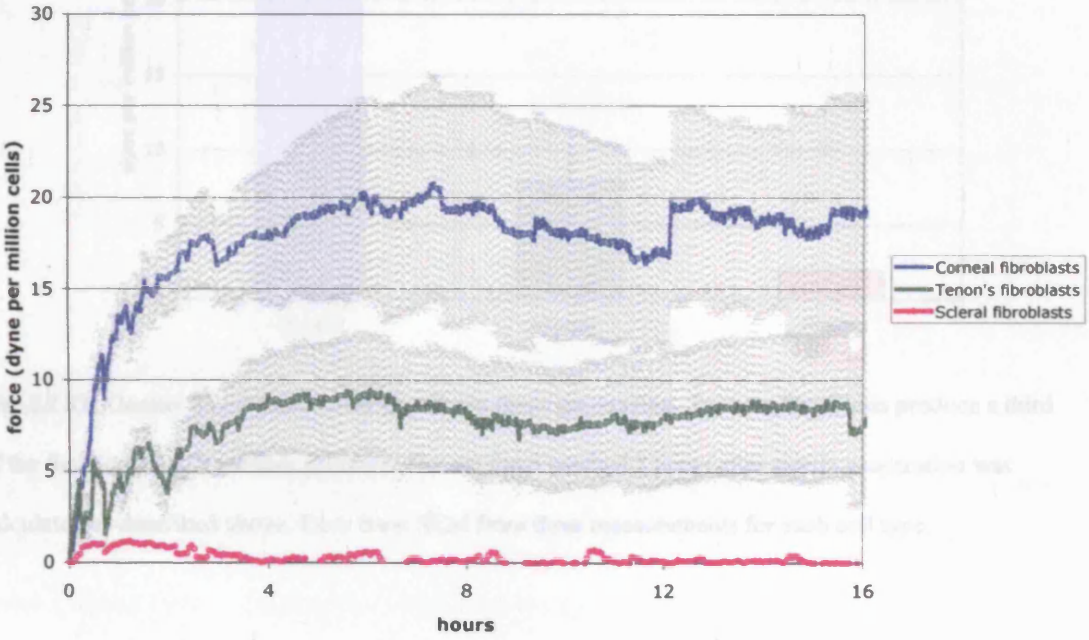

Fig. 3.1.11. Corneal fibroblasts generate more force than Tenon's fibroblasts, whilst scleral fibroblasts hardly generate any. On the culture force monitor, collagen matrices were seeded with 10^6 corneal, 10^6 Tenon's or $7x10^6$ scleral fibroblasts per ml and floated in serum-supplemented medium. Cell-free matrices were prepared as negative controls. The force associated with matrix contraction was recorded continuously for 24 hours. The maximum force reached 7 hours after matrix preparation in cell-free collagen matrices (n=5) was subtracted from the values reached by the cell-seeded matrices (corneal: n=6, Tenon's n=7, scleral n=1), and the resulting figure corrected for the cell number, to compare the mean maximum force generated by 10^6 cells of each type. The graph shows the mean force for each cell type; SEM was omitted because of number of data points. These curves were obtained by the CFM component of the SIM-CFM, separated from the microscope, under standard tissue culture conditions.

During our experiments, we had observed that the different cell types seemed to differ in cell size. As cell size might in part underlie the difference in force generation, we calculated the cell volume for each cell type. Tenon's have about 75%, and scleral fibroblasts about 22% of the volume of corneal fibroblasts (Fig. 3.1.13).

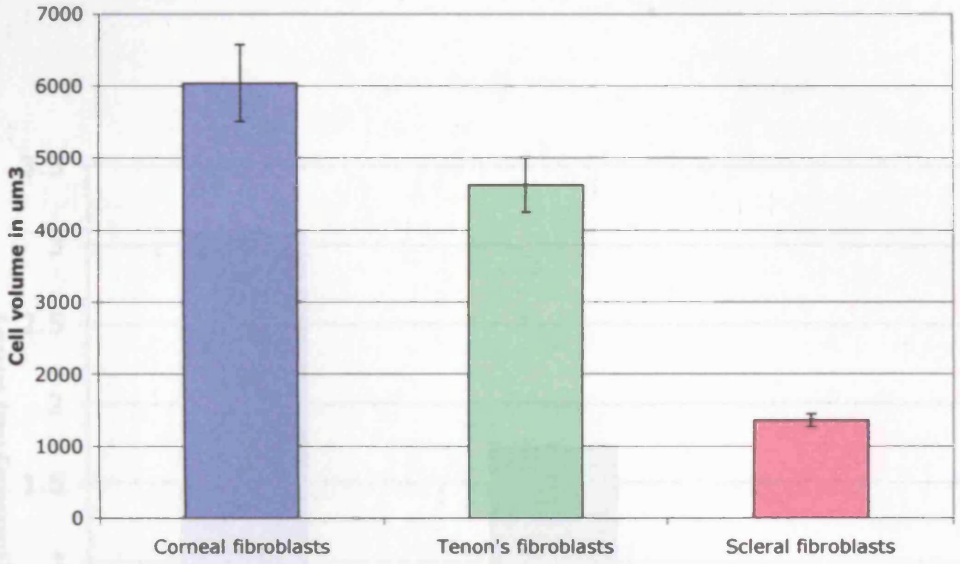

Fig. 3.1.13. Ocular fibroblasts differ greatly in size. Corneal fibroblasts are bigger than Tenon's, and much bigger than scleral fibroblasts.

Corneal, Tenon's and scleral fibroblasts were trypsinised and fixed using 3.7% formaldehyde in cytobuffer. Using a confocal microscope, photos were taken of cells in suspension. The cell diameter was measured on two axes on these digital photos using ImageJ, and the cell volume was calculated from the cell diameter. Cell numbers: Corneal (n=30), Tenon's (n=38) and scleral fibroblasts (n=22). Error bars show SEM; all differences statistically significant with $p<0.005$ (t-test assuming unequal variances).

By dividing the measured force by the cell volume, the intrinsic cellular force can be calculated. The values for intrinsic force are in a similar range for all three types of fibroblasts, indicating that it is likely that one common mechanism underlies force generation (Fig. 3.1.14). However, even the intrinsic force differs between the three cell types, suggesting that in addition to cell size, other factors are at play.

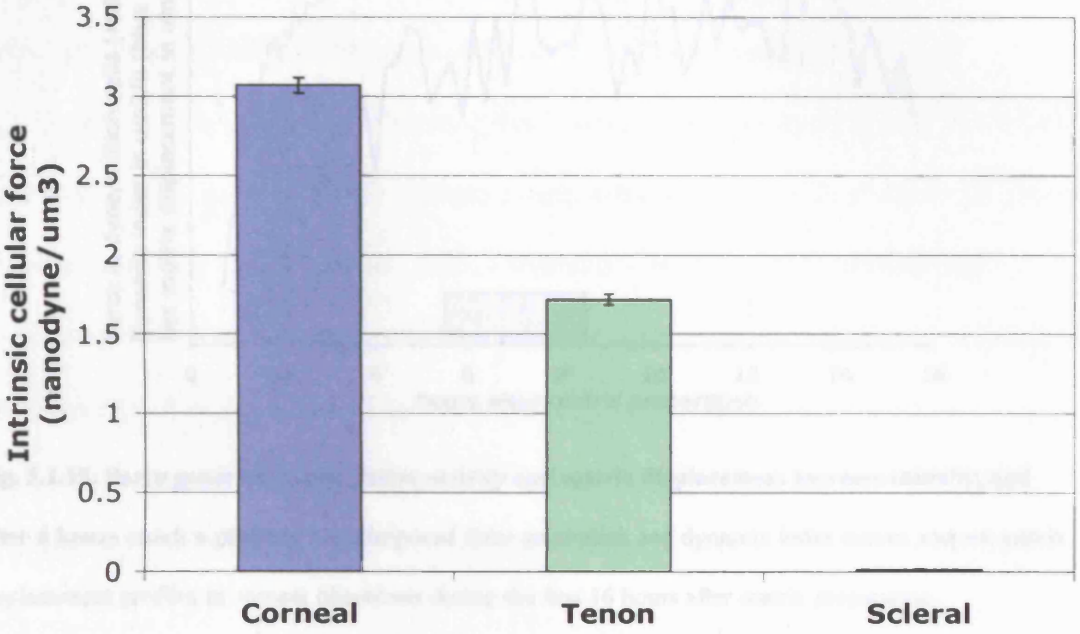

Fig. 3.1.14. The intrinsic cellular force is in the same range for all three cell types, indicating the presence of a common mechanism of force generation.

Force measured by CFM was divided by mean cell volume, resulting in the value for intrinsic cellular force (nanodyne/ μm^3).

In summary, three of the measured parameters follow a similar course, with an initial sharp increase during the first 5-7 hours after matrix preparation, followed by a plateau: maximum cell length, dynamic index, and force generation. In addition, net matrix displacement is high in the first 2 hours, and then decreases (Fig. 3.1.15).

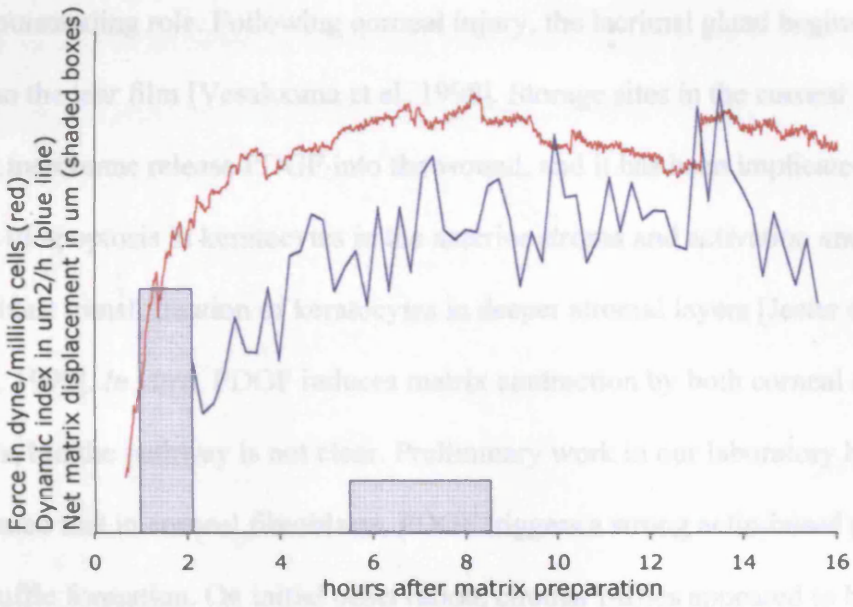

Fig. 3.1.15. Force generation, protrusive activity and matrix displacement increase initially, and after 6 hours reach a plateau. Superimposed force generation and dynamix index curves and net matrix displacement profiles in corneal fibroblasts during the first 16 hours after matrix preparation.

In conclusion, protrusive and retractile activity, not migration, is the predominant dynamic cell behaviour in the early phase of matrix contraction. It is possible to construct a device which visualises cell behaviour, cell-matrix interaction and simultaneously measures the strain exerted by cells onto the matrix. This demonstrates that protrusive activity correlates with net matrix displacement and cellular force generation. The intrinsic cellular force of the three types of ocular fibroblasts lies within the same range, indicating that cells might use a common mechanism to generate force.

3.2. The pathway from PDGF receptor to matrix contraction

Both *in vivo* and *in vitro*, PDGF plays an important role in the activation of corneal fibroblasts. Amongst all cytokines involved in corneal healing and scarring, PDGF plays an outstanding role. Following corneal injury, the lacrimal gland begins to secrete PDGF into the tear film [Vesaluoma et al. 1998]. Storage sites in the corneal epithelial basement membrane release PDGF into the wound, and it has been implicated in the induction of apoptosis in keratocytes in the anterior stroma and activation and myofibroblast transformation of keratocytes in deeper stromal layers [Jester et al. 1999; Kim et al. 1999]. *In vitro*, PDGF induces matrix contraction by both corneal and dermal fibroblasts, but the pathway is not clear. Preliminary work in our laboratory had demonstrated that in corneal fibroblasts, PDGF triggers a strong actin-based phenotype: circular ruffle formation. On initial observation, circular ruffles appeared to be associated with retraction of cellular protrusions, and this seemed to be a candidate pathway for PDGF-mediated matrix contraction. We therefore decided to explore the pathway from PDGF receptor to matrix remodelling by corneal fibroblasts in detail.

3.2.1. PDGF is an important stimulator of matrix contraction in corneal fibroblasts

We first sought to determine the role PDGF plays in stimulating matrix contraction by corneal fibroblasts as compared to the mix of growth factors. We therefore prepared collagen matrices as described before, but stimulated them with PDGF and compared

the resulting matrix contraction profile to that obtained after serum stimulation.

a) PDGF induces nearly as much matrix contraction as serum

When stimulated by PDGF-BB, corneal fibroblasts contract collagen matrix nearly as efficiently as when stimulated by serum: 24 hours after matrix preparation, contraction with PDGF-stimulation reaches 70% of that of serum stimulation (Fig. 3.2.1).

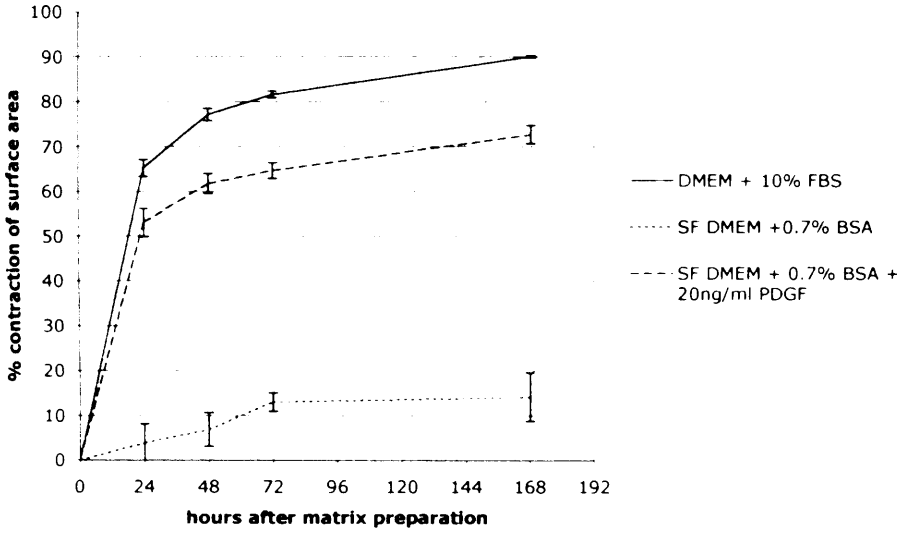

Fig. 3.2.1. In corneal fibroblasts, PDGF induces 70% of the matrix contraction observed after serum stimulation. HCF were embedded in collagen matrix at a density of 40,000 cells/ml. After 30 minutes of polymerisation, the matrices were detached from the wells they were cast in and floated in either DMEM with 10% FBS (positive control), serum-free DMEM with 0.7% BSA (negative control), or serum-free DMEM with 0.7% BSA and 20ng/ml PDGF. Digital photos were taken every 24 hours, and the progressive reduction in surface area calculated from the matrix diameter measured in Image J. Error bars represent SEM.

b) PDGF inhibitors greatly reduce serum-induced matrix contraction by corneal fibroblasts

We confirmed the importance of PDGF-mediated matrix contraction in the context of stimulation by multiple growth factors by applying three inhibitors of the PDGF pathway: anti-PDGF-receptor beta antibody and AG1295 and Trapidil, a tyrphostin and a triazolopyrimidine which inhibit PDGF-receptor phosphorylation.

We first determined the efficiency of these three PDGF antagonists in inhibiting matrix contraction after isolated PDGF stimulation. As a second step, we then used the same inhibitors on serum-stimulated matrices to determine the percentage of global contraction that can be attributed to PDGF present in serum. Lastly, we conducted cell viability studies after exposure to AG1295 and Trapidil to investigate whether toxicity might explain part of their inhibitory effect.

1. Identification of inhibitors of PDGF-mediated matrix contraction

As the literature and our own preliminary data indicated that only the BB isoform of PDGF elicits circular ruffling, we used this isoform in our matrix contraction experiments. In order to test whether matrix contraction could be inhibited by an anti-PDGF-BB-antibody, we co-administered the growth factor and its competitive antibody, varying the concentration of the antibody and observing the effect on matrix contraction. Matrix contraction induced by 20ng/ml PDGF-BB can be inhibited by application of the specific antibody at a concentration of 0.5 to 1 μg/ml (Fig. 3.2.2.).

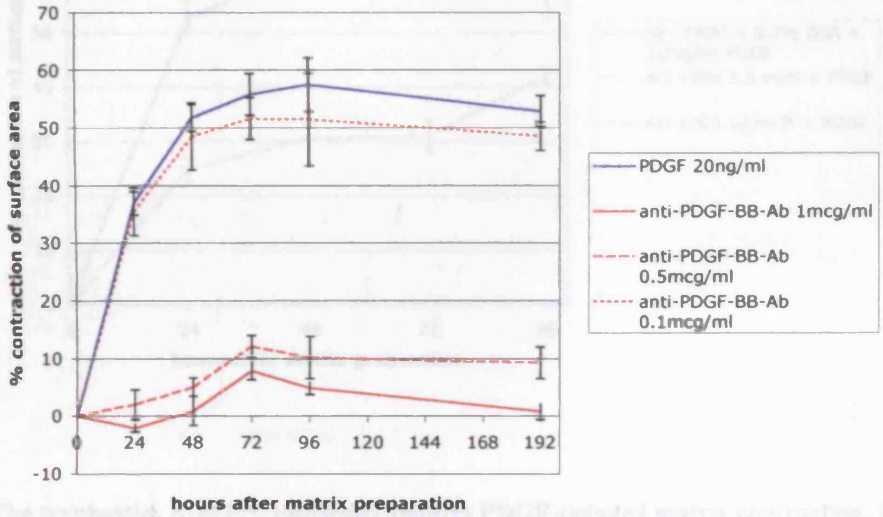

Fig. 3.2.2. Anti-PDGF-BB-antibody efficiently reduces PDGF-induced matrix contraction. HCF were embedded in collagen matrix at a density of 40,000 cells/ml. After 30 minutes of polymerisation, the matrices were detached from the casting wells and floated in serum-free DMEM with 0.7% BSA and 20ng/ml PDGF without antagonist, or with 0.5 or 1 μg antibody/ml. Digital photos were taken every 24 hours, and the progressive reduction in surface area calculated from the matrix diameter measured in Image J. The results shown are from a triplicate set of collagen matrices. Error bars represent SEM.

As the PDGF receptor is a tyrosine kinase receptor, its signalling can be inhibited by tyrphostins such as AG1295, a chemical inhibitor of PDGF receptor kinase activity. We investigated whether AG1295 reduces matrix contraction by corneal fibroblasts stimulated exclusively by PDGF. AG1295 inhibits PDGF-induced matrix contraction in dose-dependent fashion. A concentration of 10μM AG1295 halves matrix contraction (Fig. 3.2.3).

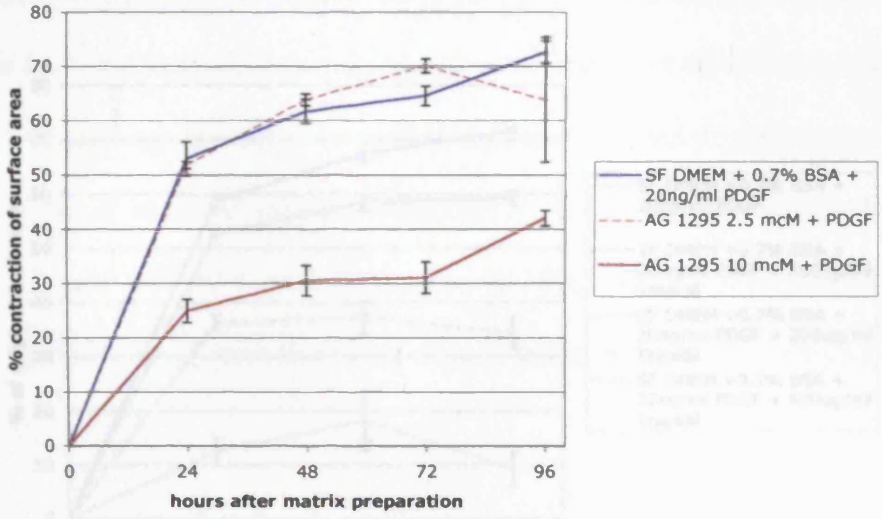

Fig. 3.2.3. The tyrphostin, AG1295, efficiently reduces PDGF-induced matrix contraction. HCF were embedded in collagen matrix at a density of 40,000 cells/ml. After 30 minutes of polymerisation, the matrices were detached from the casting wells and floated in serum-free DMEM with 0.7% BSA and 20ng/ml PDGF without AG1295, or with 2.5μM or 10μM AG1295. Digital photos were taken every 24 hours, and the progressive reduction in surface area calculated from the matrix diameter measured in Image J. The results shown are from a triplicate set of collagen matrices. Error bars represent SEM.

Trapidil, a triazolopyrimidine which also inhibits PDGF-receptor phosphorylation, has been used on other cell types to inhibit PDGF-mediated events, and inhibits corneal fibroblast proliferation *in vitro* [Knorr et al. 1999]. We investigated whether Trapidil reduces PDGF-mediated matrix contraction by corneal fibroblasts. Indeed, Trapidil inhibits PDGF-induced matrix contraction in dose-dependent fashion. A concentration of 200µg/ml Trapidil reduces matrix contraction over the first 24 hours by 39%. It also inhibits any further contraction after the early phase (Fig. 3.2.4).

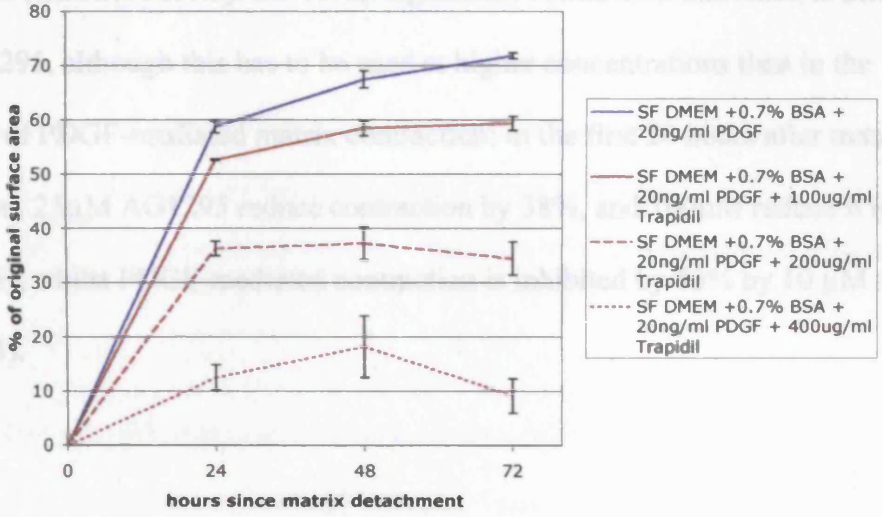

Fig. 3.2.4. The PDGF-pathway inhibitor, Trapidil, efficiently reduces PDGF-induced matrix contraction. HCF were embedded in collagen matrix at a density of 40,000 cells/ml. After 30 minutes of polymerisation, the matrices were detached from the wells they were cast in and floated in serum-free DMEM with 0.7% BSA and 20ng/ml PDGF without Trapidil, or with 100, 200 or 400 µg/ml Trapidil. Digital photos were taken every 24 hours, and the progressive reduction in surface area calculated from the matrix diameter measured in Image J. The results shown are from a triplicate set of collagen matrices. Error bars represent SEM.

2. Importance of PDGF-mediated matrix contraction by corneal fibroblasts in the presence of multiple growth factors

In order to assess whether PDGF-blockade via these three antagonists might also inhibit matrix contraction by corneal fibroblasts in the presence of a mix of growth factors, we stimulated corneal fibroblasts in collagen matrix with serum in the presence of each inhibitor. In our model, the anti-PDGF-BB-antibody has no effect on serum-induced matrix contraction, even at the highest concentration used to inhibit PDGF-induced contraction (data not shown). However, significant contraction inhibition is achieved with AG1295, although this has to be used at higher concentrations than in the inhibition of PDGF-mediated matrix contraction: in the first 24 hours after matrix preparation, 25μM AG1295 reduce contraction by 38%, and 100μM reduce it by 56% (Fig. 3.2.5), whilst PDGF-mediated contraction is inhibited by 53% by 10 μM AG1295 (Fig. 3.2.3).

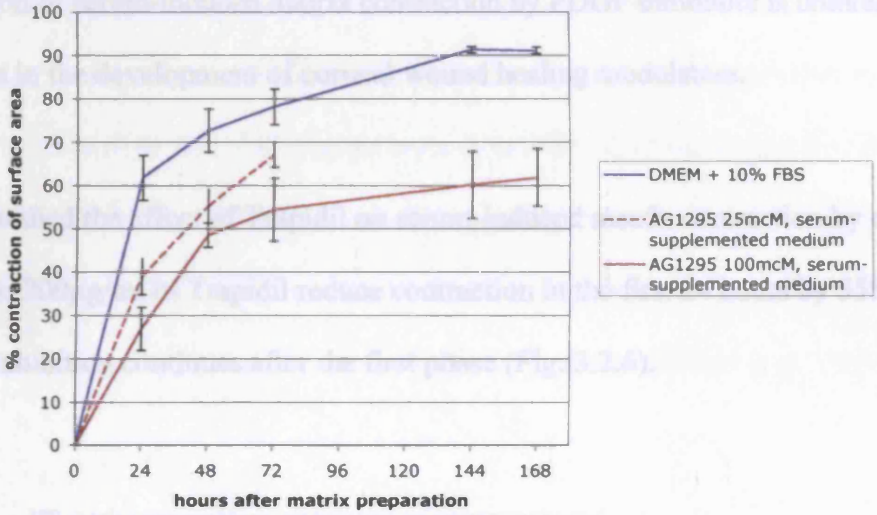

Fig. 3.2.5. AG1295 reduces serum-induced matrix contraction. The experiment was repeated as detailed in Fig. 3.2.2. Matrices were floated in DMEM with 10% FBS without AG1295, or with 25µM or 100µM AG1295. The results shown are from two triplicate sets of collagen matrices. Error bars represent SEM.

There are two possible explanations for the poor inhibition of serum-induced matrix contraction by inhibitors of the PDGF pathway: either the bovine serum used here does not contain sufficient amounts of PDGF to stimulate PDGF-mediated matrix contraction, or it does not contain sufficient amounts of isoform BB. In either case, serum and PDGF seem to induce corneal fibroblasts to contract matrix via different pathways, consistent with reports on PDGF- and LPA/serum-induced matrix contraction by dermal fibroblasts [Abe et al. 2003]. However, in the cornea, PDGF induced contraction is likely to be the physiologically more relevant pathway. Unlike in skin, the wound healing response in the avascular cornea is not initiated by bleeding, thrombus formation and fibrinolysis. Rather, trauma to epithelium and epithelial basement membrane releases growth factors, particularly PDGF, from extracellular storage places

and increases secretion of growth factors into the tear film. On this background, the lack of inhibition of serum-induced matrix contraction by PDGF inhibitors is unlikely to be of concern in the development of corneal wound healing modulators.

We also studied the effect of Trapidil on serum-induced matrix contraction by corneal fibroblasts. 200µg/ml of Trapidil reduce contraction in the first 24 hours by 55%. In addition, inhibition continues after the first phase (Fig. 3.2.6).

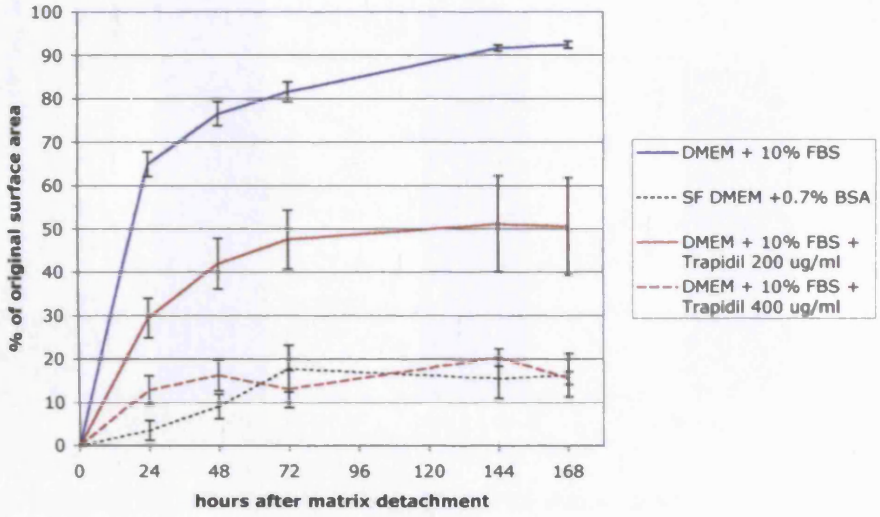

Fig. 3.2.6. Trapidil reduces serum-induced matrix contraction to a similar degree as PDGF-induced contraction. The experiment was repeated as detailed above. Matrices were floated in DMEM with 10% FBS without Trapidil, or with 200 or 400 µg/ml Trapidil. The results shown are from four (controls and Trapidil 200µg/ml) or two (Trapidil 400µg/ml) triplicate sets of collagen matrices. Error bars represent SEM.

With view to the lack of strong contraction inhibition by the PDGF-receptor antibody and the PDGF receptor tyrosine kinase inhibitor, the similarity in inhibition observed in the Trapidil experiment is surprising. One possible explanation is that in this assay and in these concentrations, Trapidil might have a cytotoxic effect on corneal fibroblasts, rather than a specific inhibitory effect on the signalling cascade. Trapidil inhibits bovine corneal fibroblast proliferation, but based on staining with trypan blue does not seem toxic to these cells when cultured in two-dimensional culture [Knorr et al. 1999].

3. Assessment of toxic effects of AG1295 and Trapidil on corneal fibroblasts

To see whether cell toxicity might contribute to the observed reductions in matrix contraction, we performed a cell viability assay for both AG1295 and Trapidil. At concentrations which interfere with protrusive activity and reduce both PDGF- and serum-induced matrix contraction, AG1295 is only mildly toxic (Fig. 3.2.7).

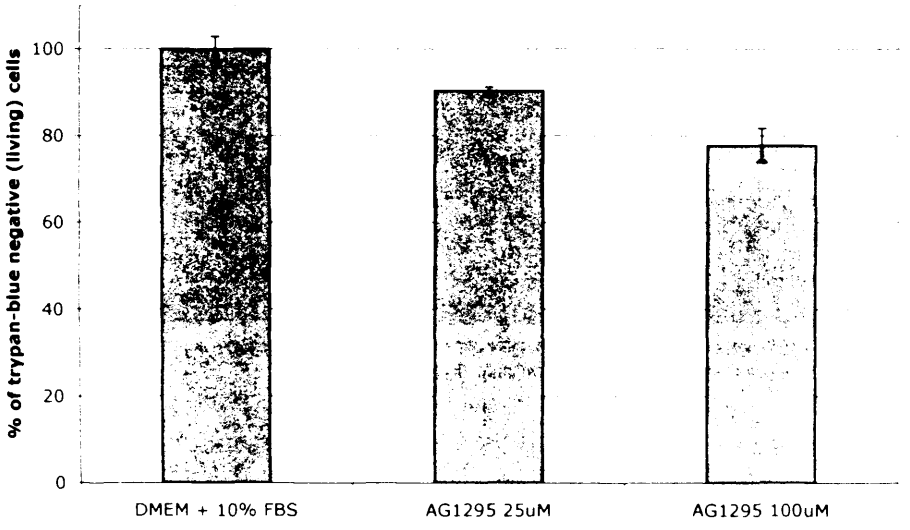

Fig. 3.2.7. The effect of AG1295 on matrix contraction is not due to cellular toxicity. HCF were embedded in collagen matrix at a density of 40,000 cells/ml. After 30 minutes of polymerisation, the matrices were detached from the wells they were cast in and floated in DMEM with 10% FBS without AG1295, or with 25μM or 100μM AG1295. After 24 hours, the collagen matrices were dissolved by collagenase, and the cells recovered by centrifugation. The vital dye, trypan blue, was added, and trypan blue-positive and -negative cells were counted. The proportion of viable cells was normalised to those observed in untreated matrices. Results shown are from a triplicate set of matrices; $p<0.05$ comparing 25μM AG1295 to DMEM with 10% FBS, and $p<0.01$ comparing 100μM AG1295 to DMEM with 10% FBS (t-test assuming unequal variances). Error bars: SEM.

Moderate concentrations of Trapidil, on the other hand, seem toxic to corneal fibroblasts in collagen matrix (Fig. 3.2.8). However, we only conducted this experiment once, and the proportion of dead cells seemed higher in this assay than in matrices used for live microscopy.

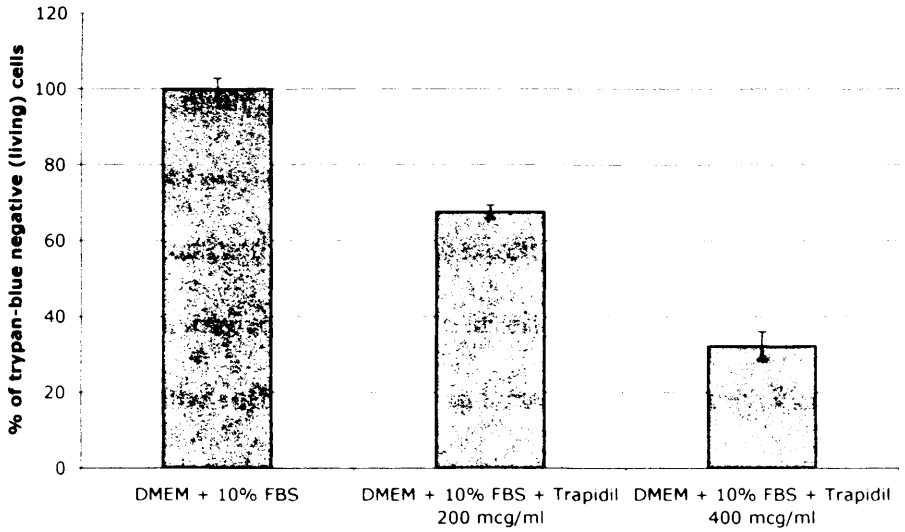

Fig. 3.2.8.Trapidil is toxic to corneal fibroblasts in collagen matrix. HCF were embedded in collagen matrix at a density of 40,000 cells/ml. After 30 minutes of polymerisation, the matrices were detached from the wells they were cast in and floated in DMEM with 10% FBS without Trapidil, or with 200 or 400 μg/ml Trapidil. After 24 hours, the collagen matrices were dissolved by collagenase, and the cells recovered by centrifugation. The vital dye, trypan blue, was added, and trypan blue-positive and -negative cells were counted. The proportion of viable cells was normalised to those observed in untreated matrices. Results shown are from a triplicate set of collagen matrices; all test statistically significant with $p<0.01$ (t-test assuming unequal variances). Error bars: SEM

In summary, PDGF is an important stimulator of matrix contraction by corneal fibroblasts. The PDGF-stimulated response reaches 70% of that induced by serum, and the use of antagonists of early steps of the PDGF pathway inhibits a significant part of serum-induced contraction.

3.2.2. PDGF stimulates a major protrusive activity in corneal fibroblasts: circular ruffling

As PDGF plays an important role in matrix contraction by corneal fibroblasts, we decided to investigate the pathway from PDGF receptor to matrix contraction in more detail. Preliminary work in our laboratory had shown that in corneal fibroblasts in two-dimensional or planar culture, PDGF elicits a dramatic actin-based cellular activity: circular ruffling. As we had previously demonstrated that acto-myosin dynamics underlie early matrix contraction, we hypothesized that the circular ruffling pathway might be involved in matrix contraction. We tested this hypothesis by first characterising the circular ruffling pathway in terms of morphology, kinetics and dose-response effects, then identified inhibitors of this phenomenon in two-dimensional cell cultures, and finally applied the same inhibitors to corneal fibroblasts in three-dimensional collagen matrix. Section 3.2.2. presents the results from the two-dimensional, and section 3.2.3. those from the three-dimensional studies.

a) Circular ruffling morphology and kinetics in corneal fibroblasts

In corneal fibroblasts grown on a rigid planar substratum, PDGF-BB induces two types of actin-based ruffling activity: peripheral ruffling at the cell edge, and the formation of circular ruffles on the dorsal cell surface (Fig. 3.2.9). As circular ruffling has not previously been described in corneal fibroblasts, we first characterised its appearance and dynamic behaviour in our model. In serum-starved cells, circular ruffles (CR) begin to form on the dorsal cell surface within minutes of stimulation with PDGF-BB. These ruffles begin in the cell periphery and then move towards the nucleus, but never move

over the nucleus. The circles close when opposing ridges meet, about 20 to 30 minutes after their first appearance. Circular ruffles only occur once after stimulation. During and after CR formation and closure, cells also show peripheral or edge ruffling.

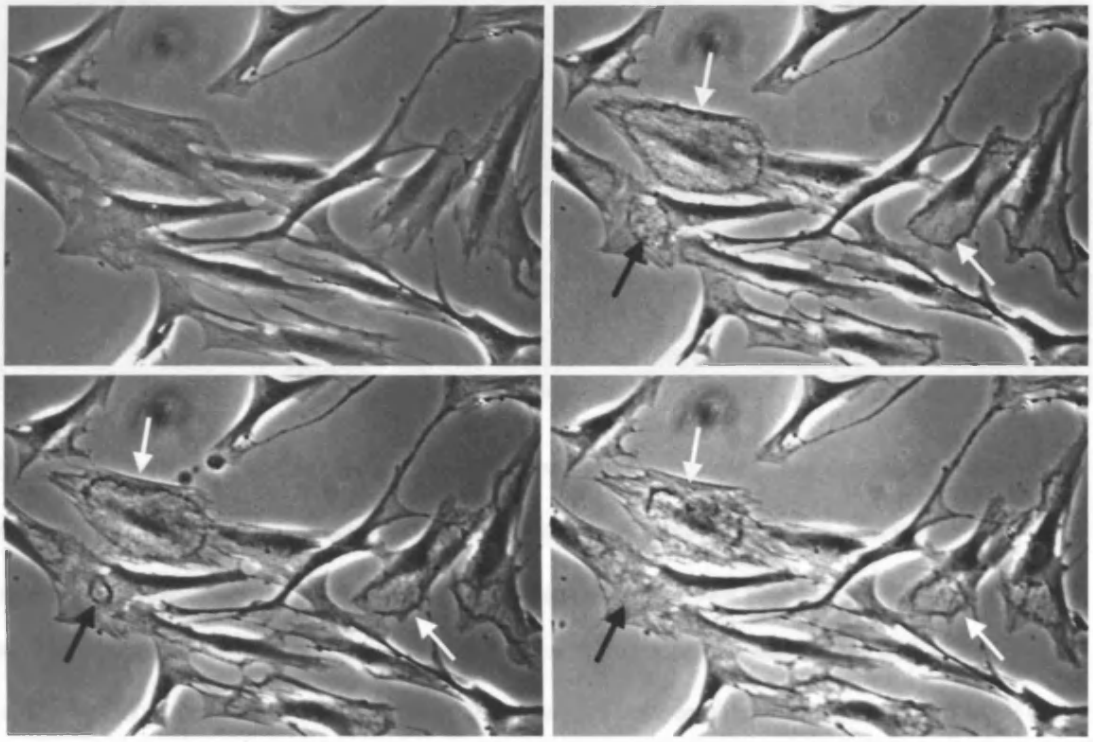

Fig. 3.2.9. In corneal fibroblasts, PDGF-BB induces a dramatic actin phenotype: circular ruffles. Human corneal fibroblasts were grown on a planar surface and serum-starved overnight. Timelapse phase contrast microscopy images were acquired every minute for 2 minutes before and 28 minutes after stimulation with 40 ng/ml PDGF-BB. Top left: prior to growth factor stimulation, the plasma membrane is smooth. Top right: 15 minutes after PDGF stimulation, CR are clearly visible as dark rings in the periphery of cells (arrows). Bottom left: 22 minutes after PDGF application, CR have constricted towards the cell centre. Bottom right: 28 minutes after stimulation, some CR have closed concentrically and disappeared (black arrow). Others are still in the process of constricting (white arrows).

To confirm that these circular ruffles are identical to those described in other cells after tyrosine kinase receptor stimulation [Dharmawardhane et al. 2000; Araki et al. 2003; Krueger et al. 2003], we confirmed that they are located on the dorsal cell surface and that they contain f-actin and components of the arp2/3 complex (Fig. 3.2.10).

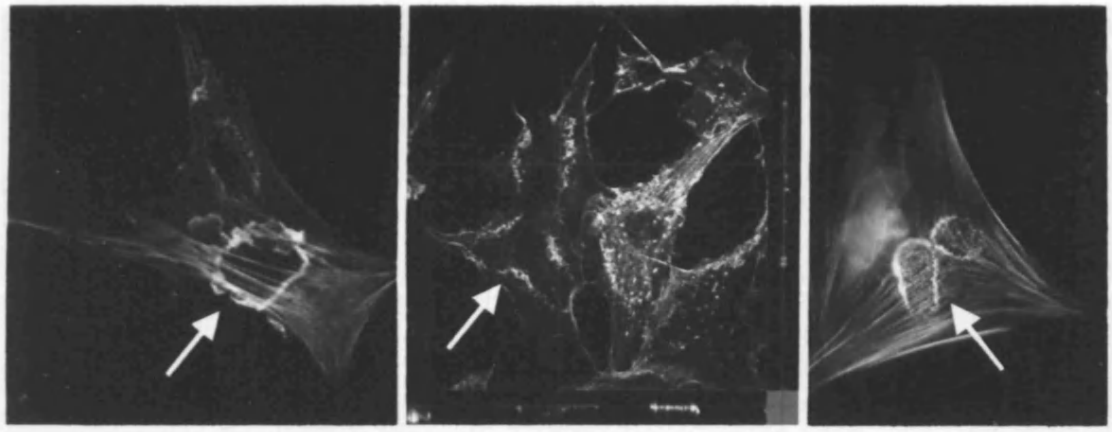

Fig. 3.2.10. Circular ruffles in corneal fibroblasts contain f-actin and components of the arp2/3 complex. HCFs were seeded on acid-washed coverslips in the presence of serum, allowed to form contacts to the substratum, then serum-starved overnight and stimulated with PDGF 50ng/ml the next day. Eight minutes after stimulation, cells were fixed with formaldehyde and stained with FITC-phalloidin (left and centre) or immunostained for the arp2/3 complex (right: monoclonal anti-arp3) and imaged on an epifluorescence microscope. Left: CR are rich in f-actin. Centre: CRs are located on the dorsal surface of the cell. Right: CRs are enriched in components of the arp2/3 complex.

The circular appearance of dorsal ruffles might be explained by a pre-existing circular arrangement or clustering of the PDGF receptor on the cell surface. In order to investigate PDGF receptor distribution, we immunostained fixed corneal fibroblasts with and without PDGF stimulation for the PDGF receptor. The receptor is distributed evenly over the cell surface. Higher intensity of staining is observed in the perinuclear area. In stimulated cells, the resulting circular ruffles are not enriched in PDGF receptor (Fig. 3.2.11). This finding is contrary to another report, which used cells expressing EGFR-GFP (epidermal growth factor receptor, coupled with green fluorescent protein),

and found homogenous receptor distribution before, but clustering in circular ruffles after stimulation [Orth et al. 2006]. The difference in results might arise from differences in technique (imaging of living versus fixed cells).

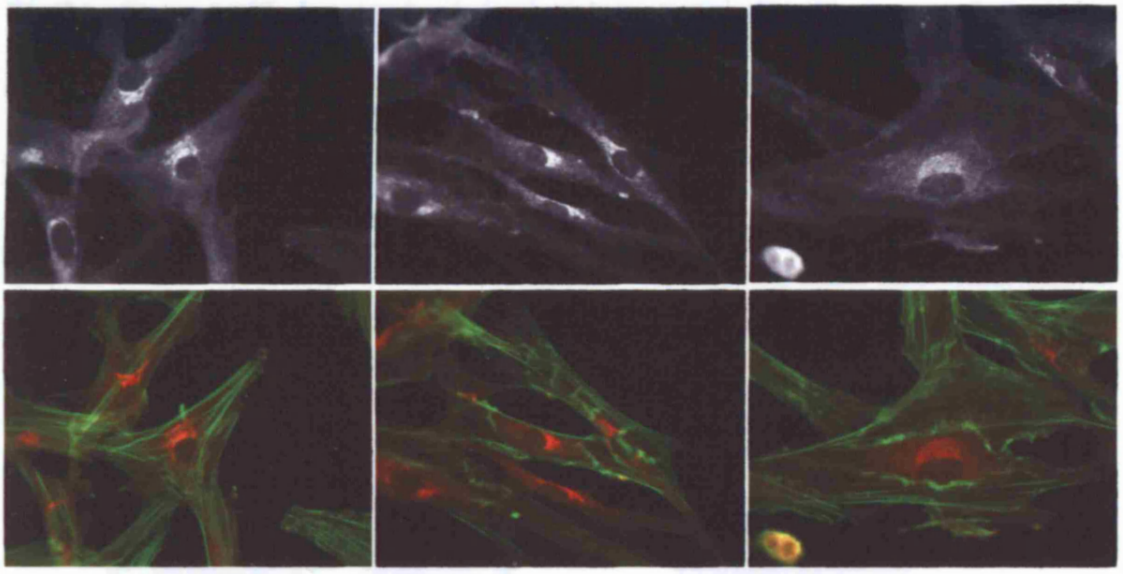

Fig. 3.2.11. PDGF receptors are distributed over the cell surface, and are not arranged in circular structures. HCFs were seeded on acid-washed coverslips in the presence of serum, allowed to form contacts to the substratum, then serum-starved overnight and stimulated with PDGF 20ng/ml the next day. Optimal stimulation time until CR ruffle formation was determined on a timelapse sequence. Six minutes after stimulation, cells were fixed with formaldehyde and immunostained for the PDGF receptor (top row, bottom row: red) and stained with FITC-phalloidin (bottom row: green) and imaged on an epifluorescence microscope. Left: unstimulated cells. Centre and right: PDGF-stimulated cells.

In areas of circular ruffling, stress fibre dissolution has been reported to occur, and it has been hypothesized that circular ruffling might prepare cells for the transition from static to motile state [Krueger et al. 2003]. On our early dynamic timelapse image sequences, circular ruffling seemed to be associated with retraction of cell processes. We therefore quantified protrusive behaviour by counting the occurrences of protrusion retraction and formation on these timelapse sequences, and found that they occur in equal proportion (Fig. 3.2.12).

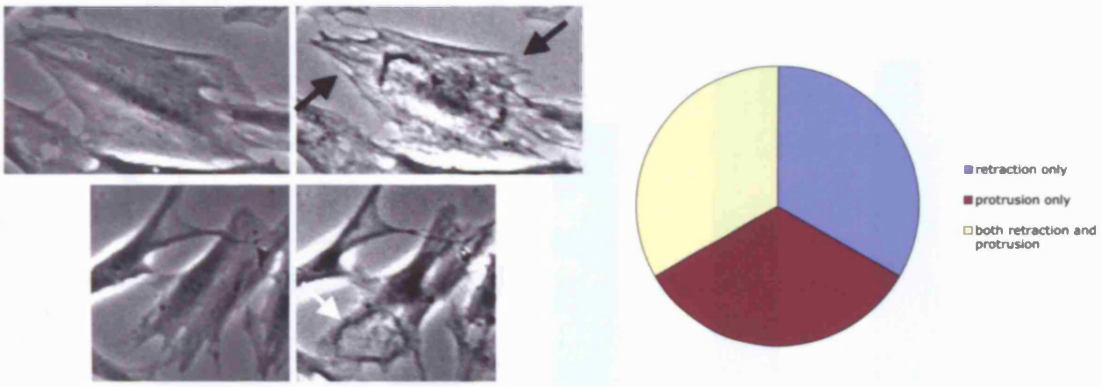

Fig. 3.2.12. Circular ruffling is associated with simultaneous retraction and protrusion of cellular processes.

Timelapse images of cells grown on a planar surface after PDGF stimulation were obtained as described. Cells were prepared and stimulated as described above. Left: cells prior to and 28 after stimulation with PDGF. Retraction (black arrows) and extension (white arrow) of protrusions in association with circular ruffles. Right: For quantitation, fifteen cells were analysed for shape change. Protrusion and retraction occurred in similar proportion.

b) Dose-response kinetics of circular ruffling

In order to optimise our experimental setup both in terms of growth factor concentration used for stimulation and time intervals used during image acquisition, we studied the dose-response kinetics of circular ruffles in our model. Higher concentrations of PDGF-BB increase the incidence of CR, until a maximal response is reached (Fig. 3.2.13).

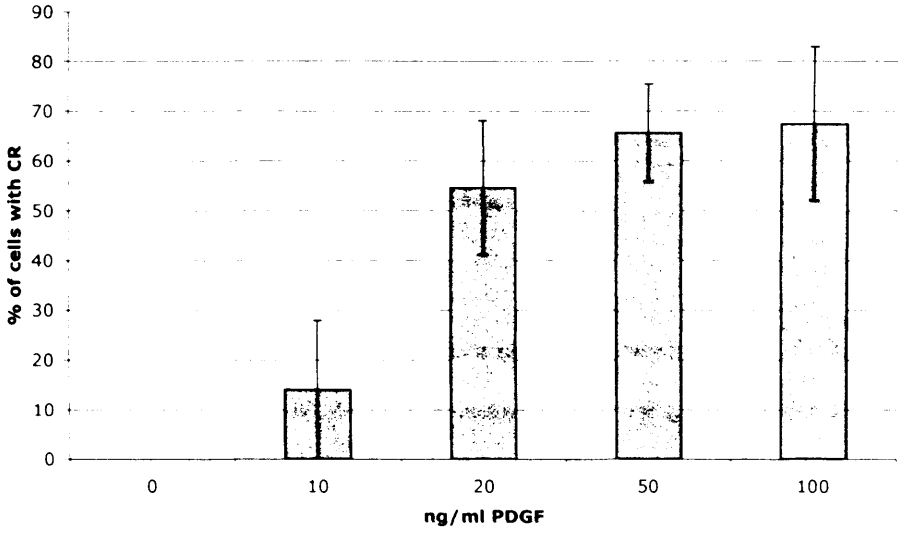

Fig. 3.2.13. The incidence of circular ruffles is dose-dependent and plateaus at stimulation with 50ng/ml PDGF.

35,000 HCFs were seeded on acid-washed coverslips in the presence of serum, allowed to attach to the substratum and spread, then serum-starved overnight and stimulated with PDGF 50ng/ml the next day. Timelapse microscopy images were acquired every 60 seconds for 5 minutes prior to and 25 minutes after stimulation with different concentrations of PDGF-BB. The number of cells with CR and the total number of cells were counted and ratioed. Shown are the means and standard errors from two independent experiments; $p>0.05$ comparing 0 versus 10 or 100 ng/ml PDGF (indicating lack of statistical significance; for the 100 ng/ml concentration this is due to the small number of experiments performed: $n=2$); $p<0.05$ comparing 0 versus 20 or 50ng/ml PDGF (t-test assuming unequal variances). Error bars: SEM.

Increasing concentrations of PDGF-BB also accelerate the appearance of CR (Fig. 3.2.14).

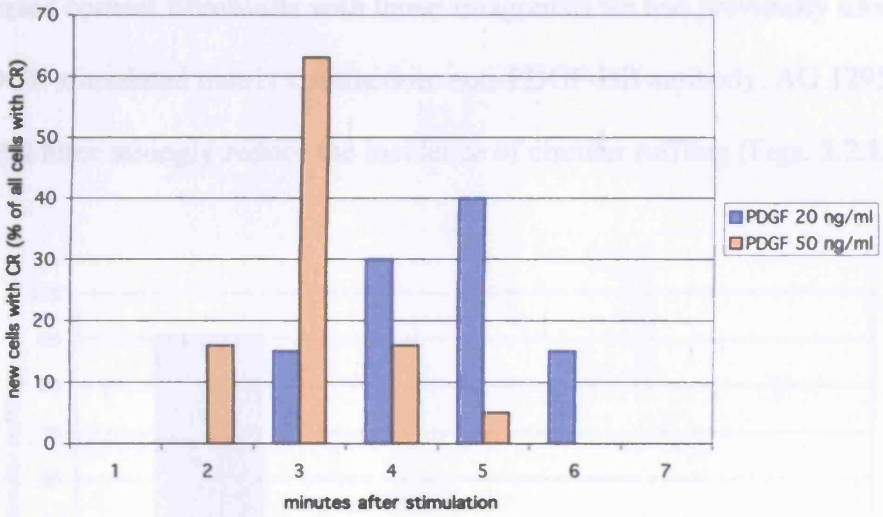

Fig. 3.2.14. Increasing concentrations of PDGF accelerate the appearance of CR. On the same timelapse images analysed for Fig. 3.2.10, the first appearance of CR was noted and related to the time elapsed since PDGF stimulation. Higher PDGF concentrations (orange) prompt faster onset of CR than lower concentrations (blue).

c) PDGF pathway blockers reduce the incidence of circular ruffling

To confirm that circular ruffles are specifically stimulated by PDGF-pathway activation, we pre-treated corneal fibroblasts with those antagonists we had previously used to inhibit PDGF-stimulated matrix contraction: anti-PDGF-BB antibody, AG 1295, and Trapidil. All three strongly reduce the incidence of circular ruffling (Figs. 3.2.15 to 17).

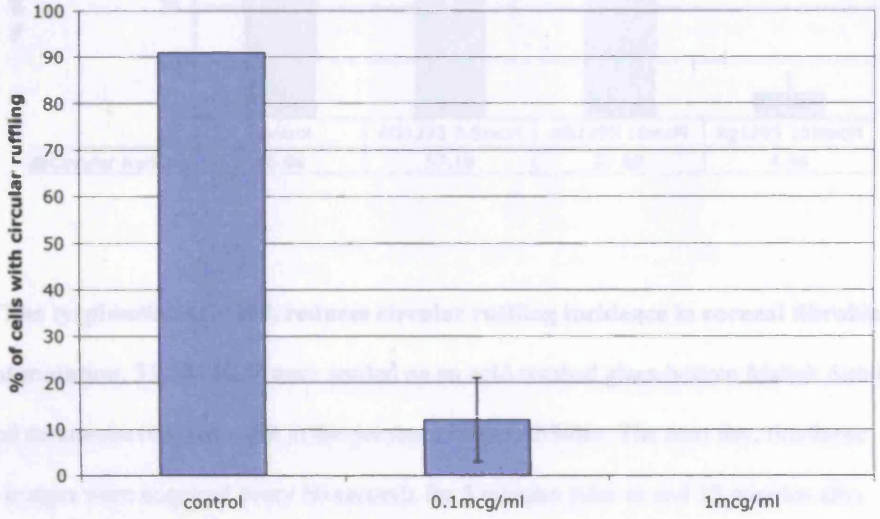

Fig. 3.2.15. Anti-PDGF-BB antibody reduces circular ruffling incidence in corneal fibroblasts after PDGF-BB stimulation. 35,000 HCF were seeded on an acid-washed glass-bottom Mattek dish (35mm diameter) and serum-starved overnight. The next day, timelapse microscopy images were acquired every 60 seconds for 5 minutes prior to and 25 minutes after stimulation with 20n/gml PDGF-BB and simultaneous application of anti-PDGF-BB antibody. The number of cells with circular ruffling and the total number of cells were counted and ratioed. Shown are the means and standard errors from one experiment; $p<0.01$ comparing control versus either antibody concentration (t-test assuming unequal variances) At antibody concentration of 1 µg/ml, circular ruffling activity is completely inhibited.

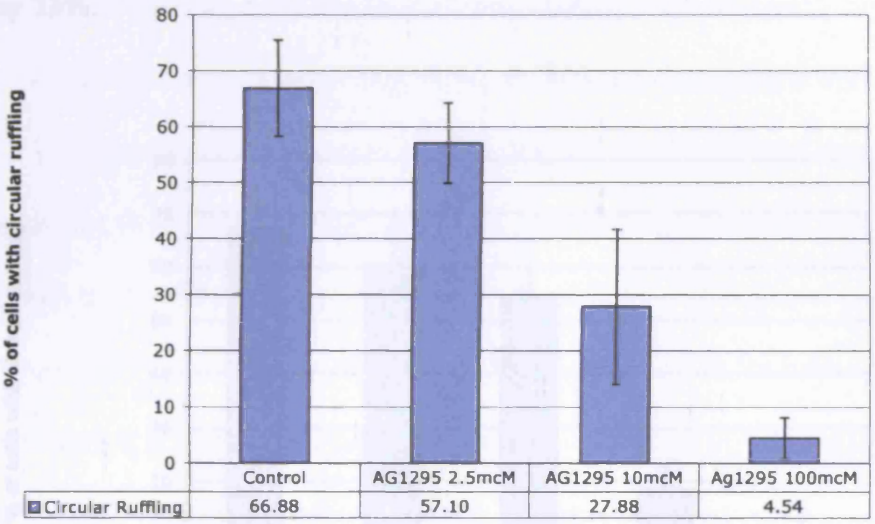

Fig. 3.2.16. The tyrphostin, AG1295, reduces circular ruffling incidence in corneal fibroblasts after PDGF-BB stimulation. 35,000 HCF were seeded on an acid-washed glass-bottom Mattek dish (35mm diameter) and serum-starved overnight in the presence of the inhibitor. The next day, timelapse microscopy images were acquired every 60 seconds for 5 minutes prior to and 25 minutes after stimulation with 20n/gml PDGF-BB in the continued presence of the inhibitor. The number of cells with circular ruffling and the total number of cells were counted and ratioed. Shown are the means and standard errors from two independent experiments; $p>0.05$ comparing control versus 2.5μM, $p<0.05$ for control versus 10μM and $p<0.01$ for control versus 100μM AG1295 (t-test assuming unequal variances).

Trapidil also reduces the incidence of CR in dose-dependent fashion (Fig. 3.2.17). Trapidil concentrations of 100μg/ml reduce circular ruffling by 19%, and 200 μg/ml reduce it by 73%.

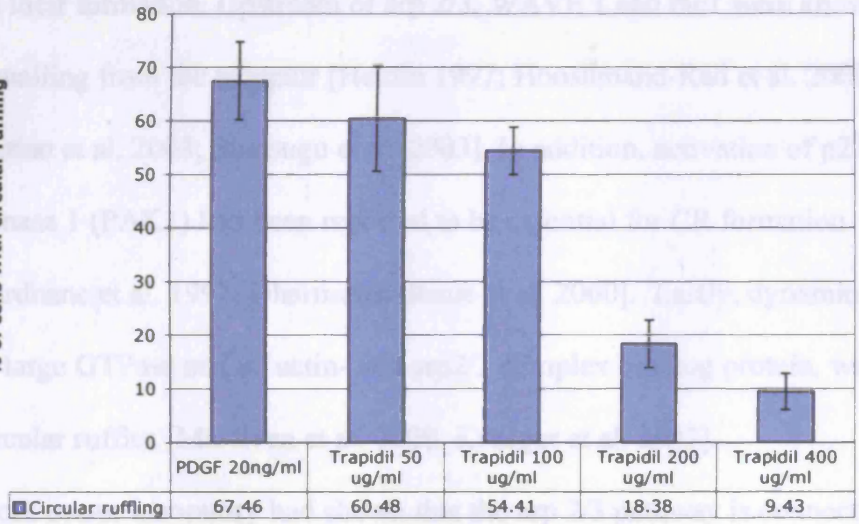

Fig. 3.2.17. Trapidil reduces circular ruffling incidence in corneal fibroblasts after PDGF-BB stimulation. 35,000 HCF were seeded on an acid-washed glass-bottom Mattek dish (35mm diameter) and serum-starved overnight in the presence of the inhibitor. The next day, timelapse microscopy images were acquired every 60 seconds for 5 minutes prior to and 25 minutes after stimulation with 20n/gml PDGF-BB in the continued presence of the inhibitor. The number of cells with circular ruffling and the total number of cells were counted and ratioed. Shown are the means and standard errors from a triplicate set of dishes; $p>0.05$ comparing PDGF control versus Trapidil 50 or 100 μg/ml, $p<0.01$ comparing PDGF control versus 200 or 400 μg/ml (t-test assuming unequal variances).

These data confirm that the circular ruffling we observed in human corneal fibroblasts is indeed a specific, PDGF-mediated phenomenon that is inhibited by known PDGF antagonists. Anti-PDGF-BB antibody competitively inhibits binding of PDGF-BB to its receptor, whilst AG 1295 and Trapidil prevent receptor phosphorylation, and all three inhibitors reduce the incidence of PDGF-induced circular ruffling in corneal fibroblasts.

d) Molecular pathways resulting in circular ruffling in corneal fibroblasts

When we began our investigation into the pathway leading to circular ruffle formation, it was known that these structures are rich in f-actin, and that the arp2/3 complex is involved in their formation. Upstream of arp 2/3, WAVE 1 and rac1 were known to mediate signalling from the receptor [Heldin 1997; Hooshmand-Rad et al. 2000; Eden et al. 2002; Anton et al. 2003; Suetsugu et al. 2003]. In addition, activation of p21-activated kinase 1 (PAK1) had been reported to be essential for CR formation [Dharmawardhane et al. 1997; Dharmawardhane et al. 2000]. Lastly, dynamin and cortactin, a large GTPase and an actin- and arp2/3 complex binding protein, were also found in circular ruffles [McNiven et al. 2000; Krueger et al. 2003].

Previous work in our laboratory had shown that the arp 2/3 pathway is connected to protrusion and ruffle formation [Machesky et al. 1998; Shao et al. 2006]. We therefore decided to investigate the role of the arp2/3 complex in circular ruffle formation by using a specific inhibitor of arp2/3-mediated protrusion formation, the WA or VCA construct. *In vitro*, the WA motif of Scar or Wasp alone is sufficient to activate arp 2/3-mediated nucleation of actin polymerization and branching of filaments. *In vivo*, the WA domain acts as a dominant negative agent, as it induces arp2/3-mediated actin polymerization throughout the cell, depleting molecules available for directed protrusion formation [Shao et al. 2006].

We micro-injected the WA domain of Scar or Wasp (Scar-/Wasp-WA) into corneal fibroblasts before stimulating them with PDGF, and found that this arp2/3 complex inhibition reduces the incidence of circular ruffles (Fig. 3.2.18).

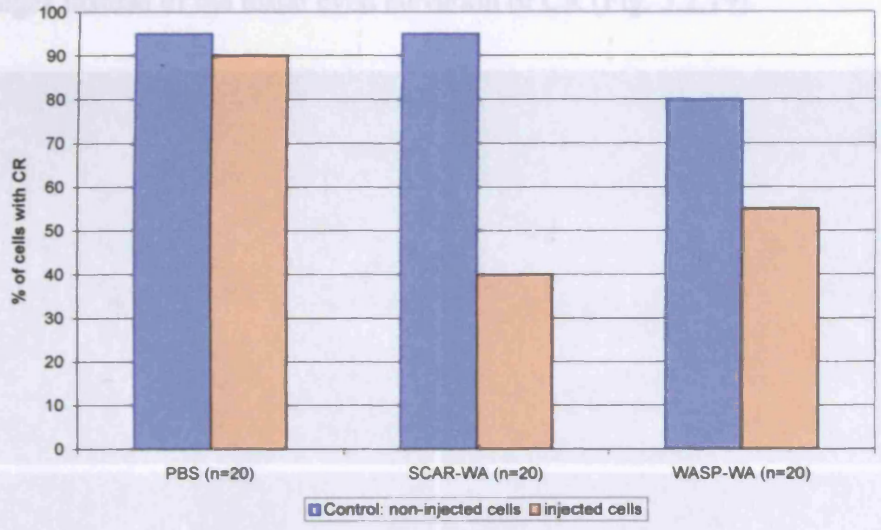

Fig. 3.2.18. Microinjection of the WA-domain of Scar or Wasp reduces the incidence of CR. HCF were seeded on acid-washed Mattek dishes and serum-starved overnight. They were micro-injected with either PBS, Scar-WA or WASP-WA, all mixed with FITC-dextran for visualisation of injected cells, allowed to recover for at least 60 minutes, stimulated with 50ng/ml PDGF, and formaldehyde-fixed 4 minutes later. Following staining with FITC-phalloidin, the proportion of cells with CR was determined as before. The graph shows the incidence of CR in 20 cells in each group (one experiment).

During the quantitation of the Scar-/Wasp-WA effect, we observed that in some cells, microinjection of the WA domain had also altered the morphology of circular ruffles in those cells which still formed CR. We noted an increased incidence of two variant types of CR: flat CR, devoid of the ridge-like elevation CR usually show, and spiky or flame-shaped ridges instead of the usual even elevation of CR (Fig. 3.2.19).

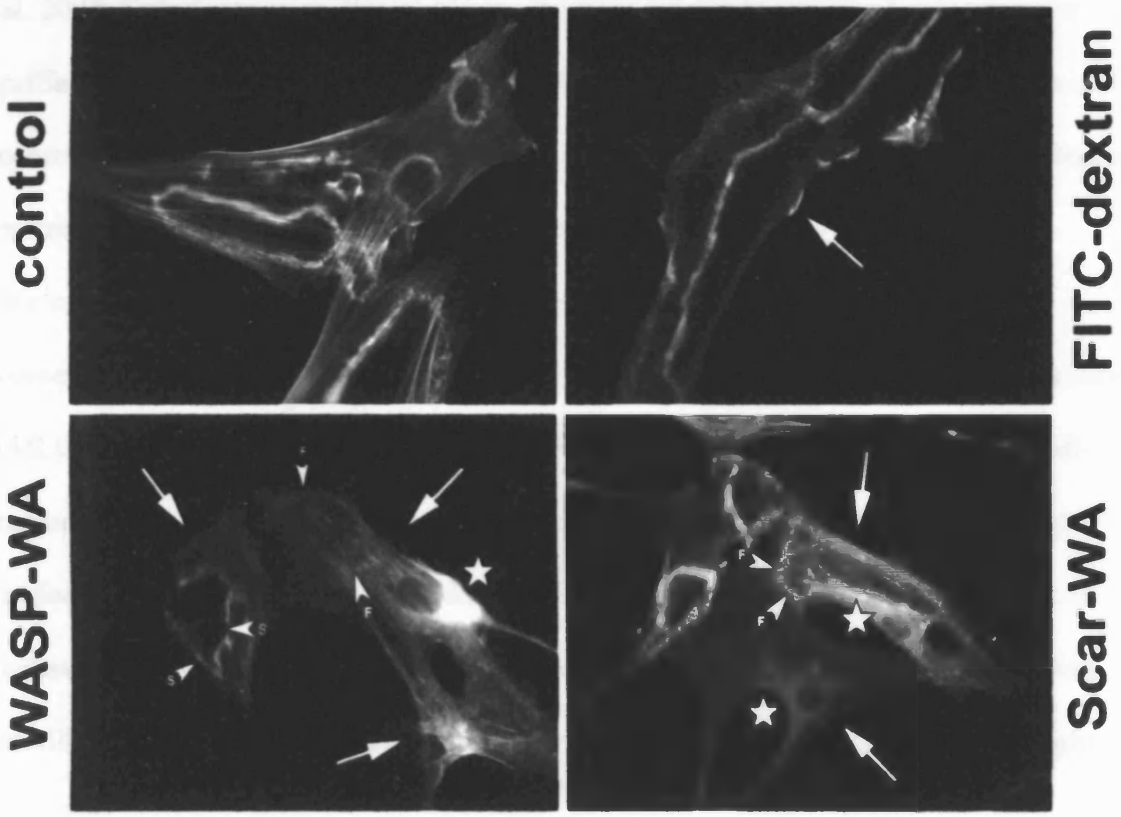

Fig. 3.2.19. Microinjection of WA domain of Scar or Wasp alters CR morphology. Cells were treated as above. Epifluorescence microscopy images show altered CR morphology in cells microinjected with WASP-WA or Scar-WA. Arrows indicate injected cells. Arrowheads S: CR with spike-like elevations, arrowheads F: flat CR. Stars: perinuclear, smooth f-actin assembly following injection of the WA-domain, indicating the functionality of the injected peptide, which induces arp2/3 mediated actin polymerisation throughout the cell, depleting actin molecules available for protrusion formation [Shao et al. 2006].

Many cell contractility events are based on interaction between actin and myosin II. The activation of myosin II is mainly regulated by two kinases: myosin light chain kinase (MLCK), and rho-associated kinase (ROCK). MLCK only phosphorylates one substrate, the light chain of myosin II. MLCK inhibition has been reported to reduce myosin II activation in the cell periphery and at the base of lamellipodia [Giannone et al. 2004; Totsukawa et al. 2004]. It has also been reported to be involved in circular ruffle formation and closure [Araki et al. 2003]. Rho kinase (ROCK) is involved in cell contractility in the cell centre and in protrusion retraction in three-dimensional collagen matrix assays [Totsukawa et al. 2004; Wyckoff et al. 2006].

We investigated the effects of inhibiting myosin II activation on circular ruffles in corneal fibroblasts. We used four inhibitors: ML-7 and ML-9, myosin light chain kinase (MLCK) blockers, Y 27632, a rho-kinase (ROCK) blocker, and blebbistatin, a small-molecule myosin II inhibitor. Blebbistatin inhibits nonmuscle myosin II and certain isoforms of muscle myosin II, but does not inhibit myosin from classes I, V and X. It behaves as an uncompetitive inhibitor and selectively inhibits the ATPase and gliding motility activities of myosin II, without inhibiting myosin light chain kinase [Straight et al. 2003].

Of these four myosin inhibitors, only the myosin light chain kinase inhibitors have a notable effect on circular ruffling: ruffles are flattened and lack the typical centripetal dynamics (Fig. 3.1.20).

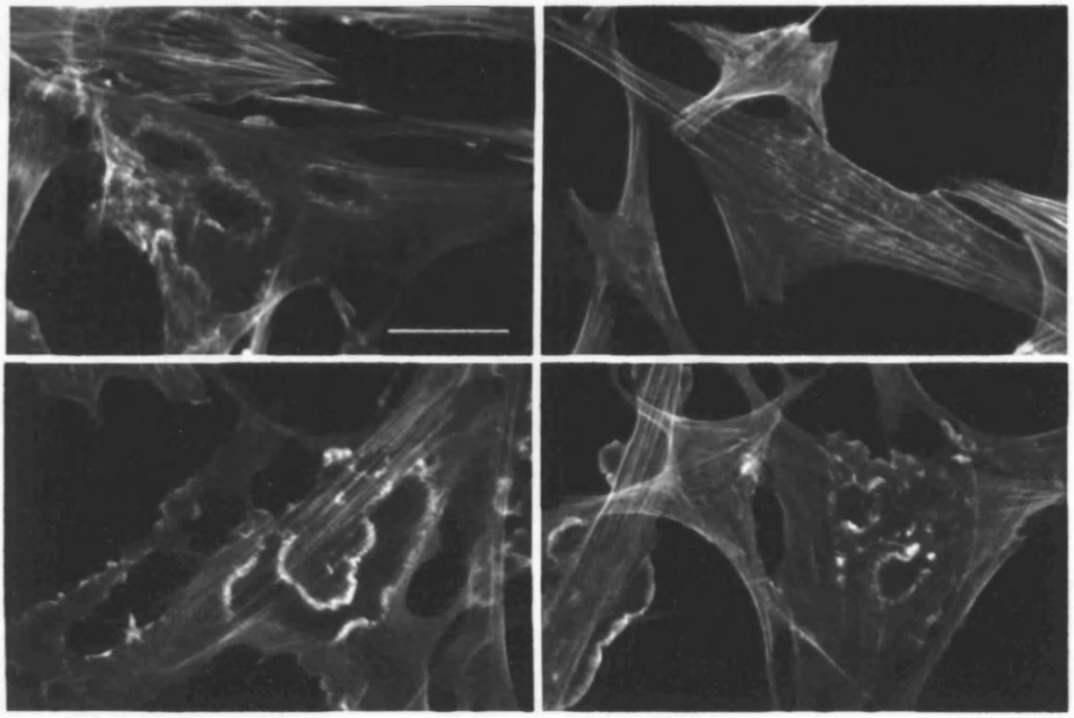

Fig. 3.2.20. Myosin light chain kinase inhibition, but not rho kinase inhibition or application of blebbistatin, alters CR morphology. Corneal fibroblasts plated on coverslips and serum-starved overnight in the presence of no inhibitor (top left), 25μM ML-7 (top right), 25μM Y27632 (bottom left) or 25μM blebbistatin (bottom right) were exposed to 50ng/ml PDGF-BB. The optimal timepoint to study circular ruffles was determined by a timelapse imaging sequence performed at the beginning of the experiment. After 7 minutes of stimulation, cells were fixed by formaldehyde and stained with FITC-phalloidin. Whilst Y27632 and blebbistatin do not affect circular ruffles, ML-7 and ML-9 induce formation of diffuse, non-concentric dorsal ruffles (ML-7 shown). Scalebar = 50μm.

Quantitation of the observed changes demonstrates that MLCK-inhibition reduces the incidence of CR in corneal fibroblasts. Rho-kinase inhibition has a moderate inhibitory effect, whereas blebbistatin has none (Fig. 3.2.21).

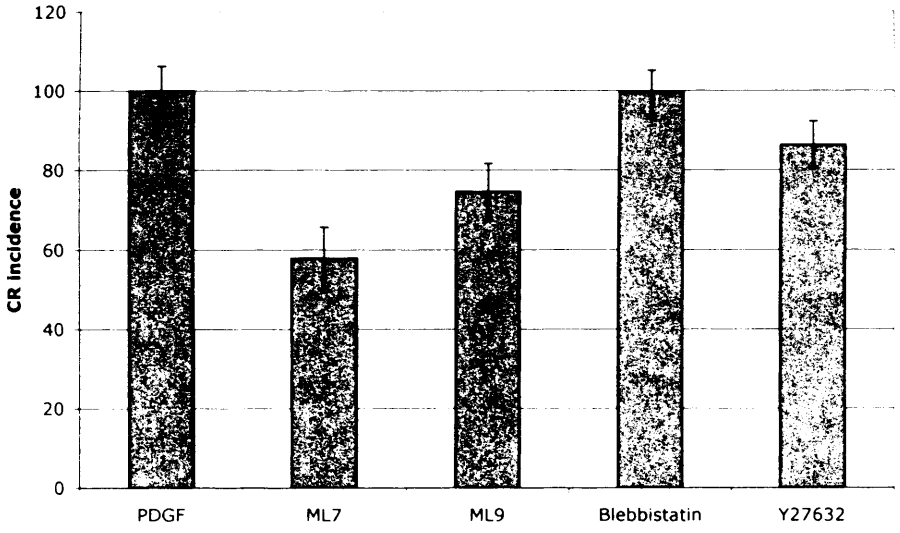

Fig. 3.2.21. Myosin light chain kinase inhibition, but not blebbistatin, reduces CR incidence. Rho kinase inhibition slightly reduces CR incidence. Cells were treated as in previous figure. Circular ruffling was quantified on 10 random photographs of each treatment, taken from two slides. Results show the mean and SE for 115 to 175 cells per group, normalised to CR incidence in the control group (one experiment). $P<0.01$ for ML7 and ML9, $p>0.05$ for blebbistatin and Y27632 versus PDGF control (t-test assuming unequal variances).

As PDGF stimulates the formation of two types of ruffles, peripheral and dorsal circular ruffles, we evaluated whether MLCK inhibition reduces both equally. MLCK inhibition specifically affects CR, but not peripheral or edge ruffling (PR). In addition, this quantitation confirms the observation that MLCK inhibition increases the formation of dorsal ruffles which lack circular arrangement and centripetal movement (Fig. 3.2.22).

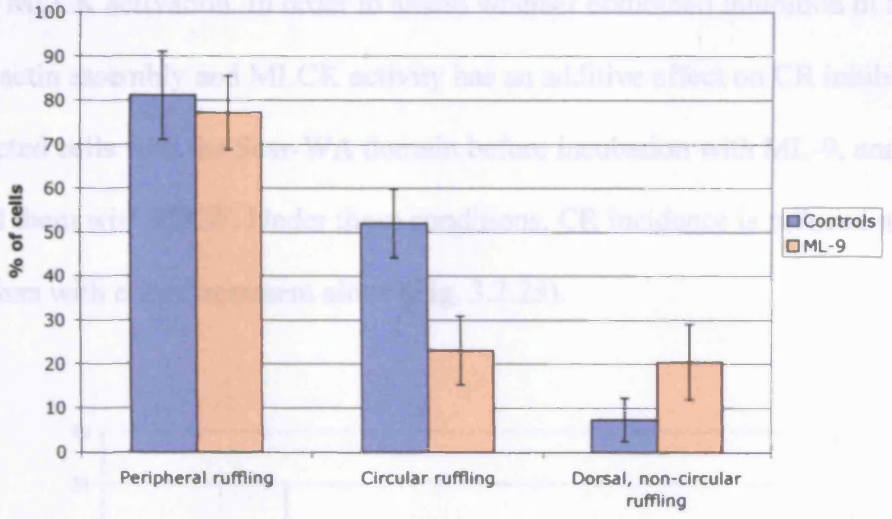

Fig. 3.2.22. Myosin light chain kinase inhibition specifically affects CR. HCFs were seeded on acid-washed Mattek dishes and serum-starved overnight. Control dishes (4 experiments) were stimulated with PDGF-BB 50ng/ml and the proportions of cells showing peripheral, circular, and dorsal (not circular) ruffling determined on timelapse images of living cells. ML-9 treated cells were pre-incubated with 25μM ML-9 for 30 minutes (2 experiments) or 60 minutes (3 experiments), then stimulated and quantified as the controls. Total number of cells counted: controls n=84, ML-9 (30 minutes) n=38, ML-9 (60 minutes) n=53, total ML-9 treated cells n=91. Shown are the mean and SEM; $p<0.05$ for circular ruffling, $p>0.05$ for peripheral and dorsal, non-circular ruffling when compared to controls (t-test assuming unequal variances).

In this experiment ML-9 has a stronger inhibitory effect on CR than in the previous figure. Differences might have arisen from the different methodology (quantitation of fixed cells versus live timelapse imaging).

In summary, the formation of circular ruffles in corneal fibroblasts can be inhibited by introducing the Scar- or Wasp-WA domain into cells, blocking arp 2/3 complex function. Formation and centripetal closure of circular ruffles can also be blocked by inhibiting MLCK activation. In order to assess whether combined inhibition of arp 2/3 mediated actin assembly and MLCK activity has an additive effect on CR inhibition, we microinjected cells with the Scar-WA domain before incubation with ML-9, and then stimulated them with PDGF. Under these conditions, CR incidence is reduced more strongly than with either treatment alone (Fig. 3.2.23).

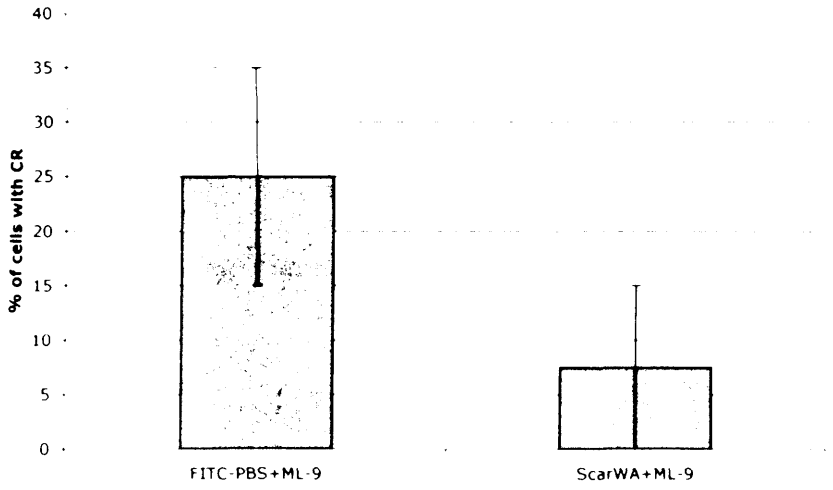

Fig. 3.2.23. Combined inhibition of actin polymerization in ruffles and myosin light chain kinase has an additive inhibitory effect on CR incidence. Cells were treated as in previous figures. Results show the mean and SEM for 40 cells micro-injected with FITC-PBS (control) and Scar-WA prior to ML-9 treatment. Data are from 2 experiments; $p>0.05$ (t-test assuming unequal variances).

In conclusion, PDGF-BB elicits a dramatic actin-based phenotype, circular ruffling, in corneal fibroblasts grown on a rigid planar substratum. The formation and/or progression of circular ruffles can be blocked fairly specifically by a combination of agents which interfere with arp 2/3-mediated actin assembly and myosin II activation.

3.2.3. The PDGF-mediated circular ruffling pathway is involved in matrix contraction by corneal fibroblasts

a) PDGF inhibition reduces dynamic cellular activity

Circular ruffles have only been demonstrated in cells grown on a planar substratum, but not in cells grown in three-dimensional collagen matrix. We therefore studied the morphological result of signalling through the circular ruffling pathway in cells in collagen matrix. In order to reproduce the conditions of the planar assay, in which cells are growth-factor starved overnight before being stimulated with PDGF, we modified our standard matrix contraction assay. Instead of adding growth factor to the medium at the time of matrix preparation, cells were serum-starved for 24 hours after seeding into the collagen matrix before PDGF was applied.

In order to determine how global matrix contraction is affected by the modification in matrix preparation, growth factor being withheld during the first 24 hours of matrix casting, we measured the contraction of fibroblast-populated matrices as described in the earlier experiments.

In the modified assay, there is slight matrix contraction during the first 24 hours, in the phase of cell spreading. This is followed by an increased rate of contraction over the 24 hours following PDGF stimulation. Contraction reaches the same plateau value as observed in the case of PDGF stimulation at the time of matrix preparation (Fig. 3.2.24).

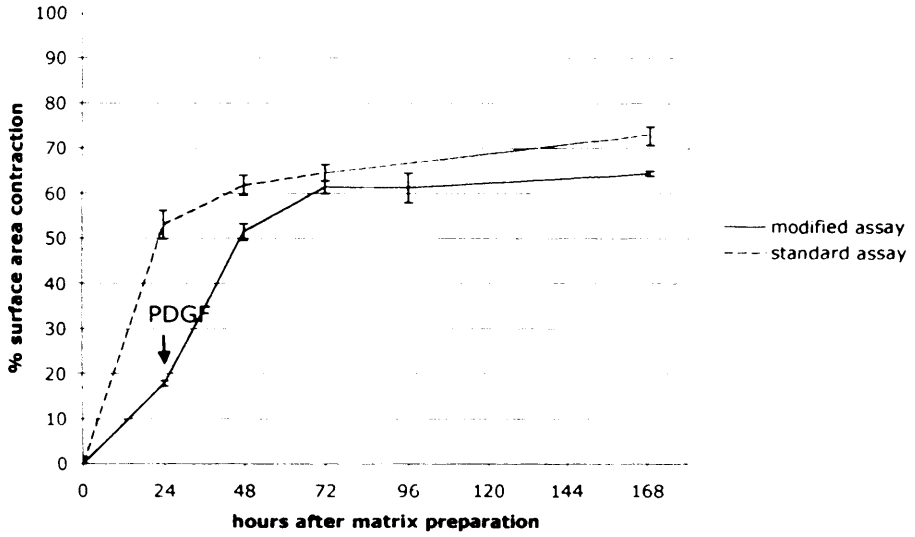

Fig. 3.2.24. Following an initial period of growth factor starvation, PDGF enhances the rate of matrix contraction. HCF-populated collagen matrices were floated in serum-free medium with 0.7% BSA for the first 24 hours after matrix preparation and then stimulated with PDGF 50ng/ml (arrow). During the first 24 hours after matrix preparation, contraction is slow, as previously shown for growth-factor starved cells in Fig. 3.2.1. This increases over the 24 hours after growth factor application. Data shown are means and SEM from one experiment with a triplicate set of matrices. For comparison, the dotted line shows rate of contraction when PDGF is added to the medium immediately after matrix preparation ("standard assay").

We then visualized cells in matrix within minutes of stimulation, initially by fixating them with formaldehyde and staining the actin cytoskeleton with phalloidin, which we had previously used to visualize circular ruffles. In three-dimensional matrix, no circular actin structures can be demonstrated. However, the appearance of the cell surface changes after PDGF stimulation: in the absence of growth factors, corneal fibroblasts have a smooth surface, but when exposed to PDGF, they develop multiple cell surface projections (Fig. 3.2.25).

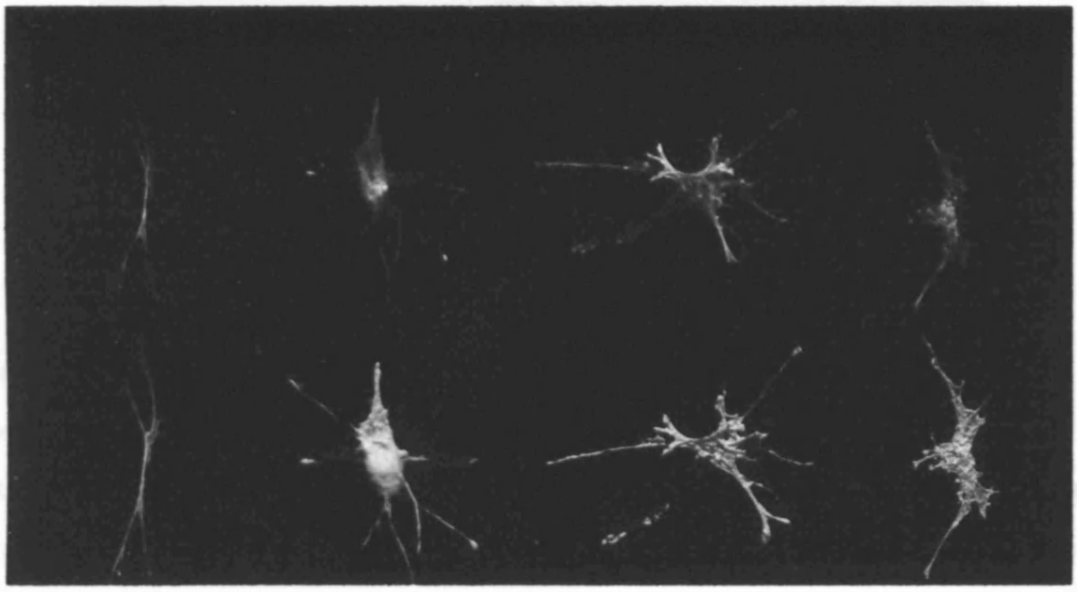

Fig. 3.2.25. When stimulated with PDGF, corneal fibroblasts in three-dimensional matrix develop surface protrusions. HCF-populated collagen matrices were floated in serum-free medium with 0.7% BSA for the first 24 hours after matrix preparation. The medium was then changed to DMEM without growth factors (left) or with PDGF 100ng/ml (right). After 15 minutes, matrices were fixed with formaldehyde and stained with FITC-phalloidin. Confocal z-stacks were reconstructed threedimensionally in Volocity, using maximum opacity rendering.

From static imaging at defined timepoints we proceeded to dynamic live timelapse imaging of the cellular response to PDGF stimulation. Initial experiments demonstrated that PDGF induces formation and retraction of protrusions similar to the dynamic activity observed in serum-stimulated cells in earlier experiments (Fig. 3.2.26), associated with traction on matrix fibres in the vicinity of protrusions (not shown).

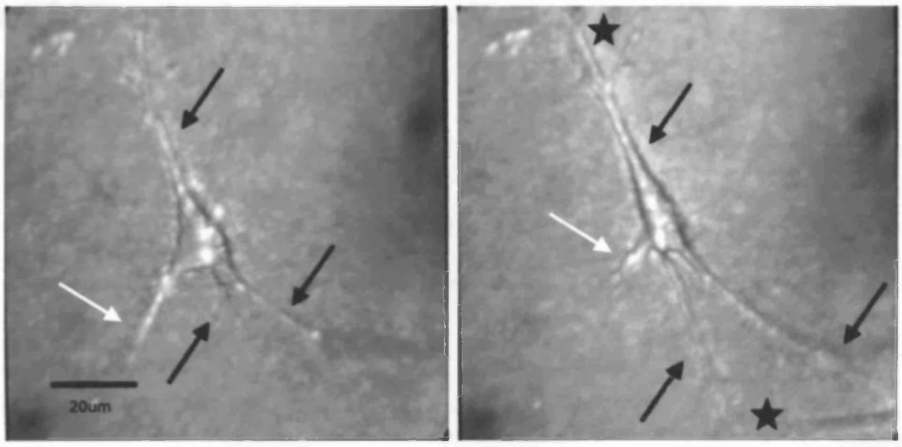

Fig. 3.2.26. PDGF triggers protrusive and retractile activity in corneal fibroblasts in three-dimensional matrix. HCF-populated collagen matrices were floated in serum-free medium with 0.7% BSA for the first 24 hours after matrix preparation and then stimulated with PDGF 100ng/ml. Acquisition of z-stack phase contrast images was started 12 minutes after addition of growth factor, and images were acquired every 10 minutes over 2 hours. Z-stacks were compressed using Openlab software. Left: corneal fibroblast at the beginning of the timelapse series, 12 minutes after PDGF stimulation. Right: same cell two hours later. Whilst one protrusion has been retracted (white arrow), others have been extended (black arrows), and have branched out (stars).

We measured the dynamic activity triggered by PDGF by calculating the dynamic index as described before. During the first four hours after PDGF stimulation, corneal fibroblasts remodel around 70% of their cell surface area measured on microscopic images every 10 minutes (Fig. 3.2.27). This value is the same as that observed after stimulation with a mix of growth factors (serum) (see fig. 3.1.5). Over the four hours of observation, the dynamic index is stable. We therefore averaged the values for each hour (Fig. 3.2.27), and in the following experiments, using different inhibitors, only compared the average dynamic index.

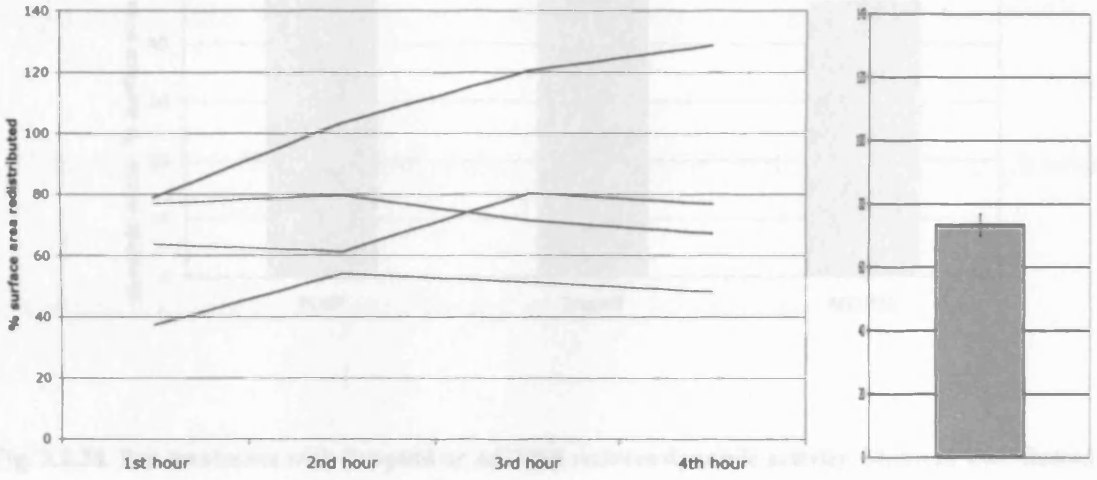

Fig. 3.2.27. After PDGF stimulation, cells remodel around 70% of their area every 10 minutes. The dynamic index largely remains stable during the first four hours after stimulation. Matrices were floated in serum-free medium with 0.7% BSA for the first 24 hours after matrix preparation and then stimulated with PDGF-BB 50ng/ml (n=4). Confocal z-stack images of individual cells were acquired every 10 minutes for 4 hours after stimulation. From these images, the dynamic index was calculated as [(areas of new protrusions)+(areas of retractions)/average cell area] for each 10 minute interval. Left: hourly averages of dynamic index in four experiments. Right: average dynamic index over four hours. Error bar: SEM over the four hours.

As we had previously demonstrated that PDGF pathway blockers such as AG1295 and Trapidil inhibit both PDGF-mediated matrix contraction and circular ruffling, we tested whether they might also have an effect on cellular dynamic activity in matrix in this assay. A concentration of 25μM AG1295 or 200μg/ml Trapidil reduces the dynamic index by 30% (Fig. 3.2.28).

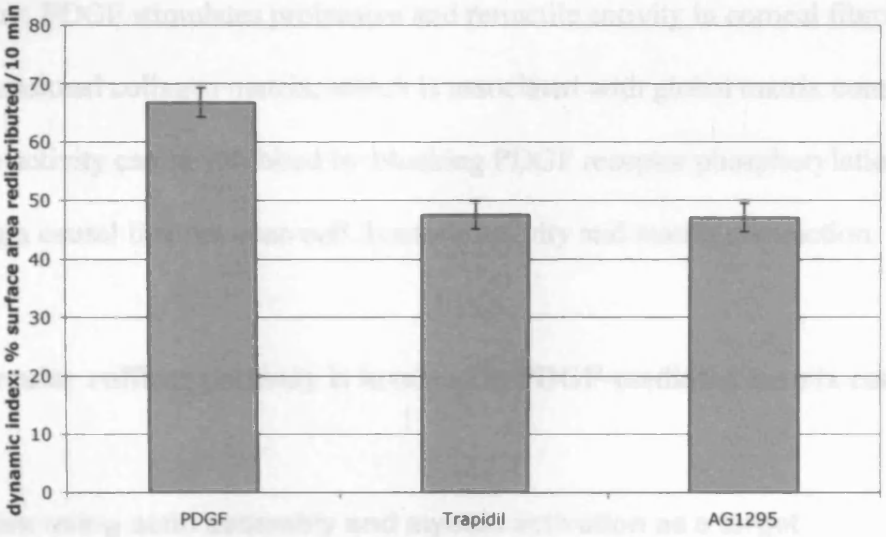

Fig. 3.2.28. Pre-treatment with Trapidil or AG1295 reduces dynamic activity. Matrices were floated in serum-free medium with 0.7% BSA without inhibitor or with 200 μg/ml Trapidil or 25μM AG1295 for the first 24 hours after matrix preparation and then stimulated with PDGF-BB 50ng/ml, in the continued presence of the inhibitor. Confocal z-stack images of individual cells were acquired every 10 minutes for 4 hours after stimulation (PDGF n=4, Trapidil n=2, AG1295 n=1). From these images, the dynamic index was calculated as [(areas of new protrusions)+(areas of retractions)/average cell area] for each 10 minute interval. In the analysis of this and all subsequent inhibitor experiments, the first three timepoints were excluded from analysis, as great fluctuation of dynamic index was systemically observed in all experiments The dynamic index was averaged over 4 hours for 4 cells for PDGF treatment, 2 cells for Trapidil treatment, and one cell for AG1295 treatment. $P<0.001$ when comparing PDGF controls with either Trapidil or AG1295 treatment (t-test assuming unequal variances).

In these experiments, we used a higher concentration of PDGF than in earlier experiments of global matrix contraction (50 versus 20 ng/ml), in order to ensure a visible behavioural response by fibroblasts after stimulation. The inhibitory effect of AG1295 and Trapidil on protrusive activity is consistent with the previously observed inhibitory effect on global matrix contraction.

In summary, PDGF stimulates protrusive and retractile activity in corneal fibroblasts in three-dimensional collagen matrix, which is associated with global matrix contraction. Protrusive activity can be inhibited by blocking PDGF receptor phosphorylation, suggesting a causal link between cell dynamic activity and matrix contraction.

b) The circular ruffling pathway is involved in PDGF-mediated matrix contraction

1. Inhibition using actin assembly and myosin activation as a target

Previous experiments demonstrated that PDGF-stimulated circular ruffles in corneal fibroblasts can be inhibited by introducing the arp 2/3 function blocking WA-domain of Scar or WASP into cells and/or by inhibiting myosin II activation through MLCK inhibition. We therefore tested whether PDGF-stimulated matrix contraction by corneal fibroblasts could equally be inhibited by these molecules, and whether combined inhibition has an additive effect as demonstrated on circular ruffling.

However, insertion of the WA-domain into cells in three-dimensional matrix through micro-injection is technically not possible, and micro-injecting cells before seeding them into collagen matrices would not allow a sufficient number of cells to be treated.

We therefore used transfection methods to insert a plasmid encoding the Scar-WA domain into human corneal fibroblasts to induce over-expression of Scar-WA and subsequent functional inhibition of arp 2/3 function. As transfection control, we transfected cells with enhanced green fluorescent protein (eGFP).

We tested the effect of overexpression of Scar in our standard matrix contraction assay, with cells being stimulated with PDGF at the time of matrix preparation. Under these conditions, Scar overexpression reduces PDGF-induced matrix contraction by HCF by 46% at 24 hours and by 56% at 48 hours (Fig. 3.2.29). Maximum transfection efficiency in these assays was 30-50% (data not shown).

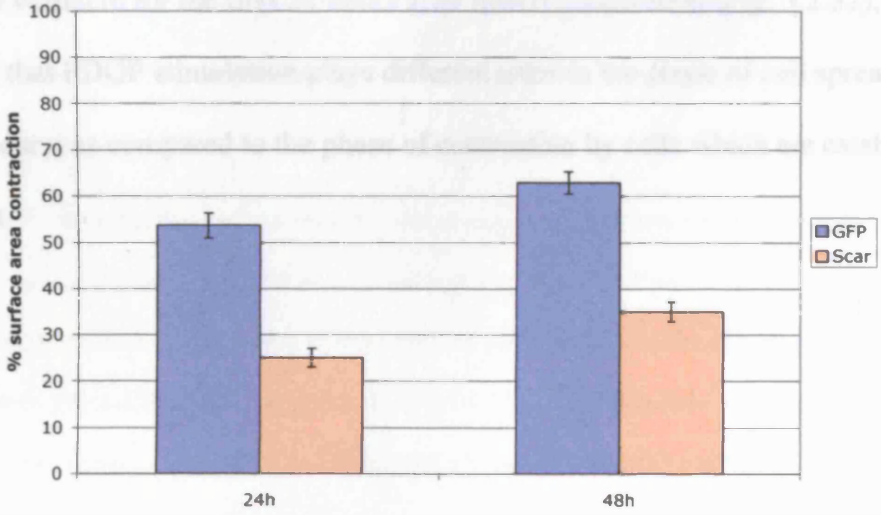

Fig. 3.2.29. PDGF-induced matrix contraction is reduced when HCF express Scar-WA. Using the transfection reagent, Fugene, HCFs were transfected with either eGFP or Scar-WA and cast into collagen matrices at a cell density of 80,000 cells/ml and incubated in DMEM with 20ng/ml PDGF-BB. Matrices were photographed immediately after floating, and 24 and 48 h later. Surface area contraction was determined as before. Shown are the mean and SEM from triplicate matrices in two independent experiments; $p<0.001$ when comparing Scar-WA- with GFP-transfected cells at either timepoint (t-test assuming unequal variances).

For myosin inhibition, the same concentrations of MLCK inhibitors ML-7 and ML-9, ROCK inhibitor Y27632, and blebbistatin were used on cells in collagen matrix as previously applied to cells on planar substratum. We conducted myosin inhibition experiments in both the standard and in the modified assay of matrix contraction: firstly, we applied the inhibitor and PDGF-BB at the time of matrix preparation (Figs. 3.2.30 and 3.2.31), and secondly, we pre-treated cells with the inhibitor from matrix preparation onwards, but only added PDGF after 24 hours (Fig. 3.2.32). Under both conditions, all myosin inhibitors have a dose-dependent inhibitory effect on PDGF-induced matrix contraction. The reduction in matrix contraction is greater when growth factors are withheld for the first 24 hours after matrix preparation (Fig. 3.2.32), indicating that PDGF stimulation plays different roles in the phase of cell spreading (first 24 hours) as compared to the phase of contraction by cells which are established in the matrix.

MLCK inhibition by either ML-7 or ML-9 reduces PDGF-induced matrix contraction (Fig. 3.2.30). In particular, incubation with 25 μM ML-9 reduces matrix contraction by 43% at 24 hours and by 48% at 48 hours.

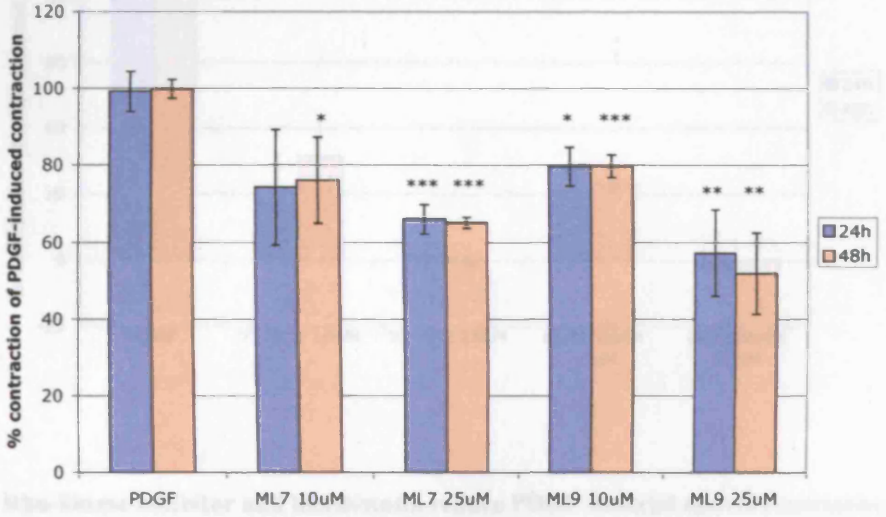

Fig. 3.2.30. MLCK inhibition reduces PDGF-induced matrix contraction. HCF were seeded into collagen matrices at a density of 40,000 cells/ml and incubated in DMEM with 20ng/ml PDGF-BB with or without ML-7 or ML-9 (10 or 25μM). Results show the mean and SEM of matrix area contraction at 24 and 48 hours, normalised to the contraction induced by PDGF, from triplicate sets of matrices in four independent experiments. All $p<0.05$ when comparing treatment with PDGF controls, except for ML-7 10μM at 24 hours, *$p<0.05$, **$p<0.01$, ***$p<0.001$ (t-test assuming unequal variances).

Although ROCK inhibition and blebbistatin did not have an effect on circular ruffling, both profoundly reduce PDGF-stimulated matrix contraction (Fig. 3.2.31).

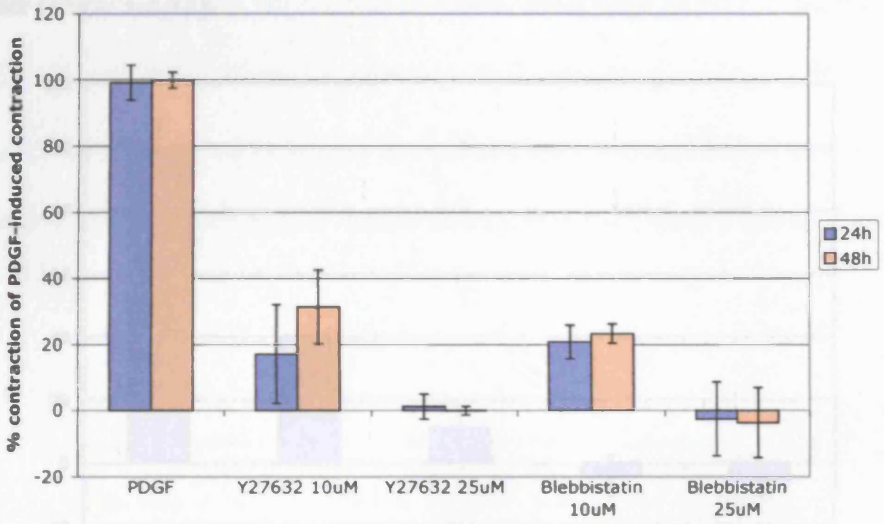

Fig. 3.2.31. Rho-kinase inhibitor and blebbistatin reduce PDGF-induced matrix contraction. HCF were seeded into collagen matrices at a density of 40,000 cells/ml and incubated in DMEM with 20ng/ml PDGF-BB with or without Y27632 or blebbistatin (10 or 25μM). Results show the mean and SEM of matrix area contraction at 24 and 48 hours, normalised to the contraction induced by PDGF, from triplicate sets of matrices in two independent experiments. All $p<0.001$ when comparing treatment with PDGF controls (t-test assuming unequal variances).

When cells are growth factor starved in the presence of a myosin inhibitor for 24 hours prior to PDGF stimulation, the inhibitory effect on subsequent matrix contraction is even greater (Figs. 3.2.32).

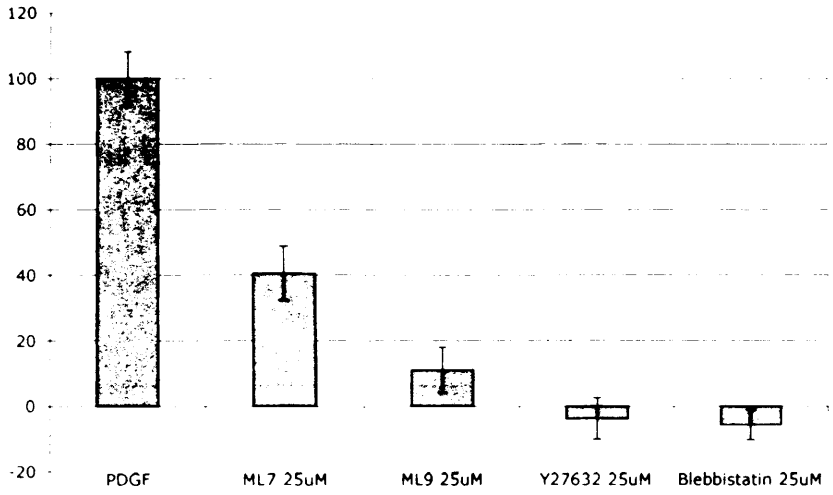

Fig. 3.2.32. Myosin inhibition strongly reduces PDGF-BB induced contraction after completion of the initial phase of cell spreading. Cells were seeded into collagen matrix and incubated for 24h in serum-free medium with 0.7% BSA with or without 25μM ML-7, ML-9, Y27632, or blebbistatin. Medium was then changed to L-15 with 50ng/ml PDGF-BB with the same inhibitor. Results show mean surface area contraction and SEM over the 24 h following medium exchange, normalised to PDGF-induced contraction. All $p<0.001$ when comparing treatment with PDGF controls (t-test assuming unequal variances).

As combined inhibition of arp 2/3-mediated actin assembly and of MLCK-mediated myosin II activation had resulted in an additive effect on circular ruffling inhibition, we also tested whether Scar-WA expression and incubation with an MLCK inhibitor had an additive effect on reducing matrix contraction. Cells transfected with eGFP were used as transfection control. Combination of Scar-WA expression and ML-9 incubation results in much greater inhibition of matrix contraction than either treatment alone (Fig. 3.2.33).

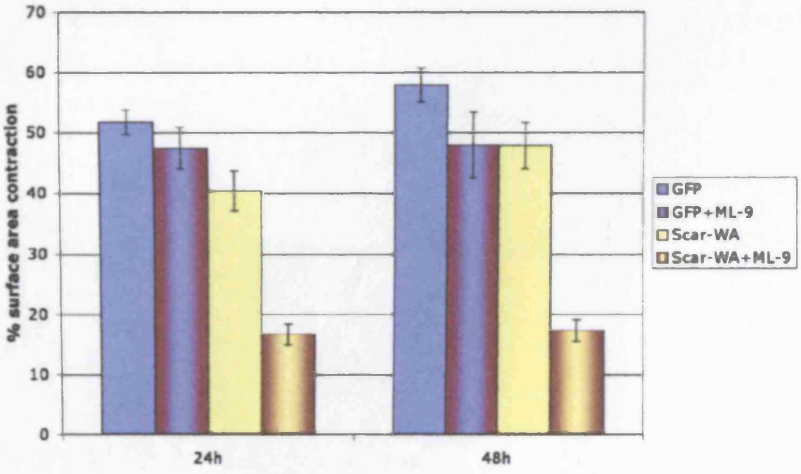

Fig. 3.2.33. Overexpression of Scar-WA combined with MLCK inhibition results in an additive inhibitory effect on matrix contraction. Using nucleofection (Amaxa^{TM}), cells were transfected with either eGFP or Scar-WA and cast into collagen matrices at a density of 40,000 cells/ml. Matrices were incubated in DMEM with 20ng/ml PDGF-BB with or without 25μM ML-9. Matrix surface area contraction at 24 and 48 hours is shown (mean and SE) from three independent experiments. $P>0.05$ when comparing GFP with GFP+ML9 at 24 and 48 hours, $p<0.01$ when comparing GFP with Scar-WA at 24 hours and $p<0.05$ at 48 hours, and $p<0.001$ when comparing GFP with Scar-WA+ML9 treatment at 24 and 48 hours (t-test assuming unequal variances).

In this experiment, Scar-WA expression did not reduce matrix contraction as much as in the previous experiment (Fig. 3.2.29). This might have been due to the different transfection methods used, which might have resulted in different transfection efficiencies, although the effect of eGFP on matrix contraction is the same in both experiments.

In order to assess whether the inhibitory effect on matrix contraction exerted by inhibition of myosin activation was due to a reduction in protrusive activity, we acquired confocal timelapse images of corneal fibroblasts pre-incubated with myosin inhibitors for 24 hours in the absence of growth factors prior to PDGF stimulation. These timelapse sequences covered the first four hours after PDGF application, and were analysed by calculating the dynamic index for individual cells as described before. MLCK inhibition slightly reduces the dynamic index, whilst ROCK inhibition increases dynamic activity, and blebbistatin has no effect (Fig. 3.2.34).

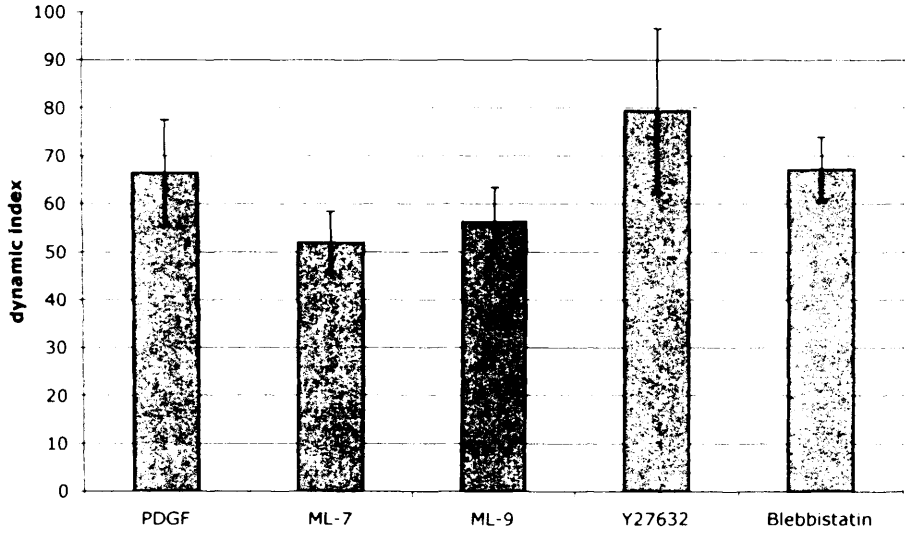

Fig. 3.2.34. Effect of myosin pathway inhibitors on protrusive activity after PDGF stimulation.

Matrices were floated in serum-free medium with 0.7% BSA without inhibitor or with 25μM ML-7, ML-9, Y27632 or blebbistatin for the first 24 hours after matrix preparation and then stimulated with 50ng/ml PDGF-BB, in the continued presence of the inhibitor. Confocal z-stack images of individual cells were acquired every 10 minutes for 4 hours after stimulation (PDGF n=4, ML-7, ML-9, Y27632 and blebbistatin n=2 each). From these images, the dynamic index was calculated as [(areas of new protrusions)+(areas of retractions)/average cell area] for each 10 minute interval.

However, both Y27632 and blebbistatin change the appearance of cellular protrusions (Fig. 3.2.35).

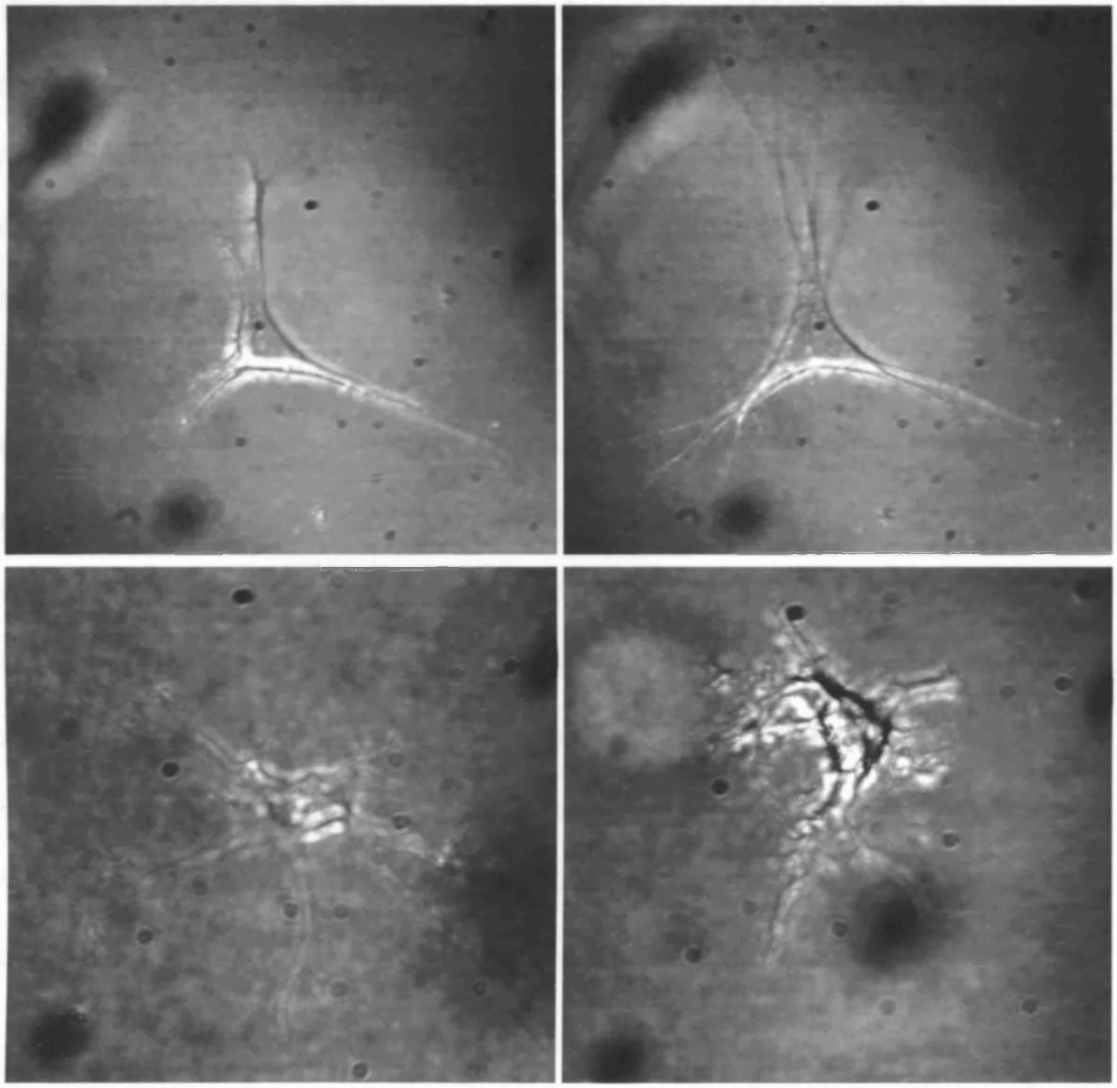

Fig. 3.2.35. Rho-kinase inhibitor Y27632 and myosin inhibitor blebbistatin dramatically change protrusion morphology. Top: serum-starved cells have straight protrusions (left), which after PDGF stimulation extend in length and branching pattern (right). Bottom left: Y27632-treated cell, with seemingly less "tone" in cell body and protrusions. Bottom right: blebbistatin-treated cell with "floppy" cell body and protrusions. MLCK inhibition does not affect protrusion morphology (not shown).

2. Inhibition using molecules specific to the circular ruffling pathway

The actin and myosin-interfering agents used are not completely specific to the circular ruffling pathway. During the course of our studies, additional information about the circular ruffling pathway became available. Specifically, the small GTPase, rab5, was demonstrated to be indispensable in the signalling pathway [Lanzetti et al. 2004]. Blocking this pathway specifically inhibits circular ruffling without affecting peripheral ruffling. The rab5 signalling pathway can be selectively inhibited by transfecting cells with plasmids encoding a dominant-negative rab5 mutant, S34N. Both overexpression and downregulation of the rab5-specific GTPase activating protein, RNTre, inhibit circular ruffling [Lanzetti et al. 2004]. We used these plasmids to observe the effect on PDGF-mediated matrix contraction in corneal fibroblasts. Expression of these plasmids leads to a strong reduction in PDGF-mediated matrix contraction (Fig. 3.2.36). In these experiments, the transfection efficiency was between 40 and 69% (GFP 69%, rab5-WT 50%, rab5-S34N 39%, RNTre 40%). The inhibitory effect on matrix contraction is therefore an underestimate of the full effect of blocking this pathway.

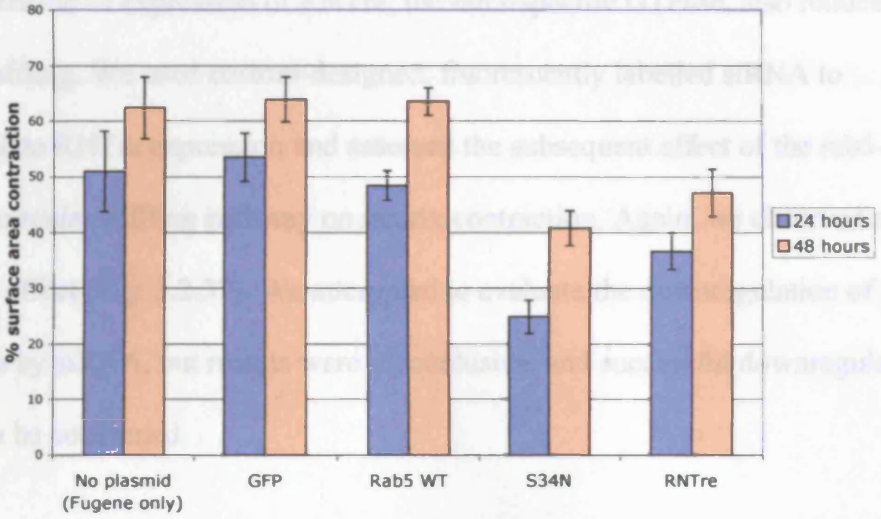

Fig. 3.2.36. Specific inhibition of the rab5 circular ruffling signalling pathway through transfection with dominant negative plasmids reduces PDGF-induced matrix contraction by 27 to 50%. Using the transfection reagent, Fugene, cells were transfected with plasmids encoding for eGFP, Rab5WT-eGFP (rab5 wild-type), S34N-myc, or RNTre-eGFP, and seeded into collagen matrices 24 hours after transfection. To ensure equal cell numbers in the different groups, cells were re-counted immediately prior to matrix preparation. Results show mean surface area contraction and SE at 24 and 48 hours after matrix preparation and incubation with 20ng/ml PDGF in two independent experiments. $P>0.05$ when comparing GFP with Fugene only or Rab5 WT at 24 and 48 hours, $p<0.01$ when comparing GFP with S34N and RNTre at 24 and 48 hours (t-test assuming unequal variances).

Downregulation of expression of RNTre, the rab5-specific GTPase, also reduces circular ruffling. We used custom-designed, fluorescently labelled siRNA to downregulate RNTre expression and assessed the subsequent effect of the rab5-mediated circular ruffling pathway on matrix contraction. Again, we observed an inhibitory effect (Fig. 3.2.37). We attempted to evaluate the downregulation of protein expression by siRNA, but results were inconclusive, and successful downregulation remains to be confirmed.

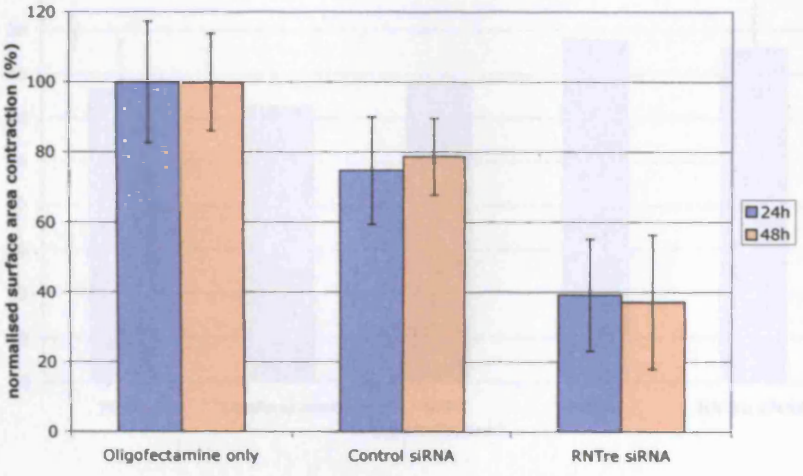

Fig. 3.2.37. Specific inhibition of the rab5 circular ruffling signalling pathway through siRNA reduces PDGF-induced matrix contraction by 50%. Using the transfection reagent, Oligofectamine, cells were transfected with eGFP-tagged siRNA to RNTre or a scrambled sequence [Lanzetti et al. 2004] and seeded into collagen matrix 24 h after transfection. Results show mean and SE of surface area contraction at 24 and 48h after matrix preparation, normalised to PDGF-induced contraction (20ng/ml) in the carrier only group in two independent experiments (one set of triplicates, one set of pairs of matrices). All $p>0.05$ when comparing oligofectamine or RNTre siRNA with control siRNA at either 24 or 48 hours (t-test assuming unequal variances).

These experiments indicate that the circular ruffling signalling pathway is indeed involved in the early phase of matrix contraction by corneal fibroblasts. We then sought to determine whether the underlying cell behavioural mechanism is the inhibition of protrusive activity. However, we find that transfection with the RNTre plasmid or RNTre-siRNA does not decrease protrusive activity, but tends to slightly increase it (Fig. 3.2.38).

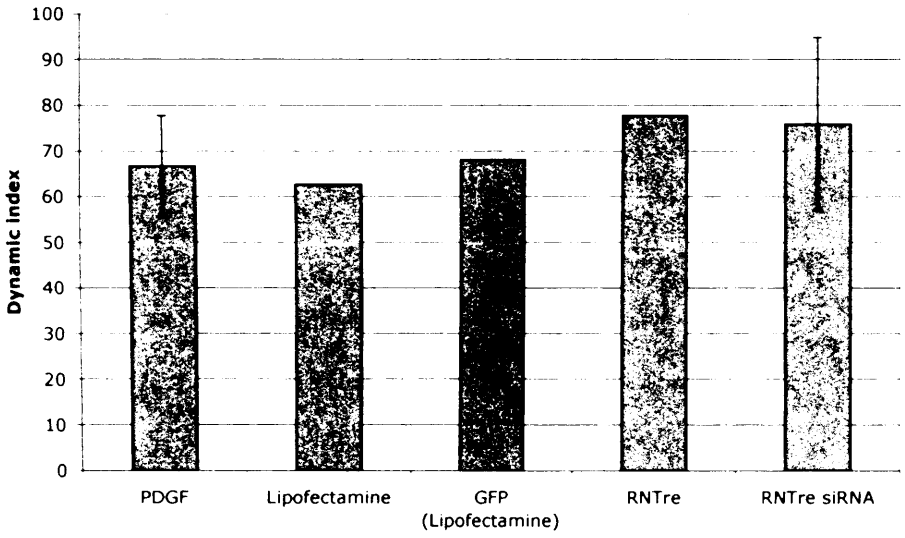

Fig. 3.2.38. Transfection with the RNTre plasmid and RNTre-siRNA transfection do not decrease protrusive activity. HCF were transfected with the RNTre plasmid or eGFP using the transfection agent, Lipofectamine 2000, or treated with RNTre siRNA using Oligofectamine. Transfected cells were embedded in collagen matrices which were floated in serum-free medium with 0.7% BSA for the first 24 hours and then stimulated with PDGF-BB 50ng/ml. Confocal z-stack images of individual cells were acquired every 10 minutes for 4 hours after stimulation (PDGF n=4RNTre n=1, RNTre siRNA n=2). From these images, the dynamic index was calculated as [(areas of new protrusions)+(areas of retractions)/average cell area] per 10-minute interval.

We also assessed whether the specific inhibitors of the rab5 signalling pathway have qualitative effects on cell or protrusion morphology. Both transfection with the RNTre plasmid and siRNA transfection seem to result in a greater number of protrusions per cell, this effect being more marked in siRNA-treated cells (Fig. 3.2.39).

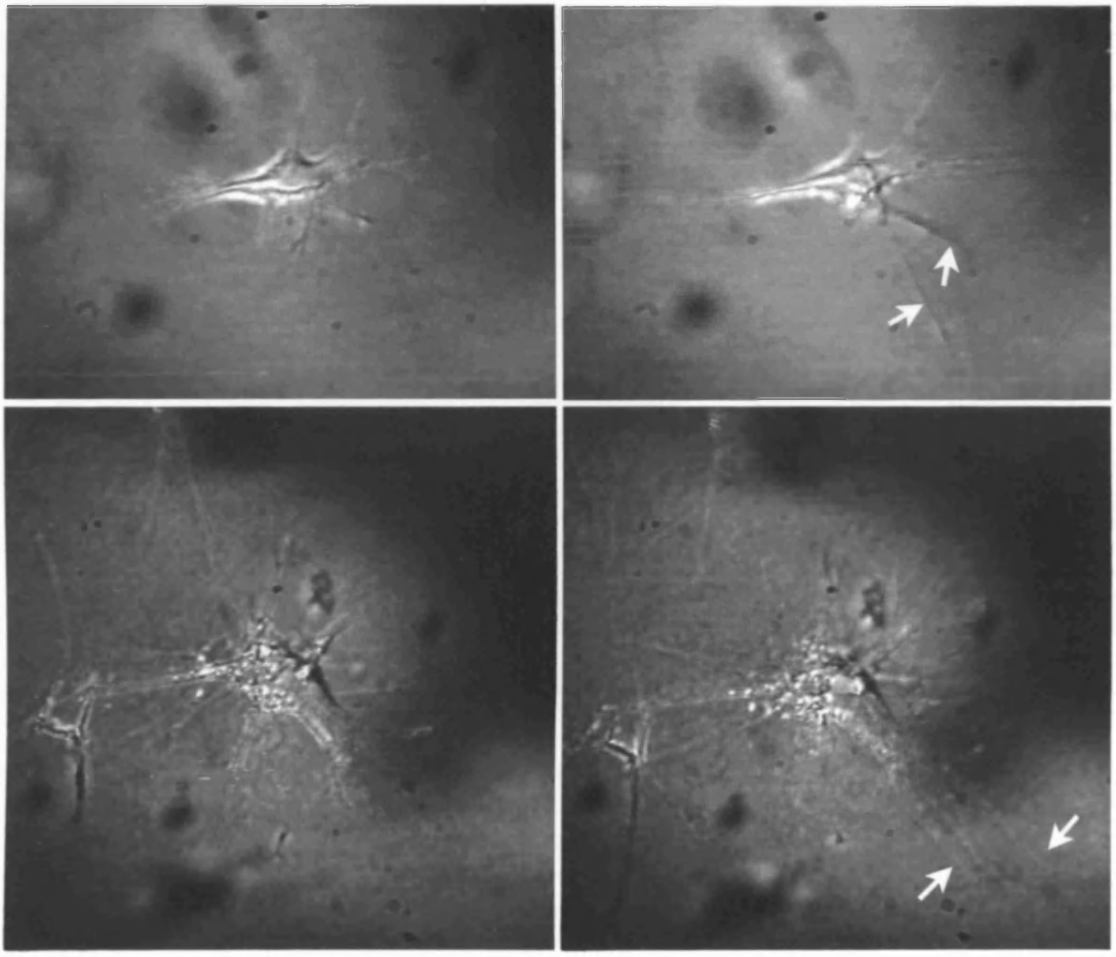

Fig. 3.2.39. Transfection with the RNTre plasmid and RNTre-siRNA transfection result in increased number of protrusions per cell. Cells were transfected with RNTre plasmid or siRNA to silence RNTre expression and then seeded into collagen matrix. After 24 hours in serum-free medium, matrices were placed on a confocal microscope, and identified through their expression of GFP/Alexa Fluor 488. Top:RNTre-plasmid transfected cells, bottom: siRNA-transfected cell with increased number of randomly oriented protrusions. Top and bottom right: extension of protrusions (white arrows) 25 minutes after PDGF stimulation.

In summary, inhibition of actin assembly and myosin activation inhibit circular ruffling pathway signalling, leading to a decrease in protrusive activity and subsequent matrix contraction. However, specific targeting of rab5, an indispensable molecule in the circular ruffling pathway, does not demonstrate a reduction in protrusive activity in matrix, although matrix contraction is significantly reduced.

3.3. Imaging tissue: confocal and two-photon microscopy combined with fluorescent probes visualise cells and matrix in conjunctiva and cornea

In the study of cell behaviour, *in vitro* collagen matrix offers advantages over traditional two-dimensional cell culture systems. It provides cells with a more physiological three-dimensional environment and allows investigations into cell-matrix interaction. However, the composition of the *in vitro* matrix is oversimplified in comparison to tissue extracellular matrix. It would therefore be desirable to adapt microscopical imaging systems to use in *ex vivo* and *in vivo* tissue.

Ex vivo imaging poses two main challenges: cell viability and poor contrast between cells and matrix. We explored possible imaging techniques for two ocular surface tissues: cornea and conjunctiva.

In order to preserve corneal transparency *ex vivo*, endothelial cell function has to be maintained to prevent stromal oedema. This can be achieved by corneal organ culture systems such as a perfusion chamber. We adapted Thiel's corneal perfusion chamber [Thiel et al. 2001] for use on a confocal microscope (Fig. 3.3.1). The main modification is a thinner base as compared to the original, as a thick base interferes with microscope light transmission.

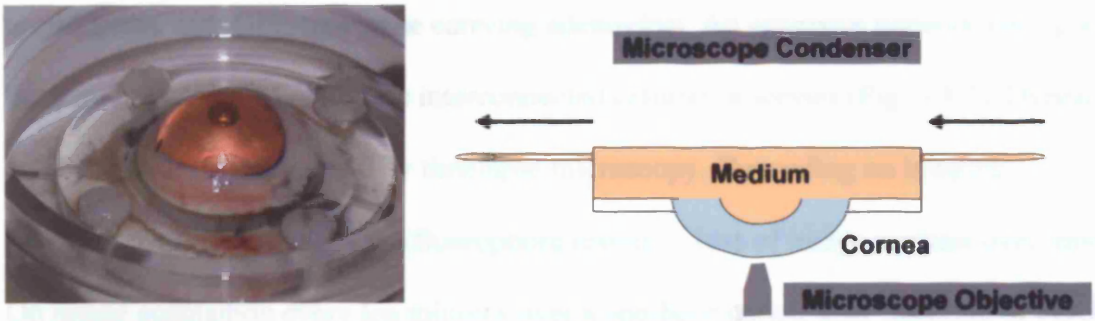

Fig. 3.3.1. Cornea in anterior segment perfusion chamber (left), which can be mounted onto an upright or an inverted microscope (right). Continuous perfusion removes metabolic waste products from the endothelium and supplies fresh nutrients.

Keratocytes can be demonstrated on a confocal laser scanning microscope after transduction with GFP-transgene carrying adenovirus. An extensive network throughout the stroma is revealed, with fine interconnected cellular processes (Fig. 3.3.2). Dynamic cell behaviour can be studied by timelapse microscopy. Depending on imaging intervals, photobleaching of the fluorophore results in loss of image contrast over time. On image acquisition every ten minutes over a one-hour period after injection of PDGF into the stroma, no significant cell movement was observed (not shown).

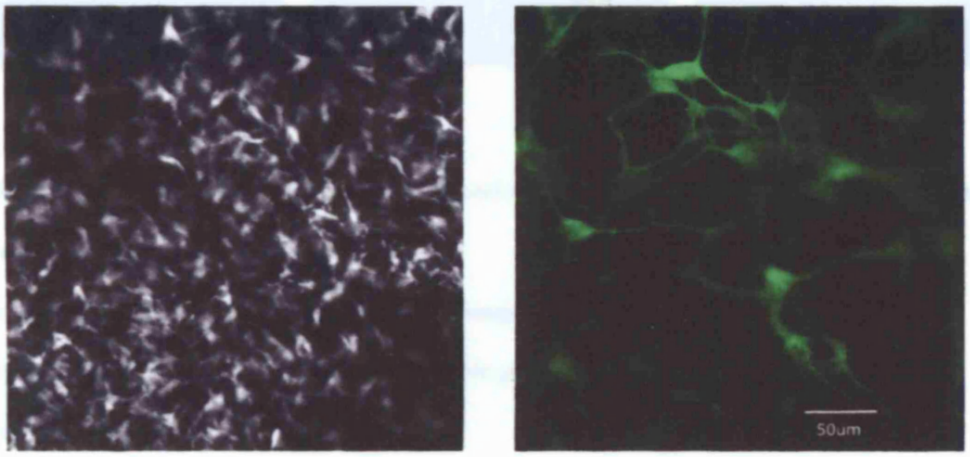

Fig. 3.3.2. Keratocyte network in corneal stroma. Visualisation by confocal laser scanning microscopy, combined with GFP-adenoviral transduction. Confocal fluorescence images of keratocytes in corneal stroma 24h after injection of GFP adenovirus and corneal organ culture in anterior segment perfusion chamber, and injection of 50µl of 100ng/ml PDGF-BB in L15, immediately before the start of image acquisition. Left: x10 objective. Right: x40 objective.

Multiphoton microscopy yields similar cellular images. In addition, the second harmonic generation properties of the collagen-rich matrix can be used to visualise corneal stroma (Fig. 3.3.3).

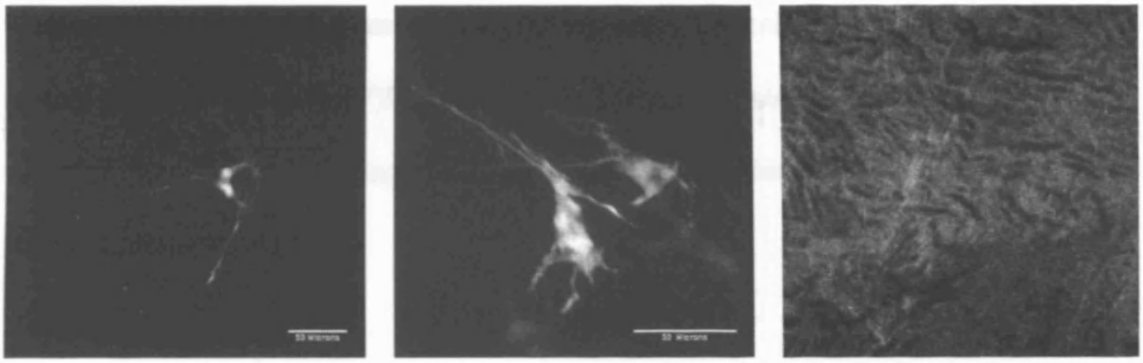

Fig. 3.3.3. GFP-transduced keratocytes and corneal stroma visualised by two-photon excitation microscopy and second harmonic generation.

Corneas were imaged 24h after injection of GFP-transgene carrying adenovirus. Left and centre: keratocytes in corneal stroma; right: second harmonic generation image of matrix. Left: x20 water objective. Centre and right: x60 dipping objective.

Another ocular surface layer of interest in the context of wound healing and scarring is the subconjunctival space, which is highly relevant after glaucoma filtration surgery. Due to their autofluorescent properties, cells and matrix in the conjunctival stroma can be visualised by two-photon excitation microscopy (Fig. 3.3.4). Different excitation wavelengths yield optimal emission signal intensity. The cellular autofluorescence is mainly generated by NAD(P)H and flavins, which are maximally excited by wavelengths of 780nm. Collagen autofluorescence is maximally stimulated by wavelengths of 920nm.

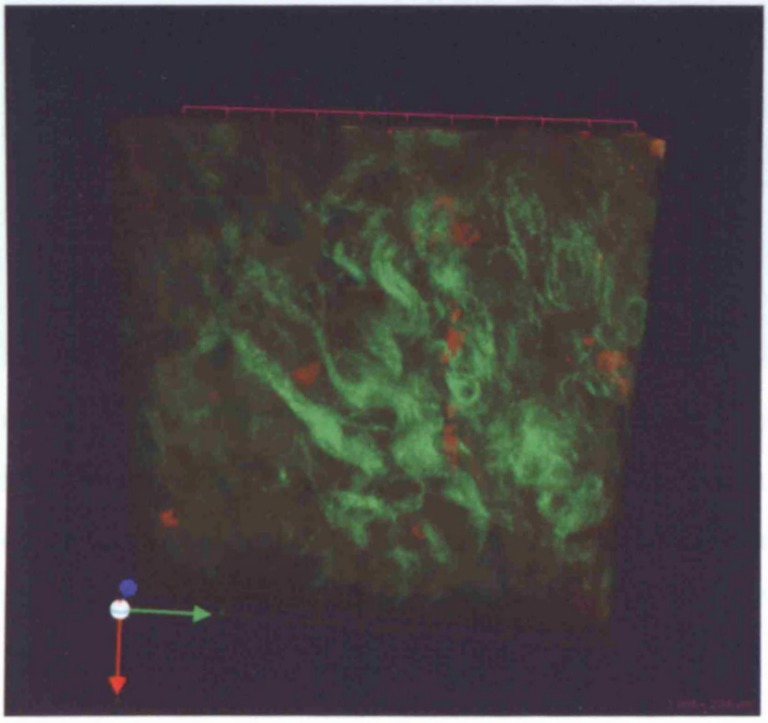

Fig. 3.3.4. Cells and matrix in the conjunctival stroma, visualised by two-photon excitation microscopy using their autofluorescent properties. Excitation wavelengths of 780nm visualises cells (red), and 920nm collagen fibres (green).

Using a confocal laser scanning microscope, stromal matrix can be visualised using reflection settings, but cells cannot demonstrated. However, vital dyes easily penetrate into the loose stroma and into the cells. Using the cell dye, CFDA-SE, conjunctival stroma and matrix can be visualised (Fig. 3.3.5).

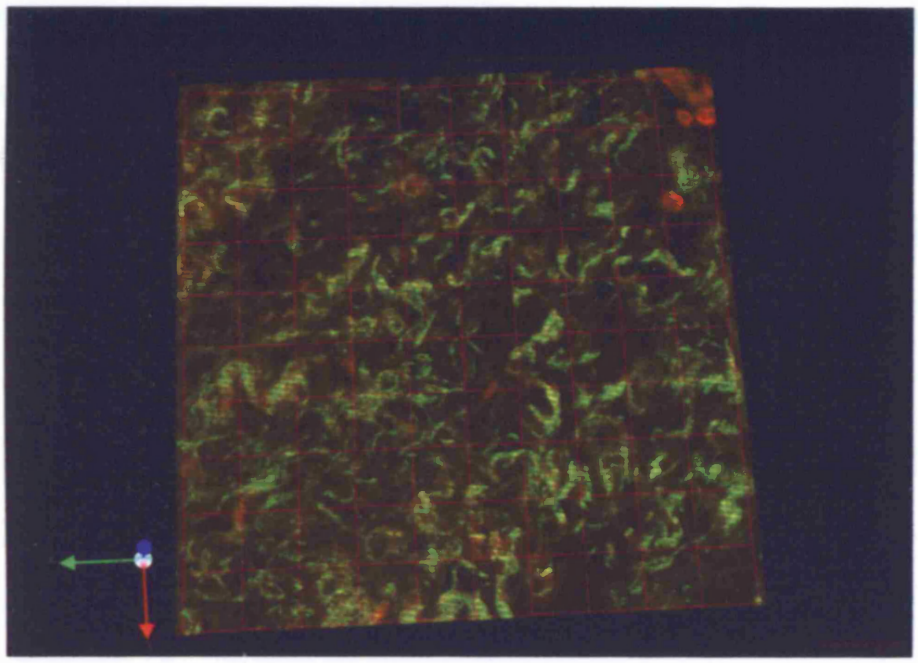

Fig. 3.3.5. Cells and matrix in the conjunctival stroma, visualised by confocal laser scanning microscopy, combined with intravital fluorescent cell staining with CFDA-SE (red) and confocal reflection microscopy settings (green). As opposed to two-photon excitation microscopy, confocal reflection settings visualise all matrix fibrils which scatter/reflect light, not only collagen fibres.

In summary, whole-tissue microscopy of conjunctival and corneal stroma can be achieved by combining optimized strategies for tissue maintenance, fluorescent cell labeling, and confocal laser and/or two-photon microscopy.

Chapter 4:

Discussion

4.1. Ocular fibroblasts differ in matrix contraction efficiency

This work is the first to systematically study and compare matrix contraction profiles of fibroblasts from different parts of the eye. Previous studies have published matrix contraction profiles of individual types of ocular fibroblasts. A direct comparison of published values is difficult, as fibroblasts from different species and different cell densities in collagen matrices were used, cells were stimulated with different cytokines, and matrices were occasionally pre-strained by maintaining attachment to the casting well for the first 24 hours. However, there is evidence that corneal fibroblasts contract matrix very rapidly, as we found in our work [Jester et al. 2003; Garrett et al. 2004]. This correlates with clinical observations. Corneal injury that reaches the stroma triggers a prompt activation of keratocytes into fibroblasts [Wilson et al. 2001]. Developmentally, corneal fibroblasts differ from Tenon's and scleral fibroblasts in that they are derived from a different embryological structure, neural crest rather than mesoderm. This might in part explain their particular receptor profile, high sensitivity to PDGF and different behavioural response.

For Tenon's fibroblasts, we observe a slower start of contraction over the first 24 hours. A similar timecourse is evident in published data, but has not been commented on before [Daniels et al. 2003]. In our model, Tenon's fibroblasts display a more sustained contractile activity, which continues over several days and results in the same final degree of matrix contraction as that achieved by corneal fibroblasts. Again, there might be a clinical parallel, as remodelling after glaucoma filtration surgery is commonly not an acute event, but continues for weeks after surgery.

Scleral fibroblasts have previously been observed to contract matrix by 20% within 24 hours of matrix preparation, which is a higher value than the less than 10% presented

here [Mazure et al. 1992]. The scleral fibroblasts selected for our work are unusual in that their protrusions are much shorter than those of corneal and Tenon's fibroblasts. We studied scleral fibroblasts from other sites from the same human donor eye as well as from other donors, and found that protrusion length varied considerably. The cells used here were isolated from regions close to the corneal limbus and differed from other scleral fibroblasts not only in protrusion length, but also other properties (A. Cambrey, unpublished data). In the context of our study of actin dynamics, we chose to use scleral fibroblasts with shorter protrusions, as they could serve as negative control in terms of dynamic cell activity and contractile behaviour. These cells had no significant matrix contracting properties when used at low density; high cell densities, however, induced a contraction profile resembling that of Tenon's fibroblasts. Clinically, scleral remodelling occurs during axial myopia and in response to elevated intraocular pressure in childhood glaucoma. These conditions develop slowly and gradually, and the slow and sustained matrix remodelling response we observed might be the underlying mechanism. Our observation that scleral fibroblasts from different parts of the eye have different properties might correlate with the predominantly posterior scleral elongation observed in axial myopia. Depending on their location, scleral fibroblasts might differ in contractile properties or might be regulated differently.

The fact that different fibroblasts show marked differences in their contractile properties might merit further exploration of cell-specific targets for the modulation of wound healing and matrix remodelling in these different tissues. We maintained all three cell types in the same culture and experimental conditions, which does not reflect their specialisation to the different extracellular matrix composition in cornea, episclera and sclera. The three cell types might also not be equally responsive in the standard media

we used, although cell growth seemed equally vigorous in all cells. In particular, the rounded morphology of the scleral fibroblasts used here may give rise to concern about the viability of these cells; however, this cell type grew to confluence faster and required flask splitting more frequently than the other two cell types.

The present experiments also studied cell behaviour in collagen type I only and over a very limited timespan, which oversimplifies the dynamic cell-matrix interactions in real tissue and makes direct correlation of *in vitro* and *in vivo* dynamics difficult. Nevertheless our results suggest that cells from different parts of the eye are intrinsically different in their behaviour. In particular, our force measurements suggest that there may be an intrinsic difference in the cells' ability to generate force, although the mechanism of force generation is likely to be common, as the values for intrinsic force are in the same range. Further work might identify markers that define these contractile properties, and this knowledge could be used to predict the contractile response of a particular tissue and to modulate contraction.

The biological tissues in which these ocular fibroblasts normally reside differ in extracellular fibre composition, and remodelling events occur over much longer periods of time. *In situ*, these fibroblasts might display behaviour different from that described here, as a matrix environment richer in diverse extracellular matrix molecules will stimulate different cell surface receptors such as different types of integrins, which act as extracellular matrix receptors [Cukierman et al. 2001]. Future work could investigate fibroblast behaviour in whole tissue, using the techniques explored in the present project.

4.2. The SIM-CFM

In order to study the link between dynamic cell behaviour and force generation, we developed a novel device, the SIM-CFM. Commercially available "cell stretchers" have several disadvantages. The most commonly used system, Flexercell^{TM} (Flexcell International), uses vacuum to deflect a membrane on which cells are cultured in monolayer. The deflecting force thereby acts at a normal to the membrane surface and to the basal cell surface, which is not the direction of strain connective tissue cells are usually exposed to [Eastwood et al. 1998]. The same problem arises with other systems, in which pushing the membrane upwards generates the deflecting force. Another major disadvantage of the vacuum based systems is that their design precludes all high-resolution live imaging, as the focus drifts enormously when the vacuum is applied.

The SIM-CFM offers a number of advantages over other "cell stretchers":

1. the measurement of forces generated by a population of cells in three-dimensional matrix, as opposed to cells grown in a single layer on a membrane
2. simultaneous live microscopic imaging of dynamic cellular behaviour and matrix changes
3. application of external tension and relaxation of internal matrix tension
4. application of external tension in the direction of strain physiological for many connective tissues, i.e. uniaxial
5. adjustment of external tension to the physiological level of tension for a particular cell type.

The SIM-CFM is an extension of the tensioning culture force monitor (t-CFM) developed by Eastwood [Eastwood et al. 1994; Eastwood et al. 1996; Brown et al. 1998; Eastwood et al. 1998; Eastwood et al. 1998]. The main advantage of the SIM-CFM over the t-CFM is its capability to perform simultaneous microscopy in addition to measuring and exerting forces. To gain morphological data, matrices studied on a conventional CFM need to be fixed and processed for microscopy. Live timelapse imaging of cell behaviour is now possible with the SIM-CFM, and we have shown that the force pattern and amplitude recorded with the SIM-CFM are comparable to values obtained with the original CFM. In addition, the use of high-resolution confocal light reflection technology simultaneously visualises individual matrix fibres. This enables us to acquire data on cell and matrix morphology as well as cellular forces at the same time.

The greater challenge of this device was to be able to observe the cells as they were contracting the matrix, but also as a mechanical strain was applied to the matrix. The design of the device, with one fixed side, means that any contraction or stretch of the matrix results in a significant unilateral horizontal displacement as well as some bilateral vertical displacement. There were concerns that this image drift might make it impossible to follow individual cell behaviour using timelapse microscopy. Indeed, a considerable difficulty is to keep cells in focus over time, as the focus drifts both laterally (xy- axes) and vertically (z- axis) during contraction and stretching. However, we have found that image drift in the xy-plane is manageable and can be compensated for by using the Registration module in Openlab^{TM} (Improvision), even when the drift is generated by applying a defined mechanical stress to the matrix. This software superimposes subsequent timelapse images which can then be manually centred onto

each other. The vertical drift is usually less dramatic because of its bilateral nature and can be compensated for during microscopy by acquiring z-stack images. For analysis, those images showing the same cells/matrix regions can be selected and connected to form a new timelapse series.

This combination of techniques results in a completely novel system with unique capabilities. Cell and three-dimensional matrix imaging before and after application of strain has to date been performed by only one other group [Voytik-Harbin et al. 2003]. However, the device used did not incorporate a culture force monitor, and rather than measuring cellular force generation only established stress-strain relationships. In addition, it was not stated whether dynamic timelapse imaging was performed, or rather acquisition of images after manual re-focussing on individual cells following application of external tension.

The SIM-CFM is therefore the first device of its kind, and has allowed us to link for the first time protrusive ability, matrix displacement and force generation in a pseudo-physiological 3D environment. Such a device will be particularly useful to study the effects of tensional changes on individual cells on a cellular and sub-cellular level.

4.3. Protrusive activity drives early contraction and force generation

The differences in *in vitro* matrix contraction in our model are most marked in the first 24 hours of matrix preparation, and the predominant cell behaviour during this phase is protrusive activity. Our data do not support either of the two main presumed mechanisms of matrix contraction, i.e. cell migration across matrices and myofibroblast transformation [Ehrlich et al. 1990; Grinnell et al. 2002; Hinz et al. 2003]. Instead, our results support the concept of matrix contraction by non-migrating fibroblasts using the "locomotion" machinery for cell-matrix interaction. [Meshel et al. 2005] We did not examine our cells for ASMA expression, but we did not observe stress fibre or actin cable formation as seen during myofibroblast transformation. In addition, it is generally accepted that myofibroblast transformation requires both TGF-β and tension, and that in free-floating matrices such as ours, this transformation does not occur [Arora et al. 1999; Hinz et al. 2003].

Whilst it has been noted that initial matrix contraction is associated with cell "spreading" from a round to a branched phenotype, the dynamic aspect of protrusive activity has not previously been investigated. Previous studies relied on static techniques and analysed cell morphology on formaldehyde-fixed matrices at defined timepoints only [Eastwood et al. 1996; Tamariz et al. 2002]. Our quantitation of dynamic protrusive activity in a three-dimensional environment demonstrates that in the presence of growth factors, the extension and retraction of protrusions is associated with net displacement of collagen fibres towards the cell. We also find that the dynamic extension and retraction of progressively longer protrusions is associated with an

increase in force generation, and that both cell length and force reach a plateau at the same time, about 6 hours after matrix preparation. Together, these findings indicate that fibroblasts use protrusive activity not only for migration, but also for cell-matrix interaction.

As a result of cell-matrix interaction, fibroblasts generate contractile force. The three types of ocular fibroblasts we studied generate different amounts of force, which has not previously been reported. The only comparative study of different types of fibroblasts demonstrated that Tenon's fibroblasts have a force generation profile different from that of dermal fibroblasts: skin fibroblasts displayed a sharp increase in force generation during the first 8-10 hours after matrix preparation, followed by a plateau at 40 to 60 dyne per million cells. Tenon's fibroblasts, on the other hand, showed a slow, but steady increase in force generation. After 24 hours, a force of 20 dyne per million cells was reached, but no plateau developed [Porter et al. 1998]. Our data support the finding of lesser contractile force in Tenon's fibroblasts. However, in our experiments, the force generation curve of Tenon's fibroblasts shows a sharp increase during the first six hours, followed by a plateau at 8 dyne per million cells. The differences in profiles obtained in these two studies might have been caused by differences in experimental setup. The development of simultaneous microscopy facility and force recordings lead us to reduce the matrix volume from 5ml (original CFM) to 2ml (SIM-CFM). In addition, donor-related differences in Tenon's fibroblasts might explain the different net force values obtained, as both experiments used primary cells from human donors, which might have differed in contractile characteristics. However, the strain measured by our miniaturised CFM setup is in the same range as that recorded on the original CFM. Both are several orders of magnitude smaller than the force recorded by other

techniques, as the CFM measures the summative strain exerted by a population of cells along only one axis. Isolated measurement of the tractional force generated by a single cellular protrusion is likely to be higher, as observed by single-cell measurements in planar culture [Lee et al. 1994].

The difference in global matrix contraction between ocular fibroblasts in our work correlates with force generation in the first 24 hours: corneal fibroblasts develop the highest force, and also contract matrix most, followed by Tenon's fibroblasts, whilst the scleral fibroblasts used here do not generate much force and do not significantly contract matrix. We identify four factors which influence the early matrix contraction profile of these cells: 1. cell size, 2. intrinsic force, 3. dynamic activity in extending and retracting protrusions and 4. net matrix displacement. In all experiments presented in this work, the scleral fibroblasts used here behave as a "negative control": their cell shape remains mostly spherical, with short protrusions only, they have a smaller cell volume than the other cell types, their dynamic activity is less, and matrix displacement and force generation are negligible. Calculation of intrinsic force demonstrates values of comparable magnitude for the three cell types studied here. The similarity in intrinsic force might explain why an increase in cell density in scleral fibroblast-populated matrices results in a global matrix contraction profile which runs parallel to that of Tenon's. However, corneal fibroblasts have higher force per volume than the other two types of fibroblasts, indicating that they might use different or additional matrix remodelling mechanisms.

We have not examined all factors relevant to matrix remodelling. In particular, we did not investigate efficiency in protrusion binding to collagen fibres via integrins and

matrix adhesions, and efficiency in permanently condensing fibres which have been pulled towards the cell body. Other studies complement our work. Integrins provide a direct link between actin cytoskeleton and extracellular matrix. Integrin engagement and focal adhesion formation are prerequisites for the generation of tractional force by fibroblasts migrating on extracellular matrix [Beningo et al. 2001]. The molecular motor of force generation, however, is the interaction between actin and myosin II, as demonstrated by MLCK inhibition in a similar model of migrating fibroblasts [Pelham et al. 1999]. Acto-myosin interaction is also the motor underlying extracellular matrix fibre displacement associated with "hand-over-hand" cycles of cell extension, matrix fibre attachment, retraction, and fibre release [Meshel et al. 2005]. Our results demonstrate this principle, described in a two-dimensional assay, in a three-dimensional collagen matrix, and the molecular pathways are discussed below.

4.4. Two types of protrusive activity, spreading and steady-state, define two phases of early matrix contraction

In the course of our experiments, we developed a modified collagen matrix contraction assay. During the first 24 hours after preparation, we maintained fibroblast-populated matrices in growth factor-free medium, prior to stimulation with PDGF. In the original assay, with PDGF present from matrix preparation onwards, the matrix is contracted by 50% within 24 hours, and by 48 hours, a plateau of 60% is reached. In the modified assay, contraction is only 20% in the first 24 hours, but after addition of PDGF reaches 50% at 48 hours and 60% at 72 hours. This means that in the modified assay, contraction over the first 24 hours after growth factor addition is only 30%, as compared to 50% in the standard assay. In the first 24 hours, dynamic activity is very high, as cells spread out from a rounded to a branched phenotype, before reaching a steady state where protrusion length remains stable, although protrusive and retractile activity continues. Compared to cells which have been stimulated with PDGF from the start, the protrusions of cells in growth factor deprived matrices are shorter and have a less branched appearance; this changes after addition of the growth factor (data not shown). However, it appears that once cells are established in the matrix, addition of growth factor does not result in as much dynamic activity as in the earlier spreading phase. The effect of all inhibitors used in our experiments is stronger when applied before growth factor stimulation. In the modified assay, matrices are pre-incubated with growth factor deprived medium including the inhibitor. After 24 hours, PDGF is added, whilst the inhibitor remains in the medium. Under these conditions, PDGF-induced matrix contraction is more profoundly reduced than in the standard assay, providing

further evidence that PDGF induces a significant effect in cells which have reached steady state in terms of their protrusive activity.

In our modified assay, dynamic activity during the spreading phase is associated with matrix contraction despite the absence of growth factors. As reported by other authors, we find that absence of growth factors reduces matrix contraction greatly, but not fully [Eastwood et al. 1996; Tamariz et al. 2002]. Reduced attachment to matrix and autocrine secretion of growth factors by fibroblasts in collagen matrix have been suggested as an explanation for residual matrix contraction [Grinnell et al. 2002; Tamariz et al. 2002]. We find that in the absence of growth factors, 10-20% of matrix surface area contraction occur within the first 24 hours, but that the contraction curve then reaches a plateau. If autocrine growth factor production was the mechanism underlying contraction in the absence of external growth factors, contraction could be expected to continue beyond the initial 24 hours. Cell spreading is a more likely explanation. The spreading activity with formation of increasingly longer protrusions seems sufficient to generate a small degree of matrix contraction even in the absence of growth factors. We did not quantify protrusive activity during the spreading phase under these conditions, but have observed that after 24 hours, growth-factor deprived fibroblasts have shorter and less branched protrusions than those in growth-factor supplemented matrices. Growth factors are required for efficient matrix binding, and are required in addition to dynamic cell activity to generate tractional force [Tamariz et al. 2002]. The growth-factor dependence of matrix contraction efficiency is therefore likely to be due to growth factor influence on dynamic cell behaviour, i.e. binding to matrix fibres and formation of longer and branching protrusions in response to matrix binding. Further work could investigate these effects by studying these specific aspects of matrix contraction in growth-factor deprived matrices.

4.5. PDGF is a major growth factor inducing matrix contraction by corneal fibroblasts

In our studies PDGF-BB stimulates 70% of the matrix contraction elicited by serum. Other authors demonstrate that matrix contraction induced by PDGF-AB is 50% of that induced by TGF-β [Jester et al. 2003]. This finding correlates well with previous reports on the relevance of PDGF-BB in corneal healing [Kim et al. 1999; Wilson et al. 2001]. In our model, chemical inhibitors of the PDGF signalling pathway reduce matrix contraction, both after stimulation with PDGF-BB and after stimulation with serum. This indicates that PDGF inhibition might be a powerful new target in the modulation of haze formation and scarring after corneal surgery or injury, and the mechanism by which PDGF stimulates matrix contraction by these cells deserves detailed analysis. Both AG1295 and Trapidil inhibited matrix contraction. Whilst AG1295 did not show any toxic cellular effects, the incidence of cell death was increased in Trapidil-treated matrices. The latter finding is surprising, as identical concentrations of Trapidil are not toxic to bovine corneal fibroblasts *in vitro* [Knorr et al. 1999]. Trapidil has also been used in clinical studies without toxic side-effects, but as administration was systemic, concentrations cannot be directly compared [Galassi et al. 1999; Serruys et al. 2001; Maresta et al. 2005]. However, it is interesting to note that in these studies, Trapidil failed to show a beneficial effect in preventing neo-intima formation after vascular interventions; this lack of clinical effect might have been caused by the use of insufficient doses. We only performed our toxicity evaluation in one experiment, and it is possible that repeat experiments could disprove this finding. Further experiments, both *in vitro* and *in vivo*, are needed to further explore the use of these agents.

4.6. The signalling pathway downstream of the PDGF receptor induces circular ruffling in corneal fibroblasts

PDGF plays an unusually important role in the activation of keratocytes and corneal fibroblasts [Wilson et al. 2001; Jester et al. 2003]. Previous work in our laboratory had indicated that in corneal fibroblasts, PDGF triggers a dramatic, actin-based phenotype, circular ruffling (unpublished data). The present work is the first report of circular ruffling in human corneal fibroblasts. Other fibroblasts in which circular ruffling has been observed after PDGF stimulation are Swiss and NIH 3T3 fibroblasts, mouse embryonic, and human fibroblasts (Detroit 551) [Plattner et al. 1999; Dharmawardhane et al. 2000; Anton et al. 2003; Hogan et al. 2004; Lanzetti et al. 2004]. Our data confirm that proteins known to be involved in the formation and closure of circular ruffles in other cells play a part in corneal fibroblasts as well, namely Scar/WAVE, the arp2/3 complex, MLCK, rab5 and the rab5 GTPase, RNtre [Araki et al. 2003; Krueger et al. 2003; Suetsugu et al. 2003; Lanzetti et al. 2004]. Circular ruffles are formed by actin filaments which push the cell membrane upwards. Actin filament elongation is catalysed by the arp2/3 complex, which in turn is activated by WAVE 1. The pathway from PDGF receptor to WAVE 1 runs through ras, PI3K and rac, as does the pathway for lamellipodia and peripheral ruffle formation. Formation of circular ruffles, however, requires additional signalling through the rab5 pathway, resulting in three simultaneous activating signals through PI3K, rac and rab5 [Lanzetti et al. 2004].

In our model, formation and centripetal closure of circular ruffles also require MLCK, but cannot be suppressed by ROCK-inhibitors or direct myosin II inhibition through blebbistatin. The pathway from PDGF/rac to MLCK/myosin activation is unknown, but activation could occur at several points of the circular ruffling pathway:

1. crosstalk between rac and rho could result in ROCK and/or MLCK activation with subsequent myosin light chain phosphorylation and myosin activation. Rac/rho crosstalk has been observed in serum-starved Swiss 3T3 fibroblasts [Ridley et al. 1992; Ridley et al. 1992].

2. p21-activated kinase (PAK) has recenly been demonstrated to be capable of **directly phosphorylating myosin light chain** [Brzeska et al. 2004]. However, this would not explain MLCK involvement, as PAK downregulates MLCK activity.

3. rab5 could interact with a myosin, but no such interaction has been reported to date. However, interaction between myosins and rab GTPases has been described in the context of plasma membrane recycling (rab11a and myosin Vb), endosomal vesicle transport (rab8p and myosin V), and melanosome capture (rab27a and myosin Va) [Lapierre et al. 2001; Fehrenbacher et al. 2003]. Several myosins are known to be present in cellular protrusions: myosin I, V, VI, VII, and X localise to lamellipodia and membrane ruffles, and myosin II exerts a contractile effect at the base of lamellipodia [Small et al. 2002; Giannone et al. 2004].

4. Actinin-4, which is part of the rab5-RNTre-f-actin-ACTN4 complex at the end of the rab5 signalling pathway, could bind to myosin. Recently, a protein complex composed of Hrs/Actinin-4/BERP/Myosin V has been reported in the context of receptor recycling [Yan et al. 2005]. There is no report of actinin-4 binding to myosin II, but another isoform of this protein, α-actinin, was found to interact with MLCK in the activation of myosin II in regular lamellipodial contraction [Giannone et al. 2004].

It is surprising that blebbistatin had no influence on circular ruffling. Whilst blebbistatin is highly specific for myosin II A and B [Straight et al. 2003], it is not known whether MLCK phosphorylates light chains of myosins other than myosin II. The lack of inhibition of circular ruffling by blebbistatin indicates that myosin II is either not involved in this phenomenon, or that it is not the only myosin mediating circular ruffles. Recently, myosin-X has been reported to be required for pseudopodial extension during phagocytosis [Chavrier 2002; Cox et al. 2002], and it might be a candidate for further investigations into circular ruffling, as it is not inhibited by blebbistatin [Straight et al. 2003].

As rho kinase (ROCK) activity results in MLC phosphorylation both through a downstream effect on MLCK and through a direct effect, the fact that ROCK inhibition does not affect circular ruffling might also be surprising. However, this finding is consistent with previous reports that MLC phosphorylation is regulated differently depending on location within the cell. Whilst myosin II activated by MLCK at the cell periphery controls membrane ruffling, ROCK regulates MLC phosphorylation in the cell centre [Totsukawa et al. 2004]. It is therefore possible that the circular ruffling pathway signals through MLCK, but not ROCK.

In summary, our work demonstrates that the signalling pathway from PDGF receptor to circular ruffling has at least three elements, which after receptor tyrosine kinase activation might run in parallel (Fig. 4.1). The point of convergence of these signals is at present unknown.

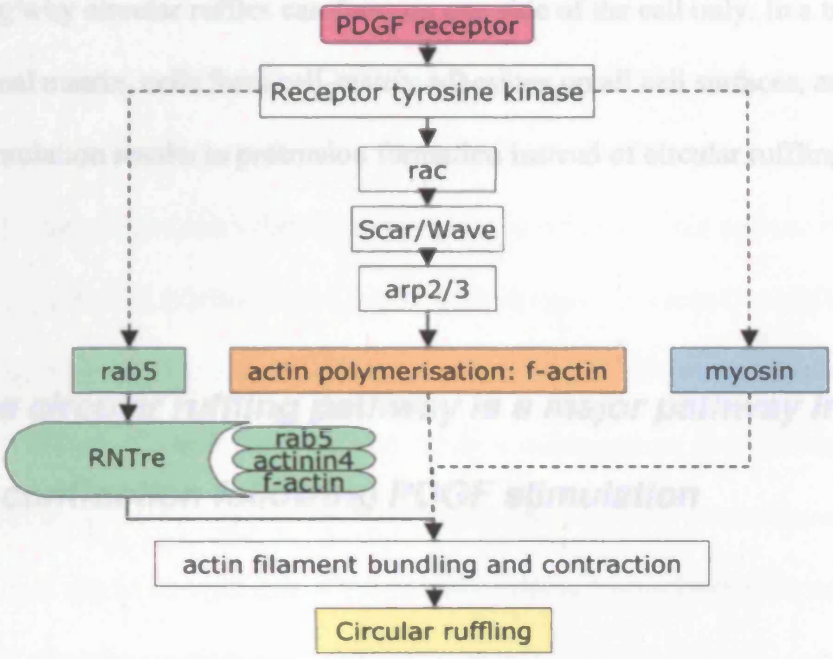

Fig. 4.1. Elements of the circular ruffling pathway. Conventional signalling through rac, Scar/Wave and arp2/3 mediates actin polymerisation and network formation. Actin filament bundling and stabilisation of the network in circular ruffles might be achieved through binding of f-actin to rab5/RNTre/actinin-4. Myosin might mediate concentric ruffle constriction and could be involved in the extension of circular ruffles.

We examined whether activation of the circular ruffling pathway in corneal fibroblasts in three-dimensional matrix also results in the formation of circular arrangements of surface protrusions. We did observe increased protrusive activity, but no circular pattern. This differs from a report that pancreatic tumour cells cultured between sheets of collagen in sandwich-like fashion form circular ruffles when stimulated with EGF (epidermal growth factor) [Orth et al. 2006]. However, fibroblast-populated three-dimensional matrix and the sandwich model differ significantly, with the latter maintaining basal/dorsal two-dimensional cell polarity as seen in other planar culture models. In the sandwich model, the cell-matrix adhesions at the basal cell surface form earlier than those on the dorsal surface, resulting in a polarised response to stimuli,

explaining why circular ruffles can form on one side of the cell only. In a truly three-dimensional matrix, cells form cell-matrix adhesions on all cell surfaces, and growth factor stimulation results in protrusion formation instead of circular ruffling.

4.7. The circular ruffling pathway is a major pathway in early matrix contraction following PDGF stimulation

Our data on the effects of PDGF mediated activation of the circular ruffling pathway in a three-dimensional collagen matrix environment allow us to develop new ideas about the potential physiological function of this signalling pathway. To date, three main functions have been proposed: fast actin remodelling in static cells preparing for cell movement, receptor internalisation, and endocytosis, in particular macropinocytosis [Krueger et al. 2003; Buccione et al. 2004; Orth et al. 2006]. The latter has been described as a result of circular ruffling in macrophages, mouse embryonic fibroblasts, 3T3 fibroblasts, Dictyostelium, and, recently and more specifically, in the form of polarised apical macropinocytosis in MDCK cells [Zhou et al. 1998; Jones et al. 1999; Plattner et al. 1999; Dharmawardhane et al. 2000; Araki et al. 2003; Hogan et al. 2004; Lanzetti et al. 2004; Mettlen et al. 2006]. It has been suggested that macropinocytosis, in particular in response to growth factor stimulation, might be relevant in facilitating cell locomotion by recycling plasma membrane and enhancing „membrane flow" [Bretscher 1996].

Because of its association with cell protrusive activity, we hypothesised that the circular ruffling pathway might be involved in matrix contraction. Indeed, specific inhibition of

this pathway by expression of the dominant negative rab5 mutant, S34N, overexpression of the rab5 GTPase, RNTre, and RNTre mRNA silencing, does inhibit PDGF-induced matrix contraction. Considering that only 50% or less of cells were successfully transfected with these plasmids, the inhibitory effect on matrix contraction is noteworthy. ROCK inhibition and blebbistatin-induced myosin II inhibition displayed a considerably stronger inhibitory effect on matrix contraction than any of the inhibitors of the rab5/circular ruffling pathway, but these broad-spectrum chemical inhibitors are likely to affect all cells and possibly other functions as well as protrusion-mediated contraction. A direct comparison of the specific rab5 inhibitors and the chemical inhibitors is therefore difficult.

The results of our studies with different myosin pathway inhibitors indicated that MLCK, ROCK and myosin II have different roles in the events leading to matrix contraction, which is consistent with other published studies. Whilst MLCK only activates MLC, ROCK phosphorylates a variety of substrates, and myosin II activation is the final step of several contractility pathways [Totsukawa et al. 2004]. Our results demonstrate that ROCK inhibition and myosin II inhibition via blebbistatin profoundly reduce matrix contraction, whilst MLCK inhibition leads to a milder reduction in contraction.

A previous study on contractility of breast gland epithelial cells reported that ROCK inhibition blocked *in vitro* matrix contraction, whilst MLCK inhibition had no effect, which is different from out findings [Wozniak et al. 2003]. However, it is known that the response to ROCK and MLCK inhibitors is cell-type specific [Totsukawa et al. 2004].

Our microscopical studies reveal that the inhibitory effect of ROCK and MLCK on matrix contraction is mediated by different mechanisms. In our analysis of cell protrusive activity, we find that whilst MLCK inhibition reduces dynamic cell activity, ROCK and myosin II inhibition have no inhibitory effect, or even tend to increase it. Whilst our quantitative method studies the overall sum of protrusion formation and retraction, other authors have analysed protrusion formation and retraction separately. From these analyses it emerges that depending on cell type and dose of the inhibitor, ROCK inhibition can induce both an increase and a decrease in protrusion formation, and that MLCK inhibition can result in protrusion formation all around the cell or in a complete collapse of protrusive activity [Katsumi et al. 2002; Worthylake et al. 2003; Totsukawa et al. 2004].

Sub-analysis of our data for protrusive and retractile activity reveals that in our model, ROCK inhibition via Y27632 induces an increase, and MLCK inhibition via ML-7 and ML-9 induces a reduction of both protrusion formation and retraction (Fig. 4.2).

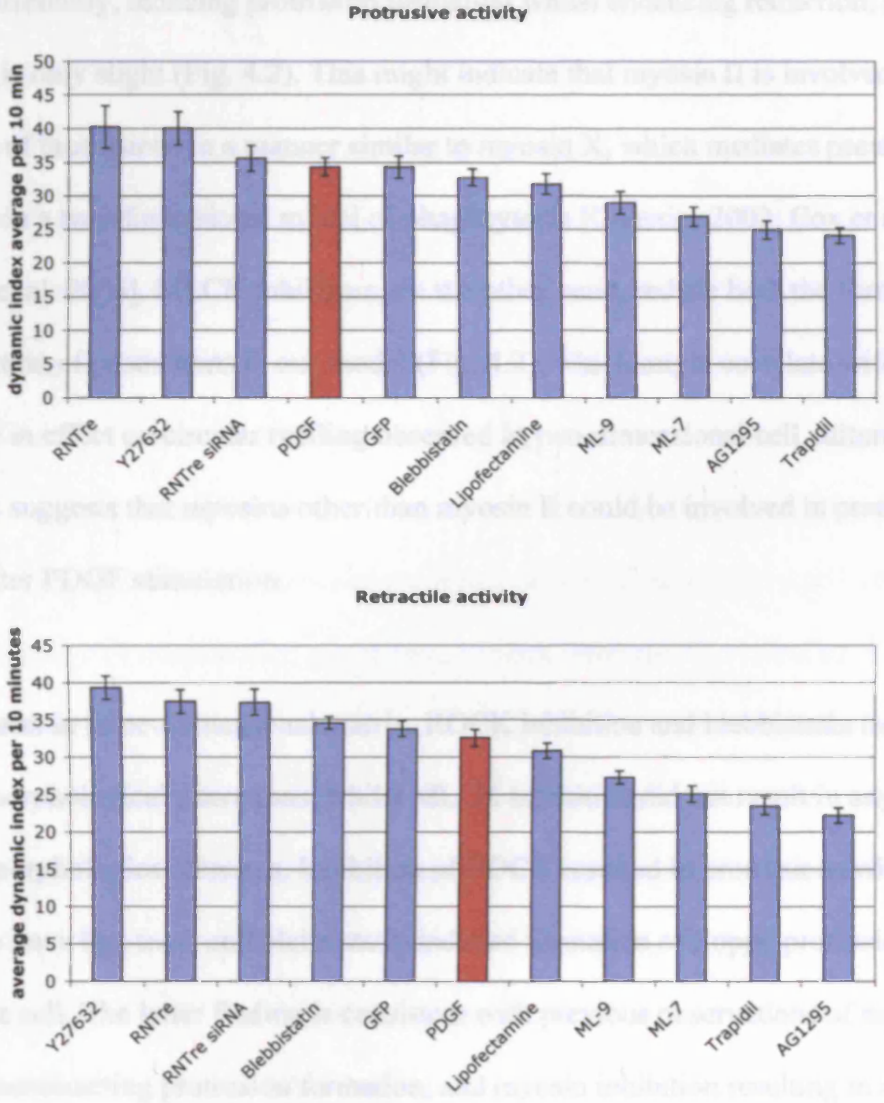

Fig. 4.2. Effect of all tested inhibitors on protrusive and retractile dynamic activity of corneal fibroblasts after PDGF stimulation. These charts summarise the data presented in Chapter 3, analysed separately for protrusion formation and retraction. Whilst MLCK inhibitors reduce both protrusive and retractile activity, ROCK inhibition increases both. Myosin II inhibition through blebbistatin might inhibit protrusive, but enhances retractile activity. Inhibition of the rab5 signalling pathway slightly increases both protrusive or retractile activity, indicating that its significant effect on matrix contraction might be mediated through another mechanism, such as recycling of integrins or receptors.

In this analysis, blebbistatin is the only inhibitor which affects protrusive and retractile activity differently, reducing protrusion formation whilst enhancing retraction, although the effect is only slight (Fig. 4.2). This might indicate that myosin II is involved in the extension of protrusions in a manner similar to myosin X, which mediates pseudopodial extension in a two-dimensional model of phagocytosis [Chavrier 2002; Cox et al. 2002; Wyckoff et al. 2006]. MLCK inhibitors, on the other hand, reduce both the formation and retraction of protrusions in our model (Fig. 4.2), which might correlate with the difference in effect on circular ruffling observed in two-dimensional cell culture. This difference suggests that myosins other than myosin II could be involved in protrusive activity after PDGF stimulation.

In fibroblasts in three-dimensional matrix, ROCK inhibition and blebbistatin induced striking morphological alterations, whilst MLCK inhibition did not result in any obvious morphological changes. Inhibition of ROCK resulted in protrusions which seemed to have less tone, and blebbistatin induced formation of floppy protrusions all around the cell. The latter finding is consistent with previous observations of myosin II activity counteracting protrusion formation, and myosin inhibition resulting in actin-mediated protrusion formation all around the cell [Wakatsuki et al. 2003; Totsukawa et al. 2004].

However, as we do not observe this phenotype after MLCK or ROCK inhibition, these two pathways might be complementary in matrix contraction activity, and blockage of one pathway could be partially compensated for by the other. Consistent with this hypothesis, a recent study of mechanisms of matrix invasion by tumour cells *in vitro* and *in vivo* demonstrated different involvement of MLCK and ROCK in protrusion formation and generation of tractional force: the authors report that formation of new

protrusions is MLCK, but not ROCK dependent, whilst force generation depends on ROCK, but not MLCK. ROCK localises to newly formed protrusions and mediates myosin light chain phosphorylation and organisation into bundles perpendicular to the direction of the extending protrusion, enabling contractile interaction between the actin network and myosin II. ROCK inhibition results in the formation of longer protrusions, but these are inefficient at penetrating matrix, and fail to form MLC bundles with the correct alignment [Wyckoff et al. 2006].

Several of our observations are consistent with this model: we also find that MLCK is required for protrusion formation. We observe that ROCK inhibition results in a slight increase in dynamic activity. However, the effect of MLCK inhibition is cell-type specific, and whilst some studies report MLCK being essential for protrusion formation, others observe that it counteracts actin-mediated protrusion formation [Totsukawa et al. 2004; Wyckoff et al. 2006]. As we do not observe protrusion formation all around the cell after MLCK inhibition, our findings suggest that in corneal fibroblasts, MLCK is essential for protrusion formation. As in the above model, ROCK inhibition might block the formation of correctly aligned MLC in the protrusions, which is required for efficient matrix contraction. Inhibition of this mechanism could explain the profound inhibitory effect on matrix contraction we observed.

Blebbistatin induces the formation of numerous floppy-appearing protrusions all around the cell, indicating both a failure to retract protrusions and a failure to form protrusions capable of penetrating matrix. The quantitative data, however, do not support the notion of inhibition of retraction (Fig. 4.2), but changes from the values observed for PDGF in the absence of inhibitors are only slight.

Another important component of protrusive activity and cell-matrix interaction is adhesion formation. Both MLCK and ROCK inhibition affect matrix adhesion dynamics. MLCK is essential for focal contact formation, whilst ROCK is essential for maturation of contacts into focal adhesions [Totsukawa et al. 2004]. Periodic contractions in lamellipodia, which might serve cells to probe the rigidity of the matrix, generate waves of actin-bound α-actinin and MLCK, which activate myosin II at the base of lamellipodia, causing contraction. This wave formation depends on MLCK, but not ROCK [Giannone et al. 2004]. The matrix response to this probing traction affects the level of tyrosine phosphorylation on the cytoplasmic side of integrins, which in turn regulates the formation and stabilisation of focal adhesions [Pelham et al. 1998]. Similarly, myosin X might serve the formation of adhesive structures and has been shown to be involved in integrin relocalisation [Zhang et al. 2004].

Taken together, our findings and previous models suggest the following mechanism of matrix contraction by corneal fibroblasts (Fig. 4.3): Protrusion formation in response to PDGF stimulation is mediated by actin polymerisation and is MLCK-dependent. MLCK is also required for adhesion formation to extracellular matrix fibres and might mediate matrix probing behaviour. ROCK is required for maturation of focal contacts into focal adhesions and for MLC alignment, which is required for effective retraction of protrusions and traction of matrix fibres towards the cell.

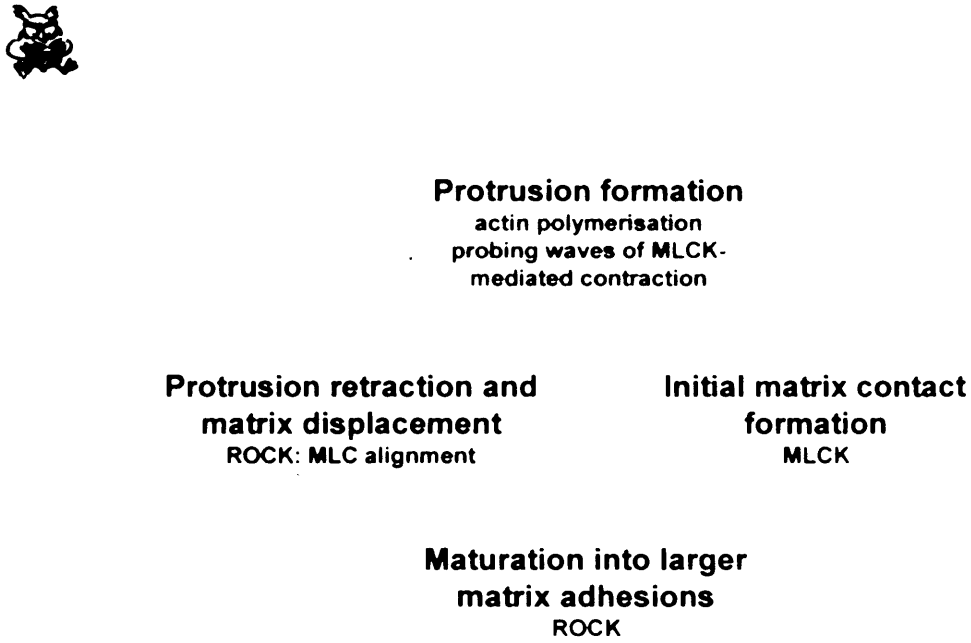

Fig. 4.3. Alternating cycles of protrusion formation, matrix binding, and protrusion retraction with matrix displacement are mediated by actomyosin dynamics.

4.8. The role of the rab5/circular ruffling pathway in matrix contraction

Based on our results on the role of actomyosin dynamics in protrusive activity and matrix contraction, and on previous suggestions for the functional role of this pathway, the rab5/circular ruffling pathway could be involved in matrix contraction activity through several mechanism:

1. As actin polymerisation is required for two-dimensional circular ruffle and three-dimensional protrusion formation, the rab5 pathway might mediate its effect through **actin-based protrusion formation.** However, unlike inhibition of actin assembly and myosin activation, inhibition of the rab5 pathway does not seem to affect protrusive activity in matrix (Fig. 4.2).

2. MLCK is required for circular ruffle formation and closure in the two-dimensional and essential for protrusion formation and matrix adhesion formation in the three-dimensional model. Rab5 might mediate its effect in three-dimensional culture through **interaction with MLCK and/or myosin in protrusion dynamics.** RNTre mRNA silencing results in a phenotype with protrusions all around the cell, as previously discussed in the context of a deficit in protrusion retraction. An interaction between rab5 and myosin II has not been reported, but several rab proteins are capable of directly binding to myosin V [Lapierre et al. 2001; Fehrenbacher et al. 2003]. It is therefore conceivable that the rab5 pathway is involved in myosin mediated contractility events. As outlined above, the rab5/RNTre/actinin-4/f-actin complex might also be

capable of binding to myosin, as actinin-4 has been found in a complex with myosin V and other molecules [Yan et al. 2005].

3. The circular ruffling/rab5 pathway might affect adhesion dynamics through **interaction with integrins.** The PDGF receptor co-localises and co-operates with membrane-spanning molecules such as integrins or the dystrophin glycoprotein complex (DGC). Integrin antagonists can inhibit PDGF-induced cell migration through matrix, and involvement of the circular ruffling pathway has been suggested [Tiger et al. 2001; Suetsugu et al. 2003; Hogan et al. 2004; Popova et al. 2004; Hoffman et al. 2005]. As protrusive and retractile activity in our model uses the same molecular "locomotion" machinery as cell migration in other models, future work with fluorescently labelled RNTre or RNTre-siRNA could investigate whether the rab5 pathway is linked to fibre displacement in our assay, and also assess integrin levels and adhesion numbers and configuration at the cell/matrix interface.

4. Both circular ruffling and the rab5 pathway have been extensively discussed in the context of **endocytosis and integrin/growth factor receptor/plasma membrane recycling** [Lanzetti et al. 2001; Lanzetti et al. 2004; Orth et al. 2006]. All of these are required for the continuous renewal of cell-matrix interaction sites, which in turn are essential for continuous cycles of protrusive activity. Consistent with an involvement of circular ruffling in growth factor receptor recycling, EGF receptor clustering has recently been observed in circular ruffles of pancreatic tumour cells expressing GFP-tagged EGF receptor [Orth et al. 2006]. Our immunostaining experiment on formaldehyde-fixed cells did not demonstrate PDGF receptor in the circular ruffles, but differences in technique might explain the differences in findings. In addition, our

dynamic characterisation of circular ruffling dynamics after stimulation with different concentrations of PDGF indicates that receptor clustering is involved. A minimum amount of PDGF is required to trigger circular ruffle formation, and although increasing PDGF concentrations accelerate the formation of circular ruffles, low concentrations do not trigger this phenotype even if the observation period is extended. Cooperation with MLCK and myosin might be part of the effect of the circular ruffling pathway on endocytosis, as MLCK is involved in endocytic cup closure [Dowrick et al. 1993; Araki et al. 2003].

In our three-dimensional collagen matrix assay, a role of the rab5 pathway in integrin or PDGF receptor recycling could in future be investigated by studying whether specific rab5 pathway blockage results in a reduction in adhesion efficiency, fibre displacement and/or protrusion formation.

4.9. Relevance to wound healing modulation and the eye

Our findings with regards to the basic mechanisms of cell-mediated matrix contraction and the central role of actomyosin-based cell protrusive activity indicate powerful new targets for the modulation of wound healing and scarring events. Instead of targeting cell proliferation, migration, and ASMA expression, our work demonstrates that matrix contraction can be inhibited efficiently by interfering with protrusive activity through inhibition of actin assembly, myosin activity and/or targeting of specific molecules involved in protrusion formation or integrin/receptor recycling.

Currently used inhibitors of ocular scarring such as 5-Fluorouracil and Mitomycin C are non-specific and cytotoxic. Newer agents such as an antibody to TGF-β2 target molecules at the beginning of the signalling cascade, and thereby affect all downstream events. However, the dosage of the TGF-β2-antibody agent has proven difficult in the complex situation of clinical use [Siriwardena et al. 2002]. Ideally, a successful modulator of contraction should target a downstream effector of a signalling cascade, such as actin or myosin, avoiding undesired effects which might be precipitated by complete suppression of growth factor signalling. The present work demonstrates that cells from different ocular tissues show different behavioural responses to particular growth factors, and modulators of contraction will need to be tailored to individual tissues.

Actin assembly inhibitors cannot easily be applied and might carry significant side-effects, as the actin cytoskeleton underlies all dynamic cellular activities, not only protrusive behaviour. Myosin inhibition, on the other hand, might be a worthwhile

therapeutic approach. Protein kinase inhibitors such as ML-7, ML-9 (MLCK inhibition), Y27632 and HA-1077 (ROCK inhibition) could specifically be applied to target tissues. Indeed, HA-1077, also known as AT877, has already been used in humans to control cerebral vasospasm after subarachnoid hemorrhage and has shown high tolerance [Shibuya et al. 1992]. In addition, HA-1077 and MLCK inhibitors reduce intraocular pressure and tissue tension following topical use in the eye in rabbit models [Honjo et al. 2001; Waki et al. 2001; Honjo et al. 2002].

Prior to testing the effects of new agents on living organisms, it would be desirable to evaluate their effect in *ex vivo* tissue. The *in vitro* approach of cultures of individual cell types in three-dimensional collagen matrix is well suited to dissect individual pathways and to learn about the specific effects of single agents, but results cannot necessarily be extrapolated to the complex situation of whole tissue. The last part of this work therefore explored imaging strategies for the study of cell-matrix interaction in whole tissue.

Whilst direct observation *in vivo* would be the ideal investigative technique, much information can be gained from *ex vivo* tissue maintained in culture, and both tissue maintenance and microscopy have seen significant advances in recent years. Three main technological innovations have been used for whole-tissue microscopy: clinical confocal microscopy, using a halogen light source, confocal laser scanning microscopy for the study of fluorescently labelled histological and cell biological specimens, and to a certain degree for live cellular imaging, and two-photon excitation microscopy for the microcopy of living tissues. However, neither of these has been entirely successful in visualising cells and cell-matrix interaction in stromal tissue on the surface of the eye, i.e. conjunctival and corneal stroma.

We have used conventional two-photon excitation microscopy to simultaneously visualise cells and matrix in conjunctival stroma, and combinations of intravital dye staining of cells and visualisation of matrix via confocal reflection technique to obtain similar images with a confocal laser scanning microscope. The corneal stroma can only be visualised using two-photon excitation microscopy, using second harmonic generation. Quiescent keratocytes can be visualised by transduction with GFP-transgene carrying adenovirus and subsequent confocal laser scanning or two-photon excitation microscopy. The acquisition of dynamic images for the study of cell behaviour requires whole-tissue culturing techniques. We report that conjunctiva can be maintained in standard tissue culture medium, and that cornea can be maintained and imaged using a modified anterior segment perfusion chamber.

The ideal setup to investigate cell behaviour and cell-matrix interaction would allow microscopic visualisation of cells and matrix *in vivo*, both in animal models and humans.

However, this goal is not yet achievable. Confocal microscopy is the best currently available technique for the study of cell behaviour on and near the ocular surface [Tervo et al. 2003]. It relies on the reflection of light by the structures under investigation. Compared to conventional microscopy, it minimises scattering of light from structures outside the focal plane, enabling optical sectioning of thin layers of the cornea. As the light source used is a halogen lamp, this type of microscopy is not harmful to the eye. However, whilst epithelial, stromal, and endothelial cells of the cornea can be visualised, keratocyte processes and matrix, with the exception of newly formed matrix, cannot [Tervo et al. 2003].

Confocal laser scanning microscopy, used in the examination of fluorescently labelled histological specimens, allows visualisation of fluorescent structures with high resolution. It offers the additional advantage of simultaneous visualisation of the stroma, using the technique of confocal reflection microscopy [Friedl et al. 2001]. This relies on the reflection and backscattering of light by the structures under observation, and has proven useful in the study of cancer cells migrating through perivascular connective tissue [Friedl et al. 2001] and of fibroblasts remodelling collagen matrix. In our experiments, confocal reflection microscopy visualised conjunctival stroma well, but not corneal stroma, where matrix fibrils are tightly and accurately aligned to prevent reflection and scatter.

However, the use of confocal laser scanning microscopy is not ideal for the imaging of living cells. The laser light, particularly the wavelengths in the UV part of the spectrum required to make use of autofluorescent properties of tissues, is toxic to cells, and incorporation of fluorophores into cells enhances phototoxicity. This limits the use of the confocal laser scanning microscope to the study of *ex vivo* specimens, or to intermittent *in vivo* studies, where cells are allowed sufficient time to recover between imaging episodes.

Two-photon excitation microscopy is a recent technique which overcomes many of the limitations of confocal laser scanning microscopy, and which makes use of the autofluorescent properties of cells and tissues. Its basic principle is the simultaneous absorption of two photons, which allows the use of two photons from the near-infrared range to excite molecules which would normally be excited by absorption of photons in the ultraviolet range. As a consequence, fluorescent imaging of these molecules is possible with far less cell damage than with previous techniques, as the exciting photons

are less harmful. In addition, excitation is limited to the focal volume of interest, reducing photobleaching and phototoxicity in neighbouring tissues [Williams et al. 2001].

Previous studies have explored the use of two-photon microscopy in the study of cornea and conjunctiva. In conjunctiva, published images are of relatively low magnification and do not demonstrate stromal cells [Teng et al. 2006]. Our study demonstrates conjunctival cells and stroma with high resolution, relying exclusively on their autofluorescent properties.

Corneal studies have delivered mixed results for different layers. Whilst epithelial and endothelial cells have been visualized, stromal cells could only be demonstrated with additional manipulation. The problem underlying keratocyte visualization is probably their low oxidative metabolic state, generating few NAD(P)H molecules which respond to the exciting photons used to stimulate autofluorescence. As a result, keratocytes generate a signal of low intensity, whilst the surrounding stroma, predominantly composed of collagen, generates an intense signal.

One way of manipulating the metabolic state of keratocytes to enhance autofluorescence is the application of sodium cyanide, which inhibits oxidative metabolism and increases fluorescence from all types of corneal cells by a factor of 2 [Piston et al. 1995]. However, this method is cell-toxic and cannot be used to image physiological cell conditions.

Another way of enhancing keratocyte fluorescence is to incorporate fluorophores into the cytoplasm. Two methods have been used: application of vital eyes, and transduction with viral vectors expressing enhanced green fluorescent protein (eGFP) [Poole et al. 1993; Foreman et al. 1996; Gatlin et al. 2003; Poole et al. 2003; Carlson et al. 2004].

The first technique has been used on small pieces of cornea, measuring 0.5 by 2mm, incubated either for four hours or overnight. Vital dyes diffuse into cells and can subsequently be imaged by epifluorescence or confocal laser scanning microscopy [Poole et al. 1993; Poole et al. 2003]. In our experiments on whole cornea, we found that penetration through epithelium or endothelium and their respective basement membranes and through the dense stromal matrix was insufficient to stain keratocytes with CFDA-SE and CMFDA (data not shown). This is in contrast to a previous report that another vital dye, calcein AM, accumulated in the cytoplasm of keratocytes in whole cornea in culture [Foreman et al. 1996]. Differences in dye properties might explain the difference in findings.

However, this technique was successful in demonstrating cells in the conjunctiva. In combination with confocal reflection microscopy, intravital cell labeling can be used for the study of cell-matrix interaction by any confocal laser scanning microscope, including dynamic events imaged by timelapse settings. However, photobleaching and phototoxicity are limiting factors.

The second method to enhance keratocyte fluorescence, transduction of keratocytes with a GFP-transgene carrying adenovirus through microinjection into the stroma of healthy rabbit corneas or through application of vector supernatant to rabbit corneas following lamellar keratectomy, has been elegantly used to render rabbit keratocytes

green fluorescent *in vivo*, but microscopy was conducted on excised tissue [Gatlin et al. 2003; Carlson et al. 2004]. Instead of the previously reported vectors, we used GFP transgene carrying adenovirus V209 with hCMV promoter, which successfully achieved keratocyte visualisation with both confocal laser scanning and two-photon excitation microscopy 24 hours after transduction.

Whilst visualization of keratocytes by two-photon microscopy has not yet been achieved under physiological conditions, the corneal stroma can be successfully imaged by using second harmonic generation. Collagen molecules are organised naturally into structures on the scale of the wavelength of light, and lack a centre of inversion symmetry. In second harmonic generation, two photons simultaneously interact with structures which lack a centre of inversion symmetry, without being absorbed. Because there is no energy loss, these processes emit radiation at exactly 1/2 of the exciting wavelength when stimulated by two exciting photons [Williams et al. 2001]. With an excitation wavelength of 800nm, different patterns of collagen fibre orientation can be visualized, and orientation can be measured with an axial resolution of 10μm. When wavelengths below 800nm are applied (730-800nm), the signal emitted from the extracellular matrix is a combination of SHG and two-photon excited fluorescence [Zoumi et al. 2002]. Second harmonic generation imaging of the cornea has been used in fresh pig eyes, and in an animal model of refractive surgery [Han et al. 2004; Teng et al. 2006].

All approaches to deliver fluorophores into cells require time until the fluorescent molecules are either taken up into the cytoplasm or begin to be expressed by the gene transcription machinery. In practical terms, this means that they can be applied to living animals and then visualised later, usually involving the animal to be sacrificed so that a specimen suitable for microscopy can be obtained. Alternatively, fluorophores can be

applied to tissue *ex vivo*, such as from an abattoir or from animals sacrificed for other studies, but then tissue culture methods need to be available to maintain the tissue until imaging can be performed. We found that for conjunctival tissue, this is not a problem, as pieces of conjunctiva can easily be maintained in standard tissue culture medium; the only artefact induced is tissue hydration. However, culture of whole cornea is difficult, as the cornea is an organ at the interface between two very different environments: on the outside, cornea *in vivo* is exposed to air, only covered by a thin layer of tear film. On the inside, it is in continuous contact with aqueous fluid. In culture, isolated cornea submerged in tissue culture media looses its transparency, due to stromal hydration, and can no longer be used as model for corneal physiology. Corneal tissue culture for the study of physiological tissue characteristics therefore has to simulate the air/fluid interface.

Several methods of corneal tissue culture have been suggested. In particular, we attempted the filling of the corneal concavity with agar/collagen mixture, which results in a hydrated cushion maintaining corneal humidity on the endothelial side, whilst the epithelial side can be exposed to humidified air, simulating the *in vivo* corneal environment (data not shown) [Foreman et al. 1996; Kabosova et al. 2003]. Whilst this is a simple and effective way to maintain corneal tissue in culture for a few days without stromal hydration, microscopic imaging proved difficult, as the "gel cushion" filling the concavity reduces light transmission, obscuring corneal details. Removing the agar-collagen mixture prior to microscopy overcomes this problem, but this prevents image acquisition over time.

The modification of Thiel's anterior segment perfusion chamber proved better suited for combined tissue maintenance and microscopy [Thiel et al. 2001]. The principle of this chamber is the perfusion of a corneoscleral button securely clamped onto a perspex

base. The perfusion allows continuous renewal of medium and removal of toxic waste products on the endothelial side of the cornea, whilst the epithelium is exposed to air. Drying of the epithelium is prevented by slight humidification at the beginning of tissue culture; placing a lid on the chamber prevents evaporation.

We reduced the height of the base of the originally described chamber to increase microscopic light transmission, and built a chamber designed to fit on the stages of both a Zeiss Axiovert 100 and a two-photon microscope. The confocal microscope has an inverted objective arrangement, but no leakage or spillage of medium from the chamber onto the objectives occurred. Overall, this is a successful setup to maintain cornea in culture for several days and to perform intermittent or continuous microscopic imaging.

In summary, the combination of vital dyes and/or viral GFP-transduction with confocal or two-photon excitation fluorescence microscopy are useful techniques to study cell-matrix interaction in whole stromal tissue. Fig. 4.4 summarises successful imaging strategies.

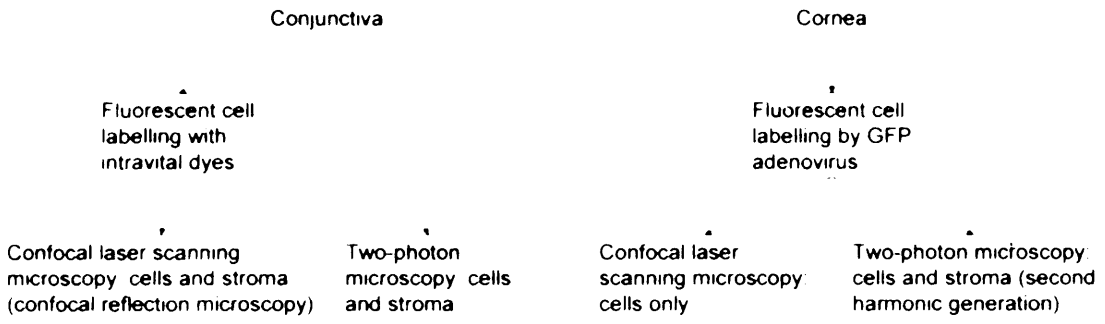

Fig. 4.4. Successful imaging strategies for imaging cells and stroma in whole conjunctiva and cornea.

Conclusions

This work demonstrates a novel mechanism to be at the basis of matrix contraction in a standard *in vitro* model of wound healing and scarring. Instead of cell migration and/or ASMA expression, we find that repeated protrusive and retractile activity generates the force required to displace matrix fibres towards the cell, resulting in net force and overall matrix contraction. This opens up the possibility of developing entirely novel treatment approaches to modulate wound healing and scarring by targeting the common and final steps of processes activated by growth factors and/or changes in mechanical tension: remodelling of the actin cytoskeleton and myosin-mediated contractility events. The discovery that the rab5/circular ruffling pathway is critically involved in matrix contraction by corneal fibroblasts indicates that specific inhibitors of this pathway might have modulatory effects on corneal scarring whilst avoiding undesired side-effects. Lastly, the combination of microscopy and tissue culture techniques with or without specific fluorescent vital cell labelling can successfully demonstrate cell-matrix interactions in living tissues, and can be used as a powerful tool to study physiological mechanisms and the effect of therapeutic agents.

In summary, this work has developed new investigative tools and has uncovered new mechanisms of cell-mediated tissue remodelling and contraction. Further work on the highly specific targets described in this thesis might not only advance our understanding of the basic mechanisms, but also significantly change the gain-to-risk-ratio in the management of wound healing and scarring.

References

Abe, M., C. H. Ho, K. E. Kamm and F. Grinnell (2003). Different molecular motors mediate platelet-derived growth factor and lysophosphatidic acid-stimulated floating collagen matrix contraction. *J Biol Chem* 278(48): 47707-12.

Ahlen, K., P. Ring, B. Tomasini-Johansson, K. Holmqvist, K. Magnusson and K. Rubin (2004). Platelet-derived growth factor BB modulates membrane mobility of beta 1 integrins. *Biochemical and Biophysical Research Communications* 314: 89-96.

Alberts, B., A. Johnson, J. Lewis, M. Raff, K. Roberts and P. Walter (2002). Chapter 16: The cytoskeleton. Molecular biology of the cell. New York, Garland Publishing.

Amano, M., K. Chihara, K. Kimura, Y. Fukata, N. Nakamura, Y. Matsuura and K. Kaibuchi (1997). Formation of actin stress fibers and focal adhesions enhanced by Rho-kinase. *Science* 275(5304): 1308-11.

Anton, I. M., S. P. Saville, M. J. Byrne, C. Curcio, N. Ramesh, J. H. Hartwig and R. S. Geha (2003). WIP participates in actin reorganization and ruffle formation induced by PDGF. *J Cell Sci* 116(Pt 12): 2443-51.

Araki, N., T. Hatae, A. Furukawa and J. A. Swanson (2003). Phosphoinositide-3-kinase-independent contractile activities associated with Fcgamma-receptor-mediated phagocytosis and macropinocytosis in macrophages. *J Cell Sci* 116(Pt 2): 247-57.

Araki, N., T. Hatae, T. Yamada and S. Hirohashi (2000). Actinin-4 is preferentially involved in circular ruffling and macropinocytosis in mouse macrophages: analysis by fluorescence ratio imaging. *J Cell Sci* 113 (Pt 18): 3329-40.

Arora, P. D. and C. A. McCulloch (1994). Dependence of collagen remodelling on alpha-smooth muscle actin expression by fibroblasts. *J Cell Physiol* 159(1): 161-75.

Arora, P. D., N. Narani and C. A. McCulloch (1999). The compliance of collagen gels regulates transforming growth factor-beta induction of alpha-smooth muscle actin in fibroblasts. *Am J Pathol* 154(3): 871-82.

Arthur, W. T., L. A. Petch and K. Burridge (2000). Integrin engagement suppresses RhoA activity via a c-Src-dependent mechanism. *Curr Biol* 10(12): 719-22.

Arvidsson, A. K., C. H. Heldin and L. Claesson-Welsh (1992). Transduction of circular membrane ruffling by the platelet-derived growth factor beta-receptor is dependent on its kinase insert. *Cell Growth Differ* 3(12): 881-7.

Assouline, M., S. J. Chew, H. W. Thompson and R. Beuerman (1992). Effect of growth factors on collagen lattice contraction by human keratocytes. *Invest Ophthalmol Vis Sci* 33(5): 1742-55.

Bailly, M., I. Ichetovkin, W. Grant, N. Zebda, L. M. Machesky, J. E. Segall and J. Condeelis (2001). The F-actin side binding activity of the Arp2/3 complex is essential for actin nucleation and lamellipod extension. *Curr Biol* 11(8): 620-5.

Barry, S. T., H. M. Flinn, M. J. Humphries, D. R. Critchley and A. J. Ridley (1997). Requirement for Rho in integrin signalling. *Cell Adhes Commun* 4(6): 387-98.

Bell, E., B. Ivarsson and C. Merrill (1979). Production of a tissue-like structure by contraction of collagen lattices by human fibroblasts of different proliferative potential in vitro. *Proc Natl Acad Sci U S A* 76(3): 1274-8.

Beningo, K. A., M. Dembo, I. Kaverina, J. V. Small and Y. L. Wang (2001). Nascent focal adhesions are responsible for the generation of strong propulsive forces in migrating fibroblasts. *J Cell Biol* 153(4): 881-8.

Benzonana, G., O. Skalli and G. Gabbiani (1988). Correlation between the distribution of smooth muscle or non muscle myosins and alpha-smooth muscle actin in normal and pathological soft tissues. *Cell Motil Cytoskeleton* 11(4): 260-74.

Bishop, A. L. and A. Hall (2000). Rho GTPases and their effector proteins. *Biochem J* 348 Pt 2: 241-55.

Bretscher, M. S. (1996). Getting membrane flow and the cytoskeleton to cooperate in moving cells. *Cell* 87(4): 601-6.

Bretscher, M. S. and C. Aguado-Velasco (1998). EGF induces recycling membrane to form ruffles. *Curr Biol* 8(12): 721-4.

Brightman, A. O., B. P. Rajwa, J. E. Sturgis, M. E. McCallister, J. P. Robinson and S. L. Voytik-Harbin (2000). Time-lapse confocal reflection microscopy of collagen fibrillogenesis and extracellular matrix assembly in vitro. *Biopolymers* 54(3): 222-34.

Brown, R. A., R. Prajapati, D. A. McGrouther, I. V. Yannas and M. Eastwood (1998). Tensional homeostasis in dermal fibroblasts: mechanical responses to mechanical loading in three-dimensional substrates. *J Cell Physiol* 175(3): 323-32.

Brzeska, H., J. Szczepanowska, F. Matsumura and E. D. Korn (2004). Rac-induced increase of phosphorylation of myosin regulatory light chain in HeLa cells. *Cell Motil Cytoskeleton* 58(3): 186-99.

Buccione, R., J. D. Orth and M. A. McNiven (2004). Foot and mouth: podosomes, invadopodia and circular dorsal ruffles. *Nat Rev Mol Cell Biol* 5(8): 647-57.

Bulinski, J. C. (2006). Cell biology. Actin discrimination. *Science* 313(5784): 180-1.

Burridge, K. and K. Wennerberg (2004). Rho and Rac take center stage. *Cell* 116(2): 167-79.

Cameron, L. A., M. J. Footer, A. van Oudenaarden and J. A. Theriot (1999). Motility of ActA protein-coated microspheres driven by actin polymerization. *Proc Natl Acad Sci U S A* 96(9): 4908-13.

Carlson, E. C., C. Y. Liu, X. Yang, M. Gregory, B. Ksander, J. Drazba and V. L. Perez (2004). In vivo gene delivery and visualization of corneal stromal cells using an adenoviral vector and keratocyte-specific promoter. *Invest Ophthalmol Vis Sci* 45(7): 2194-200.

Chavrier, P. (2002). May the force be with you: Myosin-X in phagocytosis. *Nat Cell Biol* 4(7): E169-71.

Choquet, D., D. P. Felsenfeld and M. P. Sheetz (1997). Extracellular matrix rigidity causes strengthening of integrin-cytoskeleton linkages. *Cell* 88(1): 39-48.

Chrzanowska-Wodnicka, M. and K. Burridge (1996). Rho-stimulated contractility drives the formation of stress fibers and focal adhesions. *J Cell Biol* 133(6): 1403-15.

Clark, R. A., J. M. Folkvord, C. E. Hart, M. J. Murray and J. M. McPherson (1989). Platelet isoforms of platelet-derived growth factor stimulate fibroblasts to contract collagen matrices. *J Clin Invest* 84(3): 1036-40.

Condeelis, J., M. Vahey, J. M. Carboni, J. DeMey and S. Ogihara (1984). Properties of the 120,000- and 95,000-dalton actin-binding proteins from Dictyostelium discoideum and their possible functions in assembling the cytoplasmic matrix. *J Cell Biol* 99(1 Pt 2): 119s-126s.

Connor, T. B., Jr., A. B. Roberts, M. B. Sporn, D. Danielpour, L. L. Dart, R. G. Michels, S. de Bustros, C. Enger, H. Kato, M. Lansing and et al. (1989). Correlation of fibrosis and transforming growth factor-beta type 2 levels in the eye. *J Clin Invest* 83(5): 1661-6.

Cordeiro, M. F., S. S. Bhattacharya, G. S. Schultz and P. T. Khaw (2000). TGF-beta1, -beta2, and -beta3 in vitro: biphasic effects on Tenon's fibroblast contraction, proliferation, and migration. *Invest Ophthalmol Vis Sci* 41(3): 756-63.

Cox, D., J. S. Berg, M. Cammer, J. O. Chinegwundoh, B. M. Dale, R. E. Cheney and S. Greenberg (2002). Myosin X is a downstream effector of PI(3)K during phagocytosis. *Nat Cell Biol* 4(7): 469-77.

Cui, W., M. Bryant, P. Sweet and P. McDonnell (2004). Changes in gene expression in response to mechanical strain in human scleral fibroblasts. *Experimental Eye Research* 78: 275-284.

Cukierman, E., R. Pankov, D. R. Stevens and K. M. Yamada (2001). Taking cell-matrix adhesions to the third dimension. *Science* 294(5547): 1708-12.

Dahlmann, A. H., K. Mireskandari, A. D. Cambrey, M. Bailly and P. T. Khaw (2005). Current and future prospects for the prevention of ocular fibrosis. *Ophthalmol Clin North Am* 18(4): 539-59.

Daniels, J. T., A. D. Cambrey, N. L. Occleston, Q. Garrett, R. W. Tarnuzzer, G. S. Schultz and P. T. Khaw (2003). Matrix metalloproteinase inhibition modulates fibroblast-mediated matrix contraction and collagen production in vitro. *Invest Ophthalmol Vis Sci* 44(3): 1104-10.

Daniels, J. T. and P. T. Khaw (2000). Temporal stimulation of corneal fibroblast wound healing activity by differentiating epithelium in vitro. *Invest Ophthalmol Vis Sci* 41(12): 3754-62.

Darby, I., O. Skalli and G. Gabbiani (1990). Alpha-smooth muscle actin is transiently expressed by myofibroblasts during experimental wound healing. *Lab Invest* 63(1): 21-9.

Dembo, M. and Y. L. Wang (1999). Stresses at the cell-to-substrate interface during locomotion of fibroblasts. *Biophys J* 76(4): 2307-16.

Desmouliere, A., A. Geinoz, F. Gabbiani and G. Gabbiani (1993). Transforming growth factor-beta 1 induces alpha-smooth muscle actin expression in granulation tissue myofibroblasts and in quiescent and growing cultured fibroblasts. *J Cell Biol* 122(1): 103-11.

Desmouliere, A., L. Rubbia-Brandt, A. Abdiu, T. Walz, A. Macieira-Coelho and G. Gabbiani (1992). Alpha-smooth muscle actin is expressed in a subpopulation of cultured and cloned fibroblasts and is modulated by gamma-interferon. *Exp Cell Res* 201(1): 64-73.

Desmouliere, A., L. Rubbia-Brandt, G. Grau and G. Gabbiani (1992). Heparin induces alpha-smooth muscle actin expression in cultured fibroblasts and in granulation tissue myofibroblasts. *Lab Invest* 67(6): 716-26.

Dharmawardhane, S., L. C. Sanders, S. S. Martin, R. H. Daniels and G. M. Bokoch (1997). Localization of p21-activated kinase 1 (PAK1) to pinocytic vesicles and cortical actin structures in stimulated cells. *J Cell Biol* 138(6): 1265-78.

Dharmawardhane, S., A. Schurmann, M. A. Sells, J. Chernoff, S. L. Schmid and G. M. Bokoch (2000). Regulation of macropinocytosis by p21-activated kinase-1. *Mol Biol Cell* 11(10): 3341-52.

Dowrick, P., P. Kenworthy, B. McCann and R. Warn (1993). Circular ruffle formation and closure lead to macropinocytosis in hepatocyte growth factor/scatter factor-treated cells. *Eur J Cell Biol* 61(1): 44-53.

Eastwood, M., D. A. McGrouther and R. A. Brown (1994). A culture force monitor for measurement of contraction forces generated in human dermal fibroblast

cultures: evidence for cell-matrix mechanical signalling. *Biochim Biophys Acta* 1201(2): 186-92.

Eastwood, M., D. A. McGrouther and R. A. Brown (1998). Fibroblast responses to mechanical forces. *Proc Inst Mech Eng [H]* 212(2): 85-92.

Eastwood, M., V. C. Mudera, D. A. McGrouther and R. A. Brown (1998). Effect of precise mechanical loading on fibroblast populated collagen lattices: morphological changes. *Cell Motil Cytoskeleton* 40(1): 13-21.

Eastwood, M., R. Porter, U. Khan, G. McGrouther and R. Brown (1996). Quantitative analysis of collagen gel contractile forces generated by dermal fibroblasts and the relationship to cell morphology. *J Cell Physiol* 166(1): 33-42.

Eden, S., R. Rohatgi, A. V. Podtelejnikov, M. Mann and M. W. Kirschner (2002). Mechanism of regulation of WAVE1-induced actin nucleation by Rac1 and Nck. *Nature* 418(6899): 790-3.

Ehrlich, H. P. and J. B. Rajaratnam (1990). Cell locomotion forces versus cell contraction forces for collagen lattice contraction: an in vitro model of wound contraction. *Tissue Cell* 22(4): 407-17.

Fehrenbacher, K. L., I. R. Boldogh and L. A. Pon (2003). Taking the A-train: actin-based force generators and organelle targeting. *Trends Cell Biol* 13(9): 472-7.

Foreman, D. M., S. Pancholi, J. Jarvis-Evans, D. McLeod and M. E. Boulton (1996). A simple organ culture model for assessing the effects of growth factors on corneal re-epithelialization. *Exp Eye Res* 62(5): 555-64.

Freyman, T. M., I. V. Yannas, Y. S. Pek, R. Yokoo and L. J. Gibson (2001). Micromechanics of fibroblast contraction of a collagen-GAG matrix. *Exp Cell Res* 269(1): 140-53.

Freyman, T. M., I. V. Yannas, R. Yokoo and L. J. Gibson (2002). Fibroblast contractile force is independent of the stiffness which resists the contraction. *Exp Cell Res* 272(2): 153-62.

Friedl, P. and E. B. Brocker (2000). The biology of cell locomotion within three-dimensional extracellular matrix. *Cell Mol Life Sci* 57(1): 41-64.

Friedl, P. and E. B. Brocker (2001). Biological Confocal Reflection Microscopy. Image Analysis: Methods and Applications. D.-P. Häder, CRC Press: 9-21.

Fuchshofer, R., M. Birke, U. Welge-Lussen, D. Kook and E. Lutjen-Drecoll (2005). Transforming growth factor-beta 2 modulated extracellular matrix component expression in cultured human optic nerve head astrocytes. *Invest Ophthalmol Vis Sci* 46(2): 568-78.

Funa, K. and H. Uramoto (2003). Regulatory mechanisms for the expression and activity of platelet-derived growth factor receptor. *Acta Biochim Pol* 50(3): 647-58.

Gabbiani, G. (1992). The biology of the myofibroblast. *Kidney Int* 41(3): 530-2.

Gabbiani, G., G. B. Ryan and G. Majne (1971). Presence of modified fibroblasts in granulation tissue and their possible role in wound contraction. *Experientia* 27(5): 549-50.

Galassi, A. R., C. Tamburino, A. Nicosia, G. Russo, R. Grassi, A. Monaco and G. Giuffrida (1999). A randomized comparison of trapidil (triazolopyrimidine), a platelet-derived growth factor antagonist, versus aspirin in prevention of angiographic restenosis after coronary artery Palmaz-Schatz stent implantation. *Catheter Cardiovasc Interv* 46(2): 162-8.

Galbraith, C. G., K. M. Yamada and M. P. Sheetz (2002). The relationship between force and focal complex development. *J Cell Biol* 159(4): 695-705.

Garrett, Q., P. T. Khaw, T. D. Blalock, G. S. Schultz, G. R. Grotendorst and J. T. Daniels (2004). Involvement of CTGF in TGF-beta1-stimulation of myofibroblast differentiation and collagen matrix contraction in the presence of mechanical stress. *Invest Ophthalmol Vis Sci* 45(4): 1109-16.

Gatlin, J., M. W. Melkus, A. Padgett, W. M. Petroll, H. D. Cavanagh, J. V. Garcia and J. V. Jester (2003). In vivo fluorescent labeling of corneal wound healing fibroblasts. *Exp Eye Res* 76(3): 361-71.

Geiger, B., A. Bershadsky, R. Pankov and K. M. Yamada (2001). Transmembrane crosstalk between the extracellular matrix--cytoskeleton crosstalk. *Nat Rev Mol Cell Biol* 2(11): 793-805.

Giannone, G., B. J. Dubin-Thaler, H. G. Dobereiner, N. Kieffer, A. R. Bresnick and M. P. Sheetz (2004). Periodic lamellipodial contractions correlate with rearward actin waves. *Cell* 116(3): 431-43.

Grinnell, F. (1994). Fibroblasts, myofibroblasts, and wound contraction. *J Cell Biol* 124(4): 401-4.

Grinnell, F. and C. H. Ho (2002). Transforming growth factor beta stimulates fibroblast-collagen matrix contraction by different mechanisms in mechanically loaded and unloaded matrices. *Exp Cell Res* 273(2): 248-55.

Grinnell, F., C. H. Ho, E. Tamariz, D. J. Lee and G. Skuta (2003). Dendritic fibroblasts in three-dimensional collagen matrices. *Mol Biol Cell* 14(2): 384-95.

Grinnell, F. and C. R. Lamke (1984). Reorganization of hydrated collagen lattices by human skin fibroblasts. *J Cell Sci* 66: 51-63.

Grinnell, F., M. Zhu, M. A. Carlson and J. M. Abrams (1999). Release of mechanical tension triggers apoptosis of human fibroblasts in a model of regressing granulation tissue. *Exp Cell Res* 248(2): 608-19.

Guggenheim, J. A. and N. A. McBrien (1996). Form-deprivation myopia induces activation of scleral matrix metalloproteinase-2 in tree shrew. *Invest Ophthalmol Vis Sci* 37(7): 1380-95.

Guidry, C. and F. Grinnell (1987). Contraction of hydrated collagen gels by fibroblasts: evidence for two mechanisms by which collagen fibrils are stabilized. *Coll Relat Res* 6(6): 515-29.

Gullberg, D., A. Tingstrom, A. C. Thuresson, L. Olsson, L. Terracio, T. K. Borg and K. Rubin (1990). Beta 1 integrin-mediated collagen gel contraction is stimulated by PDGF. *Exp Cell Res* 186(2): 264-72.

Hales, A. M., M. W. Schulz, C. G. Chamberlain and J. W. McAvoy (1994). TGF-beta 1 induces lens cells to accumulate alpha-smooth muscle actin, a marker for subcapsular cataracts. *Curr Eye Res* 13(12): 885-90.

Han, M., L. Zickler, G. Giese, M. Walter, F. H. Loesel and J. F. Bille (2004). Second-harmonic imaging of cornea after intrastromal femtosecond laser ablation. *J Biomed Opt* 9(4): 760-6.

Harris, A. K., D. Stopak and P. Wild (1981). Fibroblast traction as a mechanism for collagen morphogenesis. *Nature* 290(5803): 249-51.

Harris, A. K., P. Wild and D. Stopak (1980). Silicone rubber substrata: a new wrinkle in the study of cell locomotion. *Science* 208(4440): 177-9.

Heldin, C. H. (1997). Simultaneous induction of stimulatory and inhibitory signals by PDGF. *FEBS Lett* 410(1): 17-21.

Heldin, C. H. and B. Westermark (1999). Mechanism of action and in vivo role of platelet-derived growth factor. *Physiol Rev* 79(4): 1283-316.

Herman, I. M. (1993). Actin isoforms. *Curr Opin Cell Biol* 5(1): 48-55.

Hinz, B. and G. Gabbiani (2003). Mechanisms of force generation and transmission by myofibroblasts. *Current opinion in biotechnology* 14: 538-546.

Hinz, B., D. Mastrangelo, C. E. Iselin, C. Chaponnier and G. Gabbiani (2001). Mechanical tension controls granulation tissue contractile activity and myofibroblast differentiation. *Am J Pathol* 159(3): 1009-20.

Hoffman, S., S. He, M. Jin, M. Ehren, P. Wiedemann, S. J. Ryan and D. R. Hinton (2005). A selective cyclic integrin antagonist blocks the integrin receptors alphavbeta3 and alphavbeta5 and inhibits retinal pigment epithelium cell attachment, migration and invasion. *BMC Ophthalmology* 5: 16.

Hogan, A., Y. Yakubchyk, J. Chabot, C. Obagi, E. Daher, K. Maekawa and S. H. Gee (2004). The phosphoinositol 3,4-bisphosphate-binding protein TAPP1 interacts with syntrophins and regulates actin cytoskeletal organization. *J Biol Chem* 279(51): 53717-24.

Honjo, M., M. Inatani, N. Kido, T. Sawamura, B. Y. Yue, Y. Honda and H. Tanihara (2001). Effects of protein kinase inhibitor, HA1077, on intraocular pressure and outflow facility in rabbit eyes. *Arch Ophthalmol* 119(8): 1171-8.

Honjo, M., M. Inatani, N. Kido, T. Sawamura, B. Y. Yue, Y. Honda and H. Tanihara (2002). A myosin light chain kinase inhibitor, ML-9, lowers the intraocular pressure in rabbit eyes. *Exp Eye Res* 75(2): 135-42.

Hooshmand-Rad, R., L. Lu, C. H. Heldin, L. Claesson-Welsh and M. Welsh (2000). Platelet-derived growth factor-mediated signaling through the Shb adaptor protein: effects on cytoskeletal organization. *Exp Cell Res* 257(2): 245-54.

Hoppenreijs, V., E. Pels, G. Vrensen, P. Felten and W. Treffer (1993). Platelet-derived growth factor: receptor expression in corneas and effects on corneal cells. *Invest Ophthalmol Vis Sci* 34: 637-649.

Huang, H., R. D. Kamm and R. T. Lee (2004). Cell mechanics and mechanotransduction: pathways, probes, and physiology. *Am J Physiol Cell Physiol* 287(1): C1-11.

Huang, S. and D. E. Ingber (2005). Cell tension, matrix mechanics, and cancer development. *Cancer Cell* 8(3): 175-6.

Hynes, R. O. (1992). Integrins: versatility, modulation, and signaling in cell adhesion. *Cell* 69(1): 11-25.

Ingber, D. E. (1997). Tensegrity: the architectural basis of cellular mechanotransduction. *Annu Rev Physiol* 59: 575-99.

Ingber, D. E. (2003). Tensegrity II. How structural networks influence cellular information processing networks. *J Cell Sci* 116(Pt 8): 1397-408.

Jampel, H. D., N. Roche, W. J. Stark and A. B. Roberts (1990). Transforming growth factor-beta in human aqueous humor. *Curr Eye Res* 9(10): 963-9.

Jester, J. V. and J. Ho-Chang (2003). Modulation of cultured corneal keratocyte phenotype by growth factors/cytokines control in vitro contractility and extracellular matrix contraction. *Exp Eye Res* 77(5): 581-92.

Jester, J. V., J. Huang, W. M. Petroll and H. D. Cavanagh (2002). TGFbeta induced myofibroblast differentiation of rabbit keratocytes requires synergistic TGFbeta, PDGF and integrin signaling. *Exp Eye Res* 75(6): 645-57.

Jester, J. V., W. M. Petroll and H. D. Cavanagh (1999). Corneal stromal wound healing in refractive surgery: the role of myofibroblasts. *Prog Retin Eye Res* 18(3): 311-56.

Jones, N. L. and M. C. Willingham (1999). Modified LDLs are internalized by macrophages in part via macropinocytosis. *Anat Rec* 255(1): 57-68.

Kabosova, A., A. A. Kramerov, A. M. Aoki, G. Murphy, J. D. Zieske and A. V. Ljubimov (2003). Human diabetic corneas preserve wound healing, basement membrane, integrin and MMP-10 differences from normal corneas in organ culture. *Exp Eye Res* 77(2): 211-7.

Katsumi, A., J. Milanini, W. B. Kiosses, M. A. del Pozo, R. Kaunas, S. Chien, K. M. Hahn and M. A. Schwartz (2002). Effects of cell tension on the small GTPase Rac. *J Cell Biol* 158(1): 153-64.

Kessler, D., S. Dethlefsen, I. Haase, M. Plomann, F. Hirche, T. Krieg and B. Eckes (2001). Fibroblasts in mechanically stressed collagen lattices assume a "synthetic" phenotype. *J Biol Chem* 276(39): 36575-85.

Khaw, P., S. Ward, I. Grierson and N. Rice (1991). The effects of beta-radiation on proliferating human Tenon's capsule fibroblasts. *Br J Ophthalmol* 75: 580-583.

Khaw, P. T., M. B. Sherwood, J. W. Doyle, M. F. Smith, I. Grierson, S. McGorray and G. S. Schultz (1992). Intraoperative and post operative treatment with 5-fluorouracil and mitomycin-c: long term effects in vivo on subconjunctival and scleral fibroblasts. *Int Ophthalmol* 16(4-5): 381-5.

Kim, W., R. Mohan, R. Mohan and S. Wilson (1999). Effect of PDGF, IL-1alpha, and BMP2/4 on corneal fibroblast chemotaxis: expression of the platelet-derived growth factor system in the cornea. *Invest Ophthalmol Vis Sci* 40: 1364-1372.

Kirwan, R. P., M. O. Leonard, M. Murphy, A. F. Clark and J. O'Brien C (2005). Transforming growth factor-beta-regulated gene transcription and protein expression in human GFAP-negative lamina cribrosa cells. *Glia* 52(4): 309-24.

Knorr, M. and P. O. Denk (1999). Inhibitory effect of Trapidil on the proliferation of bovine corneal fibroblasts in vitro. *Graefes Arch Clin Exp Ophthalmol* 237(1): 72-7.

Kolodney, M. S. and E. L. Elson (1993). Correlation of myosin light chain phosphorylation with isometric contraction of fibroblasts. *J Biol Chem* 268(32): 23850-5.

Koumas, L., T. J. Smith, S. Feldon, N. Blumberg and R. P. Phipps (2003). Thy-1 expression in human fibroblast subsets defines myofibroblastic or lipofibroblastic phenotypes. *Am J Pathol* 163(4): 1291-300.

Krueger, E. W., J. D. Orth, H. Cao and M. A. McNiven (2003). A dynamin-cortactin-Arp2/3 complex mediates actin reorganization in growth factor-stimulated cells. *Mol Biol Cell* 14(3): 1085-96.

Langholz, O., D. Rockel, C. Mauch, E. Kozlowska, I. Bank, T. Krieg and B. Eckes (1995). Collagen and collagenase gene expression in three-dimensional collagen lattices are differentially regulated by alpha 1 beta 1 and alpha 2 beta 1 integrins. *J Cell Biol* 131(6 Pt 2): 1903-15.

Lanzetti, L., P. P. Di Fiore and G. Scita (2001). Pathways linking endocytosis and actin cytoskeleton in mammalian cells. *Exp Cell Res* 271(1): 45-56.

Lanzetti, L., A. Palamidessi, L. Areces, G. Scita and P. P. Di Fiore (2004). Rab5 is a signalling GTPase involved in actin remodelling by receptor tyrosine kinases. *Nature* 429(6989): 309-14.

Lapierre, L. A., R. Kumar, C. M. Hales, J. Navarre, S. G. Bhartur, J. O. Burnette, D. W. Provance, Jr., J. A. Mercer, M. Bahler and J. R. Goldenring (2001). Myosin vb is associated with plasma membrane recycling systems. *Mol Biol Cell* 12(6): 1843-57.

Lee, D. J., C. H. Ho and F. Grinnell (2003). LPA-stimulated fibroblast contraction of floating collagen matrices does not require Rho kinase activity or retraction of fibroblast extensions. *Exp Cell Res* 289(1): 86-94.

Lee, D. J., H. Rosenfeldt and F. Grinnell (2000). Activation of ERK and p38 MAP kinases in human fibroblasts during collagen matrix contraction. *Exp Cell Res* 257(1): 190-7.

Lee, G. M. and R. F. Loeser (1999). Cell surface receptors transmit sufficient force to bend collagen fibrils. *Exp Cell Res* 248(1): 294-305.

Lee, J., M. Leonard, T. Oliver, A. Ishihara and K. Jacobson (1994). Traction forces generated by locomoting keratocytes. *J Cell Biol* 127(6 Pt 2): 1957-64.

Lygoe, K. A., J. T. Norman, J. F. Marshall and M. P. Lewis (2004). AlphaV integrins play an important role in myofibroblast differentiation. *Wound Repair Regen* 12(4): 461-70.

Machesky, L. M. and R. H. Insall (1998). Scar1 and the related Wiskott-Aldrich syndrome protein, WASP, regulate the actin cytoskeleton through the Arp2/3 complex. *Curr Biol* 8(25): 1347-56.

Majno, G., G. Gabbiani, B. J. Hirschel, G. B. Ryan and P. R. Statkov (1971). Contraction of granulation tissue in vitro: similarity to smooth muscle. *Science* 173(996): 548-50.

Marcy, Y., J. Prost, M. F. Carlier and C. Sykes (2004). Forces generated during actin-based propulsion: a direct measurement by micromanipulation. *Proc Natl Acad Sci U S A* 101(16): 5992-7.

Maresta, A., M. Balducelli, R. Latini, G. Bernardi, T. Moccetti, C. Sosa, S. Barlera, E. Varani, E. E. Ribeiro da Silva, A. Monici Preti and A. P. Maggioni (2005). Starc II, a multicenter randomized placebo-controlled double-blind clinical trial of trapidil for 1-year clinical events and angiographic restenosis reduction after coronary angioplasty and stenting. *Catheter Cardiovasc Interv* 64(3): 375-82.

Martin, P. (1997). Wound healing--aiming for perfect skin regeneration. *Science* 276(5309): 75-81.

Mazure, A. and I. Grierson (1992). In vitro studies of the contractility of cell types involved in proliferative vitreoretinopathy. *Invest Ophthalmol Vis Sci* 33(12): 3407-16.

McNiven, M. A., L. Kim, E. W. Krueger, J. D. Orth, H. Cao and T. W. Wong (2000). Regulated interactions between dynamin and the actin-binding protein cortactin modulate cell shape. *J Cell Biol* 151(1): 187-98.

Mellstrom, K., C. H. Heldin and B. Westermark (1988). Induction of circular membrane ruffling on human fibroblasts by platelet-derived growth factor. *Exp Cell Res* 177(2): 347-59.

Meshel, A. S., Q. Wei, R. S. Adelstein and M. P. Sheetz (2005). Basic mechanism of three-dimensional collagen fibre transport by fibroblasts. *Nat Cell Biol* 7(2): 157-64.

Mettlen, M., A. Platek, P. Van Der Smissen, S. Carpentier, M. Amyere, L. Lanzetti, P. de Diesbach, D. Tyteca and P. J. Courtoy (2006). Src triggers circular ruffling and macropinocytosis at the apical surface of polarized MDCK cells. *Traffic* 7(5): 589-603.

Mizutani, T., H. Haga and K. Kawabata (2004). Cellular stiffness response to external deformation: tensional homeostasis in a single fibroblast. *Cell Motil Cytoskeleton* 59(4): 242-8.

Mochitate, K., P. Pawelek and F. Grinnell (1991). Stress relaxation of contracted collagen gels: disruption of actin filament bundles, release of cell surface fibronectin, and down-regulation of DNA and protein synthesis. *Exp Cell Res* 193(1): 198-207.

Orth, J. D., E. W. Krueger, S. G. Weller and M. A. McNiven (2006). A novel endocytic mechanism of epidermal growth factor receptor sequestration and internalization. *Cancer Res* 66(7): 3603-10.

Paavilainen, V. O., E. Bertling, S. Falck and P. Lappalainen (2004). Regulation of cytoskeletal dynamics by actin-monomer-binding proteins. *Trends Cell Biol* 14(7): 386-94.

Pasquale, L. R., M. E. Dorman-Pease, G. A. Lutty, H. A. Quigley and H. D. Jampel (1993). Immunolocalization of TGF-beta 1, TGF-beta 2, and TGF-beta 3 in the anterior segment of the human eye. *Invest Ophthalmol Vis Sci* 34(1): 23-30.

Pelham, R. J., Jr. and Y. Wang (1997). Cell locomotion and focal adhesions are regulated by substrate flexibility. *Proc Natl Acad Sci U S A* 94(25): 13661-5.

Pelham, R. J., Jr. and Y. Wang (1999). High resolution detection of mechanical forces exerted by locomoting fibroblasts on the substrate. *Mol Biol Cell* 10(4): 935-45.

Pelham, R. J., Jr. and Y. L. Wang (1998). Cell locomotion and focal adhesions are regulated by the mechanical properties of the substrate. *Biol Bull* 194(3): 348-9; discussion 349-50.

Petroll, W. M., M. Vishwanath and L. Ma (2004). Corneal fibroblasts respond rapidly to changes in local mechanical stress. *Invest Ophthalmol Vis Sci* 45(10): 3466-74.

Phillips, J. and N. McBrien (2004). Pressure-induced changes in axial eye length of chick and tree shrew: significance of myofibroblasts in the sclera. *Investigative Ophthalmology and Visual Science* 45(3): 758-763.

Piston, D. W., B. R. Masters and W. W. Webb (1995). Three-dimensionally resolved NAD(P)H cellular metabolic redox imaging of the in situ cornea with two-photon excitation laser scanning microscopy. *J Microsc* 178 (Pt 1): 20-7.

Pizzo, A. M., K. Kokini, L. C. Vaughn, B. Z. Waisner and S. L. Voytik-Harbin (2005). Extracellular matrix (ECM) microstructural composition regulates local cell-ECM biomechanics and fundamental fibroblast behavior: a multidimensional perspective. *J Appl Physiol* 98(5): 1909-21.

Plattner, R., L. Kadlec, K. A. DeMali, A. Kazlauskas and A. M. Pendergast (1999). c-Abl is activated by growth factors and Src family kinases and has a role in the cellular response to PDGF. *Genes Dev* 13(18): 2400-11.

Poole, C. A., N. H. Brookes and G. M. Clover (1993). Keratocyte networks visualised in the living cornea using vital dyes. *J Cell Sci* 106 (Pt 2): 685-91.

Poole, C. A., N. H. Brookes and G. M. Clover (2003). Confocal imaging of the human keratocyte network using the vital dye 5-chloromethylfluorescein diacetate. *Clin Experiment Ophthalmol* 31(2): 147-54.

Popova, S. N., B. Rodriguez-Sanchez, A. Liden, C. Betsholtz, T. Van Den Bos and D. Gullberg (2004). The mesenchymal alpha11beta1 integrin attenuates PDGF-BB-stimulated chemotaxis of embryonic fibroblasts on collagens. *Dev Biol* 270(2): 427-42.

Porter, R. A., R. A. Brown, M. Eastwood, N. L. Occleston and P. T. Khaw (1998). Ultrastructural changes during contraction of collagen lattices by ocular fibroblasts. *Wound Repair Regen* 6(2): 157-66.

Rada, J. A., C. A. Perry, M. L. Slover and V. R. Achen (1999). Gelatinase A and TIMP-2 expression in the fibrous sclera of myopic and recovering chick eyes. *Invest Ophthalmol Vis Sci* 40(13): 3091-9.

Ren, X. D., W. B. Kiosses and M. A. Schwartz (1999). Regulation of the small GTP-binding protein Rho by cell adhesion and the cytoskeleton. *Embo J* 18(3): 578-85.

Rhee, S. and F. Grinnell (2006). P21-activated kinase 1: convergence point in PDGF- and LPA-stimulated collagen matrix contraction by human fibroblasts. *J Cell Biol* 172(3): 423-32.

Ridley, A. J. and A. Hall (1992). The small GTP-binding protein rho regulates the assembly of focal adhesions and actin stress fibers in response to growth factors. *Cell* 70(3): 389-99.

Ridley, A. J., H. F. Paterson, C. L. Johnston, D. Diekmann and A. Hall (1992). The small GTP-binding protein rac regulates growth factor-induced membrane ruffling. *Cell* 70(3): 401-10.

Riikonen, T., J. Westermarck, L. Koivisto, A. Broberg, V. M. Kahari and J. Heino (1995). Integrin alpha 2 beta 1 is a positive regulator of collagenase (MMP-1) and collagen alpha 1(I) gene expression. *J Biol Chem* 270(22): 13548-52.

Roy, P., W. M. Petroll, H. D. Cavanagh and J. V. Jester (1999). Exertion of tractional force requires the coordinated up-regulation of cell contractility and adhesion. *Cell Motil Cytoskeleton* 43(1): 23-34.

Rubbia-Brandt, L., A. P. Sappino and G. Gabbiani (1991). Locally applied GM-CSF induces the accumulation of alpha-smooth muscle actin containing myofibroblasts. *Virchows Arch B Cell Pathol Incl Mol Pathol* 60(2): 73-82.

Sawhney, R. K. and J. Howard (2002). Slow local movements of collagen fibers by fibroblasts drive the rapid global self-organization of collagen gels. *J Cell Biol* 157(6): 1083-91.

Sawhney, R. K. and J. Howard (2004). Molecular dissection of the fibroblast-traction machinery. *Cell Motil Cytoskeleton* 58(3): 175-85.

Serini, G., M. L. Bochaton-Piallat, P. Ropraz, A. Geinoz, L. Borsi, L. Zardi and G. Gabbiani (1998). The fibronectin domain ED-A is crucial for myofibroblastic

phenotype induction by transforming growth factor-beta1. *J Cell Biol* 142(3): 873-81.

Serruys, P. W., D. P. Foley, M. Pieper, J. A. Kleijne and P. J. de Feyter (2001). The TRAPIST Study. A multicentre randomized placebo controlled clinical trial of trapidil for prevention of restenosis after coronary stenting, measured by 3-D intravascular ultrasound. *Eur Heart J* 22(20): 1938-47.

Shao, D., A. Forge, P. M. Munro and M. Bailly (2006). Arp2/3 complex-mediated actin polymerisation occurs on specific pre-existing networks in cells and requires spatial restriction to sustain functional lamellipod extension. *Cell Motil Cytoskeleton* 63(7): 395-414.

Shibuya, M., Y. Suzuki, K. Sugita, I. Saito, T. Sasaki, K. Takakura, I. Nagata, H. Kikuchi, T. Takemae, H. Hidaka and et al. (1992). Effect of AT877 on cerebral vasospasm after aneurysmal subarachnoid hemorrhage. Results of a prospective placebo-controlled double-blind trial. *J Neurosurg* 76(4): 571-7.

Siriwardena, D., P. T. Khaw, A. J. King, M. L. Donaldson, B. M. Overton, C. Migdal and M. F. Cordeiro (2002). Human antitransforming growth factor beta(2) monoclonal antibody - a new modulator of wound healing in trabeculectomy: a randomized placebo controlled clinical study. *Ophthalmology* 109(3): 427-31.

Skalli, O., P. Ropraz, A. Trzeciak, G. Benzonana, D. Gillessen and G. Gabbiani (1986). A monoclonal antibody against alpha-smooth muscle actin: a new probe for smooth muscle differentiation. *J Cell Biol* 103(6 Pt 2): 2787-96.

Small, J. V. and G. P. Resch (2005). The comings and goings of actin: coupling protrusion and retraction in cell motility. *Curr Opin Cell Biol* 17(5): 517-23.

Small, J. V., T. Stradal, E. Vignal and K. Rottner (2002). The lamellipodium: where motility begins. *Trends Cell Biol* 12(3): 112-20.

Straight, A. F., A. Cheung, J. Limouze, I. Chen, N. J. Westwood, J. R. Sellers and T. J. Mitchison (2003). Dissecting temporal and spatial control of cytokinesis with a myosin II Inhibitor. *Science* 299(5613): 1743-7.

Su, I. H., M. W. Dobenecker, E. Dickinson, M. Oser, A. Basavaraj, R. Marqueron, A. Viale, D. Reinberg, C. Wulfing and A. Tarakhovsky (2005). Polycomb group protein ezh2 controls actin polymerization and cell signaling. *Cell* 121(3): 425-36.

Suetsugu, S., D. Yamazaki, S. Kurisu and T. Takenawa (2003). Differential roles of WAVE1 and WAVE2 in dorsal and peripheral ruffle formation for fibroblast cell migration. *Dev Cell* 5(4): 595-609.

Swanson, J. A. and C. Watts (1995). Macropinocytosis. *Trends Cell Biol* 5(11): 424-8.

Tamariz, E. and F. Grinnell (2002). Modulation of fibroblast morphology and adhesion during collagen matrix remodeling. *Mol Biol Cell* 13(11): 3915-29.

Tan, J. L., J. Tien, D. M. Pirone, D. S. Gray, K. Bhadriraju and C. S. Chen (2003). Cells lying on a bed of microneedles: an approach to isolate mechanical force. *Proc Natl Acad Sci U S A* 100(4): 1484-9.

Teng, S. W., H. Y. Tan, J. L. Peng, H. H. Lin, K. H. Kim, W. Lo, Y. Sun, W. C. Lin, S. J. Lin, S. H. Jee, P. T. So and C. Y. Dong (2006). Multiphoton autofluorescence and second-harmonic generation imaging of the ex vivo porcine eye. *Invest Ophthalmol Vis Sci* 47(3): 1216-24.

Tervo, T. and J. Moilanen (2003). In vivo confocal microscopy for evaluation of wound healing following corneal refractive surgery. *Progress in Retinal and Eye Research* 22: 339-358.

Thiel, M. A., N. Morlet, D. Schulz, H. F. Edelhauser, J. K. Dart, D. J. Coster and K. A. Williams (2001). A simple corneal perfusion chamber for drug penetration and toxicity studies. *Br J Ophthalmol* 85(4): 450-3.

Tiger, C. F., F. Fougerousse, G. Grundstrom, T. Velling and D. Gullberg (2001). alpha11beta1 integrin is a receptor for interstitial collagens involved in cell migration and collagen reorganization on mesenchymal nonmuscle cells. *Dev Biol* 237(1): 116-29.

Tingstrom, A., C. H. Heldin and K. Rubin (1992). Regulation of fibroblast-mediated collagen gel contraction by platelet-derived growth factor, interleukin-1 alpha and transforming growth factor-beta 1. *J Cell Sci* 102 (Pt 2): 315-22.

Tomasek, J. J., G. Gabbiani, B. Hinz, C. Chaponnier and R. A. Brown (2002). Myofibroblasts and mechano-regulation of connective tissue remodelling. *Nat Rev Mol Cell Biol* 3(5): 349-63.

Tomasek, J. J., C. J. Haaksma, R. J. Eddy and M. B. Vaughan (1992). Fibroblast contraction occurs on release of tension in attached collagen lattices: dependency on an organized actin cytoskeleton and serum. *Anat Rec* 232(3): 359-68.

Totsukawa, G., Y. Wu, Y. Sasaki, D. J. Hartshorne, Y. Yamakita, S. Yamashiro and F. Matsumura (2004). Distinct roles of MLCK and ROCK in the regulation of membrane protrusions and focal adhesion dynamics during cell migration of fibroblasts. *J Cell Biol* 164(3): 427-39.

Tripathi, R. C., J. Li, W. F. Chan and B. J. Tripathi (1994). Aqueous humor in glaucomatous eyes contains an increased level of TGF-beta 2. *Exp Eye Res* 59(6): 723-7.

Vesaluoma, M. H. and T. T. Tervo (1998). Tenascin and cytokines in tear fluid after photorefractive keratectomy. *J Refract Surg* 14(4): 447-54.

Voytik-Harbin, S. L., B. A. Roeder, J. E. Sturgis, K. Kokini and J. P. Robinson (2003). Simultaneous mechanical loading and confocal reflection microscopy for three-dimensional microbiomechanical analysis of biomaterials and tissue constructs. *Microsc Microanal* 9(1): 74-85.

Wakatsuki, T. and E. L. Elson (2003). Reciprocal interactions between cells and extracellular matrix during remodeling of tissue constructs. *Biophys Chem* 100(1-3): 593-605.

Wakatsuki, T., R. B. Wysolmerski and E. L. Elson (2003). Mechanics of cell spreading: role of myosin II. *J Cell Sci* 116(Pt 8): 1617-25.

Waki, M., Y. Yoshida, T. Oka and M. Azuma (2001). Reduction of intraocular pressure by topical administration of an inhibitor of the Rho-associated protein kinase. *Curr Eye Res* 22(6): 470-4.

Wennstrom, S., P. Hawkins, F. Cooke, K. Hara, K. Yonezawa, M. Kasuga, T. Jackson, L. Claesson-Welsh and L. Stephens (1994). Activation of phosphoinositide 3-kinase is required for PDGF-stimulated membrane ruffling. *Curr Biol* 4(5): 385-93.

Wennstrom, S., E. Landgren, P. Blume-Jensen and L. Claesson-Welsh (1992). The platelet-derived growth factor beta-receptor kinase insert confers specific signaling properties to a chimeric fibroblast growth factor receptor. *J Biol Chem* 267(19): 13749-56.

Williams, R. M., W. R. Zipfel and W. W. Webb (2001). Multiphoton microscopy in biological research. *Curr Opin Chem Biol* 5(5): 603-8.

Wilson, S. E., R. R. Mohan, R. Ambrosio, Jr., J. Hong and J. Lee (2001). The corneal wound healing response: cytokine-mediated interaction of the epithelium, stroma, and inflammatory cells. *Prog Retin Eye Res* 20(5): 625-37.

Worthylake, R. A. and K. Burridge (2003). RhoA and ROCK promote migration by limiting membrane protrusions. *J Biol Chem* 278(15): 13578-84.

Wozniak, M. A., R. Desai, P. A. Solski, C. J. Der and P. J. Keely (2003). ROCK-generated contractility regulates breast epithelial cell differentiation in response to the physical properties of a three-dimensional collagen matrix. *J Cell Biol* 163(3): 583-95.

Wozniak, M. A., K. Modzelewska, L. Kwong and P. J. Keely (2004). Focal adhesion regulation of cell behavior. *Biochim Biophys Acta* 1692(2-3): 103-19.

Wyckoff, J. B., S. E. Pinner, S. Gschmeissner, J. S. Condeelis and E. Sahai (2006). ROCK- and myosin-dependent matrix deformation enables protease-independent tumor-cell invasion in vivo. *Curr Biol* 16(15): 1515-23.

Yamaoka, A., T. Matsuo, F. Shiraga and H. Ohtsuki (2001). TIMP-1 production by human scleral fibroblast decreases in response to cyclic mechanical stretching. *Ophthalmic Res* 33(2): 98-101.

Yan, Q., W. Sun, P. Kujala, Y. Lotfi, T. A. Vida and A. J. Bean (2005). CART: an Hrs/actinin-4/BERP/myosin V protein complex required for efficient receptor recycling. *Mol Biol Cell* 16(5): 2470-82.

Zhang, H., J. S. Berg, Z. Li, Y. Wang, P. Lang, A. D. Sousa, A. Bhaskar, R. E. Cheney and S. Stromblad (2004). Myosin-X provides a motor-based link between integrins and the cytoskeleton. *Nat Cell Biol* 6(6): 523-31.

Zhang, Z. G., I. Bothe, F. Hirche, M. Zweers, D. Gullberg, G. Pfitzer, T. Krieg, B. Eckes and M. Aumailley (2006). Interactions of primary fibroblasts and

keratinocytes with extracellular matrix proteins: contribution of alpha2beta1 integrin. *J Cell Sci* 119(Pt 9): 1886-95.

Zhao, X., K. E. Ramsey, D. A. Stephan and P. Russell (2004). Gene and protein expression changes in human trabecular meshwork cells treated with transforming growth factor-beta. *Invest Ophthalmol Vis Sci* 45(11): 4023-34.

Zhou, K., S. Pandol, G. Bokoch and A. E. Traynor-Kaplan (1998). Disruption of Dictyostelium PI3K genes reduces [32P]phosphatidylinositol 3,4 bisphosphate and [32P]phosphatidylinositol trisphosphate levels, alters F-actin distribution and impairs pinocytosis. *J Cell Sci* 111(Pt 2): 283-94.

Zoumi, A., A. Yeh and B. J. Tromberg (2002). Imaging cells and extracellular matrix in vivo by using second-harmonic generation and two-photon excited fluorescence. *Proc Natl Acad Sci U S A* 99(17): 11014-9.